國　立　交　通　大　學

電子工程學系電子研究所碩士班

碩 士 論 文

利用金屬嵌入層提升溶膠凝膠法製備之鈦酸鉍薄膜電阻轉態特性

Modification of Resistive Switching Characteristics in Sol-Gel Derived $Bi_4Ti_3O_{12}$ Thin Film Using Embedded Metal

研 究 生：黃毅函

指導教授：曾俊元 教授

中華民國九十七年七月

利用金屬嵌入層提升溶膠凝膠法製備之鈦酸鉍薄膜電阻轉態特性

Modification of Resistive Switching Characteristics in Sol-Gel Derived $Bi_4Ti_3O_{12}$ Thin Film Using Embedded Metal

研 究 生：黃毅函　　Student：Yi-Han Huang

指導教授： 曾俊元　教授　　Advisor：Prof. Tseung-Yuen Tseng

國 立 交 通 大 學

電子工程學系電子研究所碩士班

碩 士 論 文

A Thesis
Submitted to Department of Electronics Engineering and Institute of Electronics
College of Electrical and Computer Engineering
National Chiao-Tung University
in Partial Fulfillment of the Requirements
for the Degree of Master
in Electronic Engineering
July 2008
Hsinchu, Taiwan, Republic of China

中華民國九十七年七月

利用金屬嵌入層提升溶膠凝膠法製備之鈦酸鉍薄膜電阻轉態特性

研究生：黃毅函　　　　　　　　　　　　指導教授：曾俊元

國立交通大學

電子工程學系電子研究所

摘要

近來新世代非揮發性記憶元件受到廣泛的注意，諸如相變化記憶體、磁阻式記憶體、鐵電記憶體、電阻式記憶體等。其中又以電阻式記憶元件最受矚目，由於其具有低操作電壓、結構簡單、讀寫速度快、低耗能、非破壞讀取等優點，將有助於達到高密度積體整合及低操作功率的目的，因此可以期待電阻式記憶體成為未來非揮發性記憶體的主流。

本論文選用層狀鈣鈦礦結構材料（鈦酸鉍）作為電阻式記憶體的轉態層材料，利用溶膠凝膠法製備鈦酸鉍薄膜，並且首次在薄膜中間嵌入兩奈米厚度的鉻金屬層來改善轉態特性，而此結構的轉態層厚度約為二十二奈米。本論文著重在於如何降低並穩定操作電壓，除了嵌入鉻金屬外，更利用後續高溫退火步驟來實現。結果發現退火600度下，擁有最低的操作電壓(約為-2伏特)，而且，在記憶測試中，例如：耐久度、非破壞讀取、儲存能力等都擁有極佳的表現度。本實驗更利用材料分析結果去驗證電性表現，並探討嵌入金屬層對於轉態層的影響。隨後我們也探討電壓電流關係，去探討可能的電阻式記憶體的電阻轉換特性及傳導機制。

Modification of Resistive Switching Characteristics in Sol-Gel Derived $Bi_4Ti_3O_{12}$ Thin Film Using Embedded Metal

Student: Yi-Han Huang Advisor: Tseung-Yuen Tseng

Department of Electronics Engineering and Institute of Electronics
National Chiao Tung University

Abstract

In recent year, next-generation nonvolatile memories (NVM), such as OUM, MRAM, FRAM and RRAM, have attracted a lot of attention because of its ascendant advantages such as simple device structure, low operation voltage, low power consumption, long retention time, small cell size, high operation speed, low cost, good endurance, and non-destructive readout, which help for attaining to objects of high density integration and low power operation.

In this thesis, the RRAM devices manufactured based on Sol-Gel derived $Bi_4Ti_3O_{12}$ thin films are studied and developed. The electrical properties are enhanced by using embedded 2nm-Cr in BTO thin film. The thickness of switching oxide is about 22nanometer. The main point is accented on how to decrease and stabilize the operation voltage. Except using embedded metal, thermal treatment like post deposition annealing is used as well. Accidentally, the lowest operation voltage (-2V) appears at the condition with annealing at 600°C. Also, in memory test such as endurance, retention and voltage stress, the device shows the best performance. The material analyses are applied to verify the electrical phenomenon. In addition, the related conduction mechanism is discussed in detail.

誌謝

首先，要感謝我的指導老師曾俊元教授在我兩年的研究生生涯裡，提供如此良好的實驗室環境，並在專業領域上給予我許多的建議，使我能順利完成本篇論文。此外，也要感謝國家毫微米實驗室、清大貴重儀器中心、交大貴重儀器中心等單位，提供良好的研究環境讓我完成實驗。也特別感謝林晨曦博士以及林昭吟博士對本論文的建議，使論文內容更趨完善。

其次，謝謝林群傑學長、林志洋學長，在我實驗、課業以及論文上總是給予我很多實驗內容的建議。而林孟漢學長、吳明錡學長在實驗上更是給我很大的幫助，使我的論文內容更佳的完備，沒有你們的協助，我很難這麼順利畢業。也要感謝姚奕全、王聖裕、李岱螢這幾位學長在實驗細節上也提供了不少的寶貴意見，以及另外還有莊文仁、詹世偉、翁啟翔、顏宏全這幾位同學，很感謝有你們這兩年陪伴，使得我兩年的研究生活中增添了許多歡樂，而且也在實驗及課業上幫了我不少，我會好好珍惜這一份難得的友誼。李盈賢、葉昱廷、蔡承翰、孫淑炫、黃志文這幾位學弟妹，多謝你們在實驗上的幫忙。還有曾給予我協助的朋友，若沒有你們，我也不會這麼順利。也感謝女朋友旻諭這兩年的陪伴，讓我過了一段美好的研究生活。

最後還要感謝我的爸爸媽媽，很感謝你們竭盡全力的支持我讀研究所，讓我無後顧之憂能順利完成研究所學業，在此，將這份論文獻給你們。

Contents

Chinese Abstract ………………………………………………………………………. i

English Abstract ……………………………………………………………………….. ii

Acknowledgement…………………………………………………………….………….. iii

Contents …………………………………………………………………………………... iv

Table Captions ………………………………………………………………………. viii

Figure Captions ……………………………………………………………………….... ix

Chapter 1 Introduction

1.1 Memories Classification ………………………………………………………….... 1

1.2 Conventional Nonvolatile Memory ……………………………………...….... 1

1.2.1 Read Only Memory …………………………………………………………….... 2

1.2.2 Programmable Read Only Memory …………………………………...……..... 2

1.2.3 Mask-Programmed Read Only Memory ………………………………….…..... 3

1.2.4 Erasable and Programmable Read Only Memory ………………………….. 3

1.2.5 Ultraviolet-Erase EPROM ……………………………………………………. 3

1.2.6 One-Time Programmable (OTP) Read Only Memory…………………….... 4

1.2.7 Electrically Erasable and Programmable Read Only Memory……………... 4

1.2.8 Flash Memory…………………………………………………………............ 4

1.3 Promising Next-Generation Nonvolatile Memory ……………………………... 6

1.3.1 Ovonic Unified Memory ………………….………….……………........ 6

1.3.2 Magnetic Random Access Memory…………………………………………... 6

1.3.3 Ferroelectric Random Access Memory ……………………………………. 8

1.3.4 Resistance Random Access Memory …………………………………....... 10

1.4 Resistance Random Access Memory …………………………………………... 10

1.4.1 Metal-Insulator-Metal Structure………………………………………………. 10

1.4.2 Operation Method……………………………………………………………….. 11

1.4.3 Introduction to Perovskite materials……………………………………….. 11

1.4.4 Resistive Switching Mechanisms…………………………………………….. 12

1.5 Important Criteria for RRAM…………………………………………………... 16

Chapter 2 Experiment Details 23

2.1 Experimental Process Flow ……………………………………………………….. 23

2.2 Sample Preparation………………………………………………………………... 24

2.2.1 RCA Cleaning of Silicon Substrate ……………………………………….... 24

2.2.2. Furnace Oxidation of Silicon Substrate……………………………………… 24

2.2.3. Deposition of Bottom Electrode……………………………………………... 25

2.2.4. Deposition of $LaNiO_3$ Thin Films………………………………………………. 25

2.2.5. Rapid Thermal Annealing Process of $LaNiO_3$ Thin Films………………… 25

2.2.6. Deposition of $Bi_4Ti_3O_{12}$ Thin Films……………………………………….. 26

2.2.7. Post Deposition Annealing Process of $Bi_4Ti_3O_{12}$ Thin Films…………….... 26

2.2.8. Deposition of Top Electrode…………………………………………………….. 27

2.3 Electrical Measurement and Material Analyses………………………………… 27

2.3.1 Current-Voltage (I-V) Measurement………………………………………... 27

2.3.2 X-Ray Diffraction…………………………………………………………...... 28

2.3.3 Atomic Force Microscopy …………………………………………………….. 28

2.3.4 Scanning Electron Microscopy ………………………………………………….. 29

2.3.5 Transmission Electron Microscopy………………………………………………. 29

2.3.6 Secondary Ion Mass Spectrometer…………………………………………… 29

Chapter 3 Results and Discussion

3.1 Pure BTO thin film ………………………………………………………….... 34

3.1.1 Thickness of pure BTO thin film………………………………………….... 34

3.1.2 Forming process…………………………………………………………….. 35

3.1.3 Operation mode and voltage……………………………………………….... 35

3.1.4 Memory test for endurance…………………………………………………. 36

3.1.5 Thermal effect of post deposition annealing……………………………….... 36

3.1.6 Summary for thinner pure BTO thin film………………………………….... 36

3.2 The effect of embedded metal in BTO thin film………………………………… 37

3.2.1 Materials for embedded metal………………………………………………. 37

3.2.2 The effect of thermal treatment…………………………………………….... 37

3.2.3 Resistive switching properties of embedded Cr BTO thin film…………….. 38

3.3 Physical property analyses of 2nm Cr embedded…………………………….. 39

3.3.1 X-Ray Diffraction………………………………………………………….... 39

3.3.2 Scanning Electron Microscope…………………………………………….... 39

3.3.3 Atomic Force Microscope………………………... ……………………… 40

3.3.4 Transmission Electron Microscope…………………………………………….. 40

3.4 Electrical Property Analyses of 2nm Cr Embedded…………………………… 41

3.4.1 Resistive Switching Characteristics……………………………………… 41

3.4.2 Memory Test……………………………………………………………….... 42

3.4.3 Curve Fitting of Current-Voltage Plots…………………………………….... 43

3.4.4 The relation between temperature and current……………………………… 44

3.4.5 Possible mechanism………………………………………………………… 45

3.5 Electrical Property Analyses for 2nm Pt Embedded……………………………… 45

3.5.1 Resistive Switching Characteristics……………………………………… 45

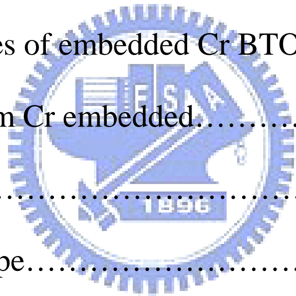

3.5.2 Curve Fitting of Current-Voltage Plots…………………………………….. 46

3.5.3 The relation between temperature and current……………………………… 47

3.5.4 Possible mechanism……………………………………………………… 47

Chapter 4 Conclusions

4.1Conclusions …………………………………………………………………. 83

References 84

Figure Captions

Chapter 1

Figure 1.1 A schematic of an MTJ memory cell. Arrows indicate possible directions of magnetic movement………………………………………………………... 19

Figure 1.2 MRAM array………………………………………………………………. 19

Figure 1.3 Hysteresis loop of FRAM cell capacitor…………………………………… 20

Figure 1.4 RRAM consists of a transistor and a resistor. The transistor is fabricated in the front end and the resistor in the back end……………………………… 20

Figure 1.5 Schematic view of stacked memory layers. The cell sizes decrease from $4F^2$ to $4F^2/n$ for n layers………………………………………………………… 21

Figure 1.6 Equivalent circuit of an array for the write operation of a given bit resistor……………………………………………………………............... 21

Figure 1.7 Equivalent circuit of an array for the reset operation of a given bit resistor……………………………………………………………………. 22

Figure 1.8 Perovskite structure. The red spheres are oxygen atoms, the deep blue are smaller metal cations and the green/blue are the larger metal cations……………………………………………………………………. 22

Chapter 2

Figure 2.1 The illustration of the experiment flow…………………………………… 30

Figure 2.2 The cross section view of conventional BTO structure…………………… 31

Figure 2.3 The cross section view of modified BTO structure………………………….. 31

Figure 2.4 The illustration of the sample preparation flow……………………………. 32

Figure 2.5 The illustration of the BTO thin film fabricated by sol-gel method………… 33

Chapter 3

Figure 3.1	The forming curve and first cycle of pure BTO thin film without PDA……..	48
Figure 3.2	Endurance of pure BTO thin film without PDA……………………………....	48
Figure 3.3	Electrical properties of 10nm Cr embedded BTO thin film without PDA…..	49
Figure 3.4	Electrical properties of 10nm Cr embedded BTO thin film with PDA 500°C.	49
Figure 3.5	Electrical properties of 10nm Cr embedded BTO thin film with PDA 600°C.	50
Figure 3.6	Electrical properties of 10nm Cr embedded BTO thin film with PDA 700°C.	50
Figure 3.7	Electrical properties of 5nm Cr embedded BTO thin film without PDA……	51
Figure 3.8	Electrical properties of 5nm Cr embedded BTO thin film with 500°C PDA...	51
Figure 3.9	Electrical properties of 5nm Cr embedded BTO thin film with 600°C PDA...	52
Figure 3.10	Electrical properties of 5nm Cr embedded BTO thin film with 700°C PDA...	52
Figure 3.11	Forming process of various Cr thicknesses in the embedded BTO thin film…	53
Figure 3.12	Resistive switching I-V curves of various Cr thicknesses in the embedded BTO thin film……………………………………………………………………	53
Figure 3.13	XRD pattern of LNO/Pt and LNO/SiO_2 bottom electrode…………………....	54
Figure 3.14	XRD pattern of embedded Cr BTO thin film with different thermal treatment…………………………………………………………………………	54
Figure 3.15	Top view SEM images of embedded Cr BTO thin film without PDA……….	55
Figure 3.16	Top view SEM images of embedded Cr BTO thin film with PDA 500°C……	55
Figure 3.17	Top view SEM images of embedded Cr BTO thin film with PDA 600°C……	56
Figure 3.18	Top view SEM images of embedded Cr BTO thin film with PDA 700°C……	56
Figure 3.19	2D and 3D AFM image of the embedded Cr BTO thin film without PDA…..	57
Figure 3.20	2D and 3D AFM image of the embedded Cr BTO thin film with PDA 500°C.	58
Figure 3.21	2D and 3D AFM image of the embedded Cr BTO thin film with PDA 600°C.	59
Figure 3.22	2D and 3D AFM image of the embedded Cr BTO thin film with PDA 700°C.	60
Figure 3.23	TEM image of the embedded Cr BTO thin film without PDA………………	61
Figure 3.24	TEM image of the embedded Cr BTO thin film with PDA 600°C…………..	61

Figure 3.25 SIMS for proving the La diffusion of bottom electrode LNO 62

Figure 3.26 The statistics for forming voltage of different annealing temperatures……… 62

Figure 3.27 Forming I-V curves of different annealing temperatures…………………….. 63

Figure 3.28 Switching I-V curves of different annealing temperatures…………………... 63

Figure 3.29 Statistics of operation voltage with different annealing temperatures………. 64

Figure 3.30 The statistics of ON and OFF state resistance with different annealing temperatures……………………………………………………………….. 64

Figure 3.31 Accumulative plots for turn-on and turn-off voltage……………………… 65

Figure 3.32 Switching cycles of embedded 2nm-Cr device without PDA……………….. 65

Figure 3.33 Switching cycles of embedded 2nm-Cr device with PDA 500°C…………… 66

Figure 3.34 Switching cycles of embedded 2nm-Cr device with PDA 600°C……………. 66

Figure 3.35 Switching cycles of embedded 2nm-Cr device with PDA 700°C……………. 67

Figure 3.36 Write/Erase cycles test for ON-State and OFF-state of sample without PDA.. 67

Figure 3.37 Write/Erase cycles test for ON-State and OFF-state of sample with PDA 500°C………………………………………………………………………. 68

Figure 3.38 Write/Erase cycles test for ON-State and OFF-state of sample with PDA 600°C………………………………………………………………………. 68

Figure 3.39 Write/Erase cycles test for ON-State and OFF-state of sample with PDA 700°C………………………………………………………………………. 69

Figure 3.40 Endurance comparisons of different devices………………………………… 69

Figure 3.41 Retention test at room temperature of embedded 2nm-Cr with PDA 600°C device………………………………………………………………………. 70

Figure 3.42 Retention test at 85°C of embedded 2nm-Cr with PDA 600°C device………. 70

Figure 3.43 Voltage stress at room temperature of embedded 2nm-Cr with PDA 600°C device………………………………………………………………………. 71

Figure 3.44 Voltage stress at 85°C of embedded 2nm-Cr with PDA 600°C device………. 71

Figure 3.45 Curve fitting at positive bias region for embedded 2nm-Cr device without PDA……………………………………………………………………….... 72

Figure 3.46 Curve fitting at negative bias region for embedded 2nm-Cr device without PDA……………………………………………………………………….... 72

Figure 3.47 Curve fitting at positive bias region for embedded 2nm-Cr device with PDA 600°C…… 73

Figure 3.48 Curve fitting at negative bias region for embedded 2nm-Cr device with PDA 600°C…… 73

Figure 3.49 ON-State conductivity of measurement at various temperatures…… 74

Figure 3.50 OFF-State conductivity of measurement at various temperatures…… 74

Figure 3.51 The activation energy of ON and OFF states…… 75

Figure 3.52 Electrical property of embedded 2nm-Pt device without PDA…… 75

Figure 3.53 Electrical property of embedded 2nm-Pt device with PDA 500°C…… 76

Figure 3.54 Electrical property of embedded 2nm-Pt device with PDA 600°C…… 76

Figure 3.55 Electrical property of embedded 2nm-Pt device with PDA 700°C…… 77

Figure 3.56 Statistics for resistance of ON-State and OFF-State at various temperatures... 77

Figure 3.57 Curve fitting at positive bias region for embedded 2nm-Pt device without PDA…… 78

Figure 3.58 Curve fitting at negative bias region for embedded 2nm-Pt device without PDA…… 78

Figure 3.59 Curve fitting at positive bias region for embedded 2nm-Pt device with PDA 600°C…… 79

Figure 3.60 Curve fitting at negative bias region for embedded 2nm-Cr device with PDA 600°C…… 79

Figure 3.61 ON-State conductivity of measurement at various temperatures for embedded 2nm-Pt device with PDA 600°C…… 80

Figure 3.62 OFF-State conductivity of measurement at various temperatures for embedded 2nm-Pt device with PDA 600°C…… 80

Figure 3.63 SIMS for proving the Pt diffusion in BTO thin film…… 81

Figure 3.64 Illustrations of conduction mechanism in embedded 2nm-Pt devices… 81

Figure 3.65 Comparison in device yield…… 82

Chapter 1

Introduction

1.1 Memories Classification

In this chapter, many kinds of memories are introduced generally. Basically, memories can be divided into two opposing categories: volatile and nonvolatile memory. In each category, there will be several kinds of memories. In this thesis, however, I would like to focus on the nonvolatile memory (NVM) and give a roughly introduction about each kind of NVMs.

1.2 Conventional Nonvolatile Memory

In 1967, D. Kahng and S. M. Sze proposed the first floating gate nonvolatile memory [1]. In recent year, NVM has been widely used in the portable devices, such as flash memory device, cell phone, digital camera, mp3 players, and personal digital assistant. Nonvolatile memory is typically used for the task of secondary storage, or long term persistent storage. The most widely used form of primary storage today is a volatile form of random access memory (RAM), meaning that when the computer is shut down, anything contained in RAM is lost. Unfortunately, most forms of nonvolatile memory have limitations that make them unsuitable for use as primary storage. Typically, nonvolatile memory either costs more or performs worse than volatile random access memory. Nonvolatile data storage can be categorized in electrically addressed systems random access memory and mechanically addressed systems hard disks, optical disc and magnetic tape. Electrically addressed systems are expensive, but fast, whereas mechanically addressed systems have a low price per bit, but are slow. Nonvolatile memory may one day eliminate the need for comparatively

slow forms of secondary storage systems, like hard disks.

Following the popularity of mobile equipments, nonvolatile memory plays an important role in the electronic industries. The nonvolatile memory should keep the stored information without power supply for a long time. [2-3]

1.2.1 Read Only Memory

The very first ROMs are hardwired devices that contain a preprogrammed set of data or instructions. The contents of the ROM have to be specified before chip production, so the actual data can be used to arrange the transistors inside the chip. Hardwired memories are still used, though they are now called masked ROMs to distinguish them from other types of ROM. The primary advantage of a masked ROM is its low production cost. Unfortunately, the cost is low only when large quantities of the same ROM are required.

1.2.2 Programmable Read Only Memory

One step up from the masked ROM is the PROM, which is purchased in an undetermined state. If you look at the contents of an undetermined PROM, you would see that the data is made up entirely of 1's. The process of writing your data to the PROM involves a special piece of equipment called a device programmer. The device programmer writes data to the device one word at a time by applying an electrical charge to the input pins of the chip. Once a PROM has been programmed in this way, its contents can never be changed. If the code or data stored in the PROM must be changed, the current device must be discarded. As a result, PROMs are also known as one-time programmable devices.

1.2.3 Mask-Programmed Read Only Memory

One of the earliest forms of nonvolatile read only memory, the mask-programmed read only memory was rewired at the design stage to contain specific data. Once the mask was used to manufacture the integrated circuits, the data was cast in stone and could not be changed. Whatever 1s and 0s were in memory, it left the factory there for life. The mask read only memory was therefore useful only for large-volume production, such as for read only memories containing the startup code in early microcomputers.

1.2.4 Erasable and Programmable Read Only Memory

An EPROM is programmed in exactly the same manner as a PROM. However, EPROMs can be erased and reprogrammed repeatedly. To erase an EPROM, you simply expose the device to a strong source of ultraviolet light. (A window in the top of the device allows the light to reach the silicon.) By doing this, it is practically to reset the entire chip to its initial-undetermined-state. Though more expensive than PROMs, their ability to be reprogrammed makes EPROMs an essential part of the software development and testing process.

1.2.5 Ultraviolet-Erase EPROM

The original erasable nonvolatile memories were EPROM's; these could be readily identified by the distinctive quartz window in the centre of the chip package. These operated bt trapping an electrical charge on the gate of a filed effect transistor in order to change a 1 to 0 in memory. To remove the charge, one would place the chip under an intense short wavelength fluorescent ultraviolet lamp for 20-30 minutes, returning the entire chip to its original blank state.

1.2.6 One-Time Programmable (OTP) Read Only Memory

An OTP is electrically an EPROM, but with the quartz window physically missing. Like the fuse PROM it can be written once, but cannot be erased. It has largely replaced PROM chips in electronic production as an EPROM with no window is inexpensive to manufacture and can e programmed using identical equipment to that used to write to the UV-window EPROM.

1.2.7 Electrically Erasable and Programmable Read Only Memory

EEPROMs are electrically-erasable-and-programmable. Internally, they are similar to EPROMs, but the erase operation is accomplished electrically, rather than by exposure to ultraviolet light. Any byte within an EEPROM may be erased and rewritten. Once EEPROM is written the new data, the new data will remain in the device forever or at least until it is electrically erased. The primary tradeoff for this improved functionality is higher cost, though write cycles are also significantly longer than writes to a RAM. So EEPROM is used for main system memory.

1.2.8 Flash Memory

Flash memory [4-6] is non-volatile computer memory that can be electrically erased and reprogrammed. It is a technology that is primarily used in memory cards and USB flash drives for general storage and transfer of data between computers and other digital products. It is a specific type of EEPROM (Electrically Erasable Programmable Read-Only Memory) that is erased and programmed in large blocks; in early flash the entire chip had to be erased at once. Flash memory costs far less than byte-programmable EEPROM and therefore has become the dominant technology wherever a significant amount of non-volatile, solid-state storage is needed. Example applications include PDAs (personal digital assistants), laptop computers, digital

audio players, digital cameras and mobile phones. It has also gained popularity in the game console market, where it is often used instead of EEPROMs or battery-powered SRAM for game save data.

Flash memory is non-volatile, which means that no power is needed to maintain the information stored in the chip. In addition, flash memory offers fast read access times (although not as fast as volatile DRAM memory used for main memory in PCs) and better kinetic shock resistance than hard disks. These characteristics explain the popularity of flash memory in portable devices. Another feature of flash memory is that when packaged in a "memory card," it is enormously durable, being able to withstand intense pressure, extremes of temperature, and even immersion in water. However, flash memory has some drawbacks including low operation speed, high operation voltage and low endurance. Furthermore, following the device scaling, the tunneling oxide will be shrunken, which leads to larger keakage current.

In addition, flash memory offers fast read access times (although not as fast as volatile DRAM memory used for main memory in PCs) and better kinetic shock resistance than hard disks. These characteristics explain the popularity of flash memory in portable devices. Another feature of flash memory is that when packaged in a "memory card," it is enormously durable, being able to withstand intense pressure, extremes of temperature, and even immersion in water.

Although technically a type of EEPROM, the term "EEPROM" is generally used to refer specifically to non-flash EEPROM which is erasable in small blocks, typically bytes. Because erase cycles are slow, the large block sizes used in flash memory erasing give it a significant speed advantage over old-style EEPROM when writing large amounts of data.

1.3 Promising Next-Generation Nonvolatile Memory

1.3.1 Ovonic Unified Memory (OUM)

OUM uses the unique behavior of chalcogenide glass, which can be switched between two states, polycrystalline and amorphous, with the application of heat.

PCM cell can be constructed in a number of different ways, but there are two notable methods. In one method, diodes are used as selection elements instead of transistors. This cuts down on cost, since a diode is smaller and cheaper than a transistor. Taking this one degree further, Macronix pioneered cross-point PCM, which is composed simply of a self-aligned chalcogenide cell sandwiched between the address lines (that is, with no transistor or diode selection element). In this manner, the chalcogenide itself serves as the rectifying element so the low-resistance crystalline state is never used. Instead, the cell is manipulated between distinct amorphic states. This type of cell is very low cost since it only requires two masking steps.

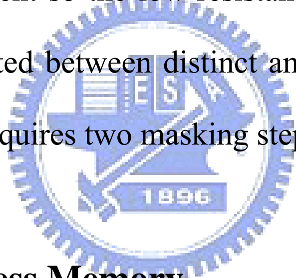

1.3.2 Magnetic Random Access Memory

Magnetic random access memory (MRAM) [7-8] is a nonvolatile computer memory technology, which has been in development since the 1990s. Continued increases in density of existing memory technologies cause flash memory and DRAM to face the problems of worse performances. MRAM is, however, in a niche role in this market, and its proponents are believed that the advantages are so overwhelming that MRAM will eventually become mainstream memory.

Unlike conventional RAM chip technologies, the data in MRAM are not stored as electric charge, but by magnetic dipole polarization, in a structure of so-called magnetic tunnel junction (MTJ). The material of MTJ stack includes two magnetic layers separated by a thin dielectric barrier and a mechanism to pin the polarization of

one of the magnetic layers in a fixed direction, as shown in Figure 1.1.[9]. The polarization direction of the free magnetic layer is used for information storage. The resistance of the memory bit is either low or high, depending on the relative polarization (parallel or antiparallel) of the free layer with respect to the pinned layer. An applied field can switch the free layer between the two states. A memory device is built from a grid of such "cells". In an MRAM array, is shown in Figure 1.2 [9], orthogonal lines pass under and over the bit, carrying current that produces the switching field. The bit is designed so that it will not switch when current is applied to just one line, but will always switch when current is flowing through both lines that cross at the selected bit.

Reading is accomplished by measuring the electrical resistance of the cell. A particular cell is (typically) selected by powering an associated transistor, which switches current from a supply line through the cell to ground. Due to the magnetic tunnel effect [10], the electrical resistance of the cell changes due to the orientation of the fields in the two plates. If the two plates have the same polarity this is considered to mean "0", while if the two plates are of opposite polarity the resistance will be higher and this means "1".

Data written to the memory cells can be used a variety of methods. In the simplest way, a pair of write lines, above and below the cell, arranged at right angles to each other. When current is passed through the cell, an induced magnetic field [11] is created at the junction, which the writable plate picks up. This pattern of operation is similar to core memory, a system commonly used in the 1960s. This approach requires a fairly substantial current to generate the field, however, which makes it less interesting for low-power uses, one of primary disadvantages of MRAM. Additionally, as the device is scaled down in size, there comes a time when the induced field overlaps adjacent cells over a small area, leading to potential false writes. This

problem, the half-select (or write disturb) problem, appears to set a fairly large size for this type of cell. One experimental solution to this problem was to use circular domains written and read using the giant magnetoresistive effect [12-15], but it appears this line of research is no longer active.

Another approach, the toggle mode, uses a multi-step write with a modified multi-layer cell. The cell is modified to contain an "artificial antiferromagnet" where the magnetic orientation alternates back and forth across the surface, with both the pinned and free layers consisting of multi-layer stacks isolated by a thin "coupling layer". The resulting layers have only two stable states, which can be toggled from one to the other by timing the write current in the two lines so one is slightly delayed, thereby "rotating" the field. Any voltage, less than that of the full write level, actually increases its resistance to flipping. That means that other cells located along one of the write lines will not suffer from the half-select problem, allowing for smaller cell sizes.

1.3.3 Ferroelectric Random Access Memory

Ferroelectric random access memory (FRAM) is a type of nonvolatile computer memory. It is similar in construction to dynamic random access memory (DRAM), which is currently used in the majority of a computer's main memory, but uses a ferroelectric layer to achieve nonvolatility. Although the market for nonvolatile memory is currently dominated by flash memory, FRAM offers a number of advantages, notably lower power usage, faster write speed and a much greater maximum number (exceeding 10^{16} for 3.3 V devices) of write-erase cycles.

The 1T-1C storage cell design in an FRAM is similar in construction to the storage cell in widely used DRAM in that both cell types include one capacitor and one access transistor. In a DRAM cell capacitor, a linear dielectric is used, whereas in

an FRAM cell capacitor, the dielectric structure includes ferroelectric material, typically lead zirconate titanate [16-17] (PZT).

As shown in the Figure 1.3[18], a ferroelectric material has a nonlinear relationship between the applied electric field and the apparent stored charge. Specifically, the ferroelectric characteristic has the form of a hysteresis loop, which is very similar in shape to the hysteresis loop of ferromagnetic materials. The dielectric constant of a ferroelectric is typically much higher than that of a linear dielectric because of the effects of semi-permanent electric dipoles formed in the crystal structure of the ferroelectric material. When an external electric field is applied across a dielectric, the dipoles tend to align themselves with the field direction, produced by small shifts in the positions of atoms and shifts in the distributions of electronic charge in the crystal structure. After the external electric field is removed, the dipoles retain their polarization state. Typically binary "0"s and "1"s are stored as one of two possible electric polarizations in each data storage cell. For example, in the figure a "1" is encoded using the negative remnant polarization "-Pr", and a "0" is encoded using the positive remnant polarization "+Pr".

Operationally, FRAM is similar to DRAM. Writing is accomplished by applying a field across the ferroelectric layer by charging the plates on either side of it, forcing the atoms inside into the "up" or "down" orientation (depending on the polarity of the charge), thereby storing a "1" or "0". Reading, however, is somewhat different than in DRAM. The transistor forces the cell into a particular state, say "0". If the cell already held a "0", nothing will happen in the output lines. If the cell held a "1", the re-orientation of the atoms in the film will cause a brief pulse of current in the output as they push electrons out of the metal on the "down" side. The presence of this pulse means the cell held a "1". Since this process overwrites the cell, reading FRAM is a destructive process, and requires the cell to be re-written if it was changed.

1.3.4 Resistance Random Access Memory

Resistance random access memory (RRAM) has great potential for the purpose to replace flash memory. The more details about RRAM will be mentioned in the next section.

1.4 Resistance Random Access Memory

It was intensively studied from the 1960s to early 1980s for device applications. RRAM has many attracting points enabling it to be easily combined with these density multiplying technologies. For examples, its simple cell structure, CMOS-friendly materials and low process temperature make it easy to add up another memory layer on top of the other ones. Even multi-level programming might be possible by controlling the set compliance current. Also, $4F^2$ 1D1R cross-point array structure can be realized sue to its unipolarly programmable device properties. By combining multi-layer and 1D1R cross-point structure, memory density can enormously increase in the way already demonstrated in the multi-layer anti-fuse one time programmable ROM.

1.4.1 Metal-Insulator-Metal Structure

Research the physical mechanisms and electrical properties of RRAM always use the simple Metal-Insulator-Metal (MIM) structure which is not a complete memory device.

M= top electrode

I= dielectric layer (the materials have resistive switching characteristics)

M= bottom electrode.

1.4.2 Operation Method

Different from conventional 1T1C memory structure, RRAM is composed of one transistor and one resistor. In order to increase packaging density, the transistor is fabricated in the front-end-process while the resistor is formed in the back-end-process, as shown in Figure 1.4[19]. The resistor is formed in metal/insulator/metal (MIM) stacked structure and also can be fabricated in the metal/insulator/metal/insulator/metal stacked array structure to increase density, as shown in Figure 1.5[20]. The RRAM cell has smaller size than that of others memory. Figure 1.6 and Figure 1.7[21] indicate the operation method of write and erase for RRAM. When a dc voltage is applied on the word line to turn on the bit transistor and a voltage pulse is applied to the bit line while the source of the bit transistor is grounded, vice versa. For the reading operation, the memory cell is selected by the word line and a reading pulse is applied to bit line to sense the leakage current while the source of the bit transistor is grounded. After that, the leakage current is compared to the reference value and the stored information is determined. RRAM has the non-destructive readout property and the memory state would not be destroyed by the read operation.

1.4.3 Introduction to Perovskite materials

The materials for RRAM can be divided into five categories, including silicon, perovskite materials, $PrCaMnO_3$ (PCMO), polymer and binary metal oxides. In this thesis, the focused point would be on the perovskite materials.

The perovskite structure with the chemical formula ABO_3 is shown in Figure 1.8[18]. The structure is very versatile and is useful in technological applications such as ferroelectrics, catalysts, sensors, and superconductors. The general crystal structure is a primitive cube, with the A-cation in the middle of the cube, the B-cation in the

corner and the anion, commonly oxygen, in the centre of the face. The structure is stabilized by the 6 coordination of the B-cation (octahedron) and 12 of the A-cation. The packing of the ions can be thought of the A and O ions together forming a cubic close packed array, where the B ions occupy a quarter of the octahedral holes. Although the primitive cube is the idealized structure, differences in radius between the A and B cations can alter the structure to a number of different distortions of which tiling is the most common one. With perovskite tilt the BO_6 octahedron twists along one or more axes to accommodate the difference. Complex perovskite structures contain two different B-site cations. This results in ordered and disordered variants. The perovskite structure shares the property of ferroelectricity with garnet and olivine. Many superconducting ceramic materials have perovskite-like structures. In this thesis, the perovskite structure - $Bi_4Ti_3O_{12}$ is used for the switching oxide materials.

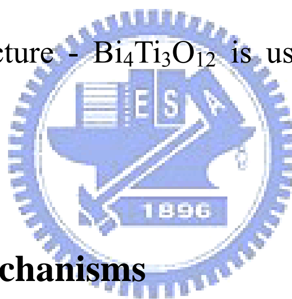

1.4.4 Resistive Switching Mechanisms

The basic carrier conduction mechanisms in insulating films are Schottky emission, Frenkel-Poole emission, tunneling or thermal emission, space-charge-limited current, ohmic conduction and ionic conduction. At present, in addition to the $SrZrO_3$ (SZO) [22], $SrTiO_3$ (STO) [23], and $PrCaMnO_3$ (PCMO) [24] perovskite, and many binary oxides [25] have been considered as the candidates for the RRAM device application. However, the microscopic mechanism of the resistive switching is not yet understood [26]. Although several theoretical models were proposed, they could not explain the whole experimental results of the RRAM materials. For the switching mechanisms of RRAM can be classified in detail: conduction paths, charger transfer, dipole rearrangement, phase transformation, formation of depletion, and energy gap states modulation.

I. Conduction Paths [27-35]

Combing scanning electron mircroscopy and electron and electron-beam-induced current imaging with transport measurements, it is shown that the current flowing is confined in areas localized at defects, proposed by Rossel et al. These local conduction regions are defined as the conduction paths are the also called conduction filaments. The conduction filaments are conduction channels formed in the dielectric layer to change the conductivity. The conduction filaments could be possibly composed of various kinds of point defects, such as oxygen vacancies, ionic and electronic defects. Initially, the device is in the origin-state. When applying a dc voltage or voltage pulse to the device, the electric field will line up the point defects inside the dielectric layer and form a low resistance channel for conducting electron. The first resistive switching is called as forming process. In the previous reports, Kinoshita *et al.* proposed that the forming process is equivalent to dielectric breakdown via performing time dependent dielectric breakdown test. Then, after forming process, the device becomes very high conductive, called on-state. When the voltage is applied to the on-state of the device, this channel will be broken and the conductivity will be switched back to low conductive state, called off-state. The voltage used to switch the device from off-state to on-state is defined as turn-on voltage, and the voltage used to switch back to off-state is defined as turn-off voltage. Moreover, the resistive switching mechanism is related to formation and rupture of the conduction paths.

II. Charge Transfer [36-38]

When defects and impurities in the insulator form energy states within energy gap, one can utilize various dopants to induce different acceptor and donor levels. The charge transfer processes via donor and acceptor levels create carriers and transport

within the insulator. After applying a voltage pulse to the device, the transitional element dopants inside the dielectric layer may change their valences. Therefore, the donor and acceptor levels are also changed. An opposite direction of pulse voltage source will help to restore the transitional element dopants to the original valence. Change transfer process via different donor or acceptor levels results in different resistance. Beck et al. proposed that the charge transfer processes via Cr^{3+} and Cr^{4+} in SZO films as studied by photocurrent and luminescence measurement appear to be a plausible mechanism for carrier creation and transport within the insulator.

III. Dipole Rearrangement [39]

The mechanism of resistive switching characteristics is mainly attributed to the materials have an inner permanent dipole moments. When a voltage pulse is applied to the device, the dipoles in a local range will be rearranged according to the electric field and form first resistance state. The disorder of the local dipole changes the resistance of the material and causes the second resistance state. In contract, applying an opposite direction voltage pulse will restore the arrangement of the dipoles and reverse the material to the first resistance state. This mechanism is usually proposed to be the origin of the conductivity change in ferroelectric and some organic materials.

IV. Phase Transformation [40]

The concept of this mechanism is that the crystallinity of the film was varied by adding electrical signal and one can know that polycrystalline film has lower resistivity than that of an amorphous one. The phase transformation mechanism is the resistive switching mechanism in OUM, utilizing the chalcogenide materials. When a voltage pulse is applied to the device, the current flows through the device will produce a thermal energy. Different gradients of temperature will lead to different

phases in the chalcogenide layer. The width of voltage pulse can be controlled to obtain the different resistance states.

V. Formation of Depletion Layer [41]

The depletion region is composed of a layer of unscreened dopant ions. Schottky barrier are formed at the interfaces between electrode and insulator. In some repots, the resistive switching devices using polymer materials as dielectric layers show that a capacitance change is achieved after applying a voltage pulse to the device. In the polymer, it is attributed that the dopants are not chemically bound to the polymer and may drift slowly under applying an electric field, resulting in the change of capacitance in the depletion layer. This phenomenon should be caused by a drift of some negatively charged ions to the interface between the top electrode and the polymer when a positive voltage is applied to the top electrode, and a reverse process will occur when a negative voltage is applied to the top electrode. The resistive switching is caused by field induced migration of some ions, leading to the capacitance change at the same time. Because of the depletion layer, there will be a displacement current which can be measured during a voltage sweep. This mechanism is mainly found in the polymer material.

1.5 Important Criteria for RRAM

I. Operation Voltage

The flash memory has the large operation voltage which is considered as a drawback for application. The large operation voltage causes the reliability issue and the chip would be required to design the circuit for ascending voltage. Therefore, the operation voltage less than 10V should be more appropriate for application.

II. Endurance

The endurance characteristics give the memory threshold voltage window, which is the difference between the threshold voltages in the programmed/written state and the erased states, as a function of the number of programming cycles. Nonvolatile memories can be programmed and erased frequently at the expense of introducing permanent tunneling oxide damage such as oxide breakdown and trap-up. This implies that the total number of program operations is limited. The damaging of the memory cell during cycling is normally referred to as "degradation" and the number of cycles the memory can withstand is called "endurance". For the nonvolatile memory with non-destructive readout such as flash memory, the endurance should be larger than 10^6. If the goal is to replace DRAM, the endurance should be larger than 10^{12}. So far the best reported endurance of RRAM is only about 10^6.

III. Operation Speed

So far the operation time of flash memory is just about 1ms. For the goal of replacing flash memory, the operation time of RRAM should be smaller than 1ms. If the goal is to replace the SRAM or DRAM, the operation time of RRAM should be about 10ns. Of course, the faster the operation speed is, the better the performance is.

Furthermore, the operation speed of the write and erase may be not the same.

IV. Resistance Ratio

The resistance ratio of application specification should be larger than 5 at least. Generally speaking, if the resistance ratio of the device is larger, the device performance is better. The higher resistance ratio will have larger sensing margin to read the stored information. If the resistance ratio is too small, the sensor amplifier can not distinguish the stored information correctly, leading to misreading. The resistance ratio would decay due to process damages, operation times, etc. In the stage of resistive film deposition, the resistance ratio should be larger than 100.

V. Retention

When a nonvolatile memory cell can no longer hold the charges in the floating gate, it is said to have affected its retention capability. Retention is a measure of the time that a nonvolatile memory cell can retain the charges whether it is powered or non-powered. In floating gate memories, the stored charges can leak away from the floating gate through the blocking oxide or through the tunneling oxide. This leakage caused by mobile ions and oxide defects, result in a shift of the threshold voltage of the memory cell. To improve the retention characteristics of the memory cell, various improvements to the quality of the blocking and tunneling oxides become very important. Retention can be quantified by measuring or estimating the time it takes for the floating gate to discharge when it is intended to keep the information stored. The specification of the retention is too strict for all the nonvolatile memory devices. So far, the reported retention time of RRAM is about several months. If the retention time is not up to 10 years, it could be compensated by external circuit design and is applied to specific applications.

VI. Readout Disturbance

A typical memory array undergoes stresses that arise during programming and erasing commonly referred to as disturbs. The four principal memory cell disturbs that can occur in an array are dc erase, dc program, program disturb, and read disturb. The two common disturbs that can impact memory cells during programming are dc program and program disturb. Memory cell disturbs can also occur during erasing and is called dc erase. Finally, during "read" operation when the memory is read to determine the state (logic 0 or 1), memory cell disturb can also occur and is called read disturb. If the readout is destructive, the information should be written again after reading operation. However, so far the reported RRAM are all non-destructive readout. The reading time is about 10 ns and the read voltage is usually smaller than 1V. The small read voltage and short reading time would still disturb the memory states. Therefore, the readout testing is required. The specification of readout disturbance for replacing DRAM should be larger than 10^{12}. So far the reported results are usually larger than 10^{12}. Therefore, the readout disturbance should not be an issue for RRAM.

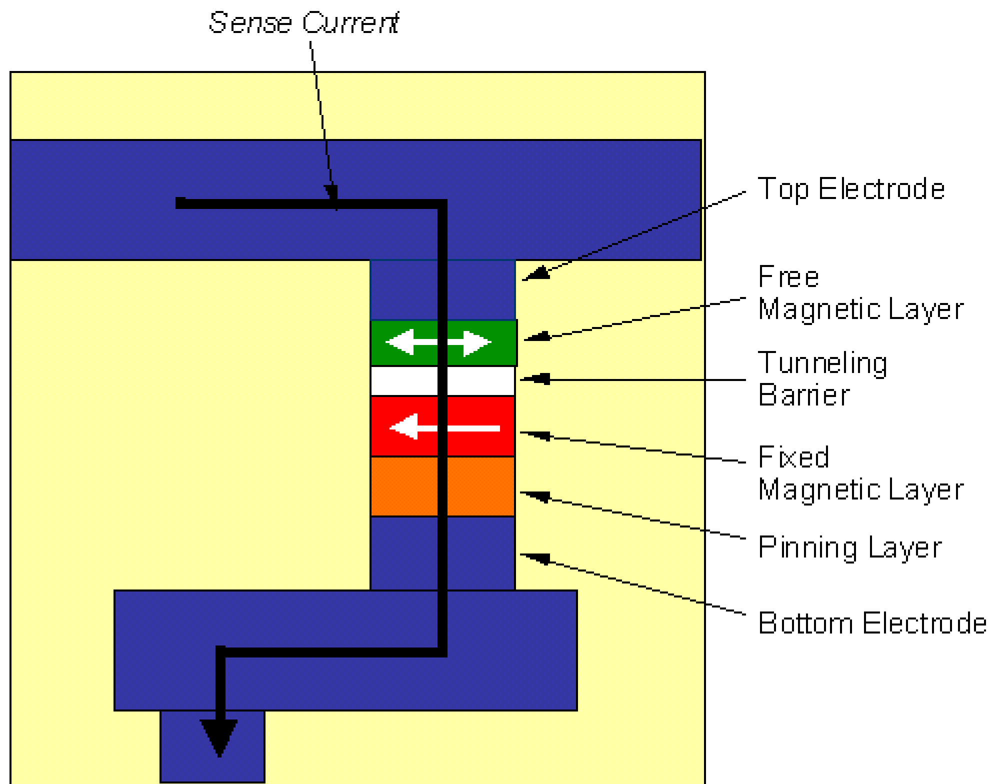

Figure 1.1 A schematic of an MTJ memory cell. Arrows indicate possible directions of magnetic movement [9]

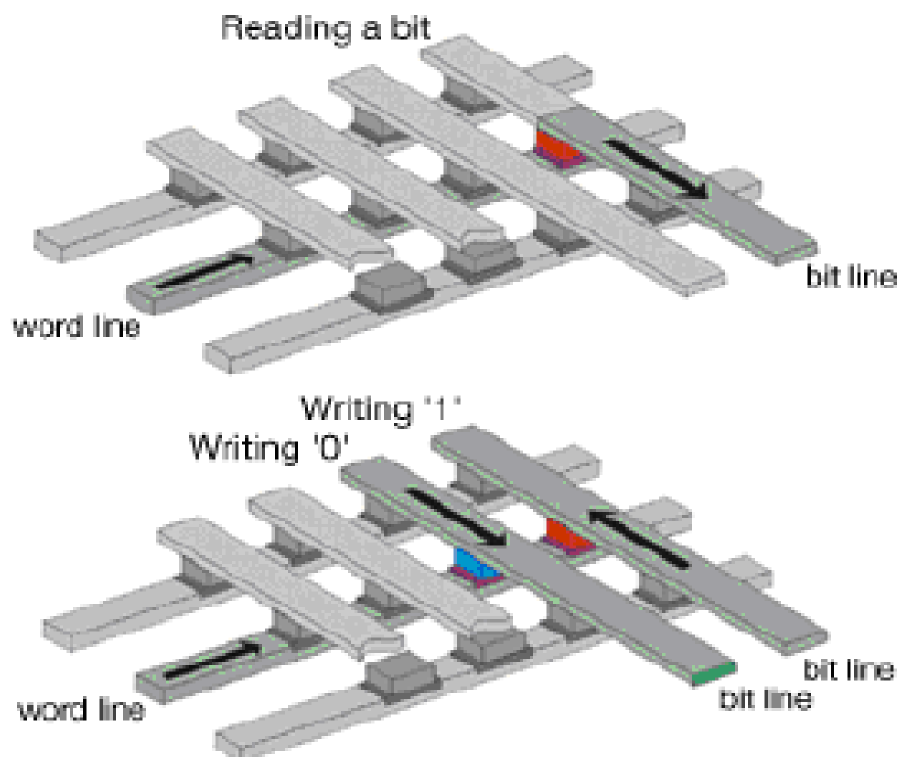

Figure 1.2 MRAM array [9]

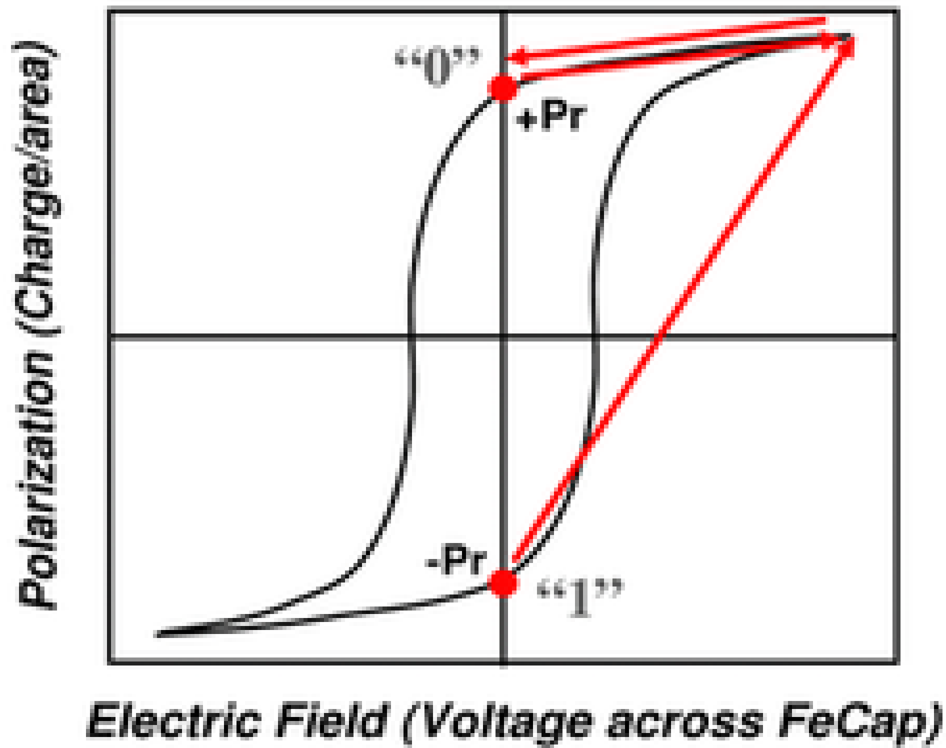

Figure 1.3 Hysteresis loop of FRAM cell capacitor [18]

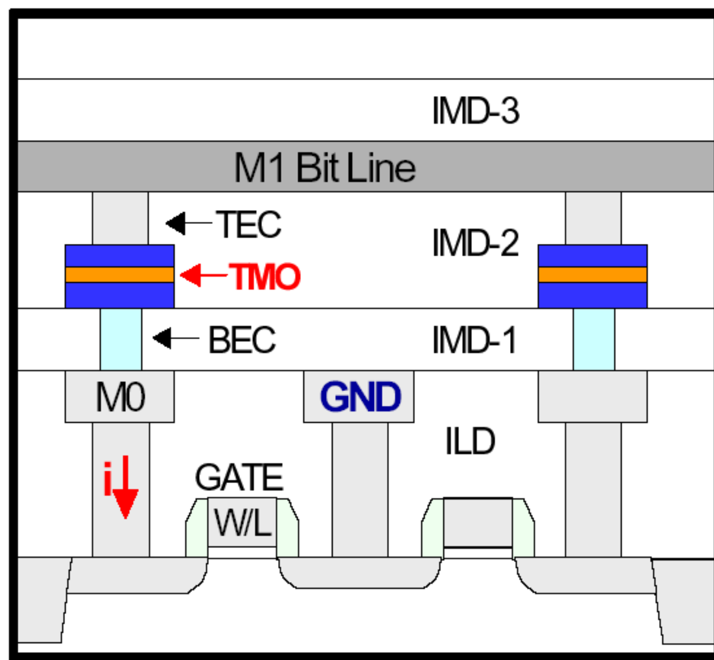

Figure 1.4 RRAM consists of a transistor and a resistor. The transistor is fabricated in the front end and the resistor in the back end [19].

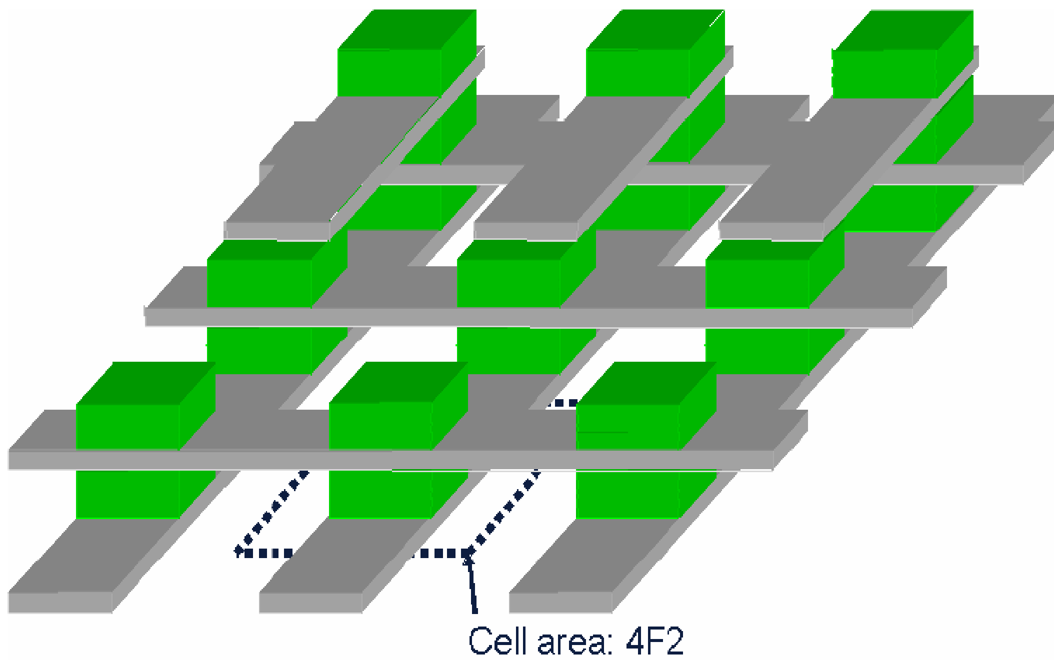

Figure 1.5 Schematic view of stacked memory layers. The cell sizes decrease from $4F^2$ to $4F^2/n$ for n layers [20].

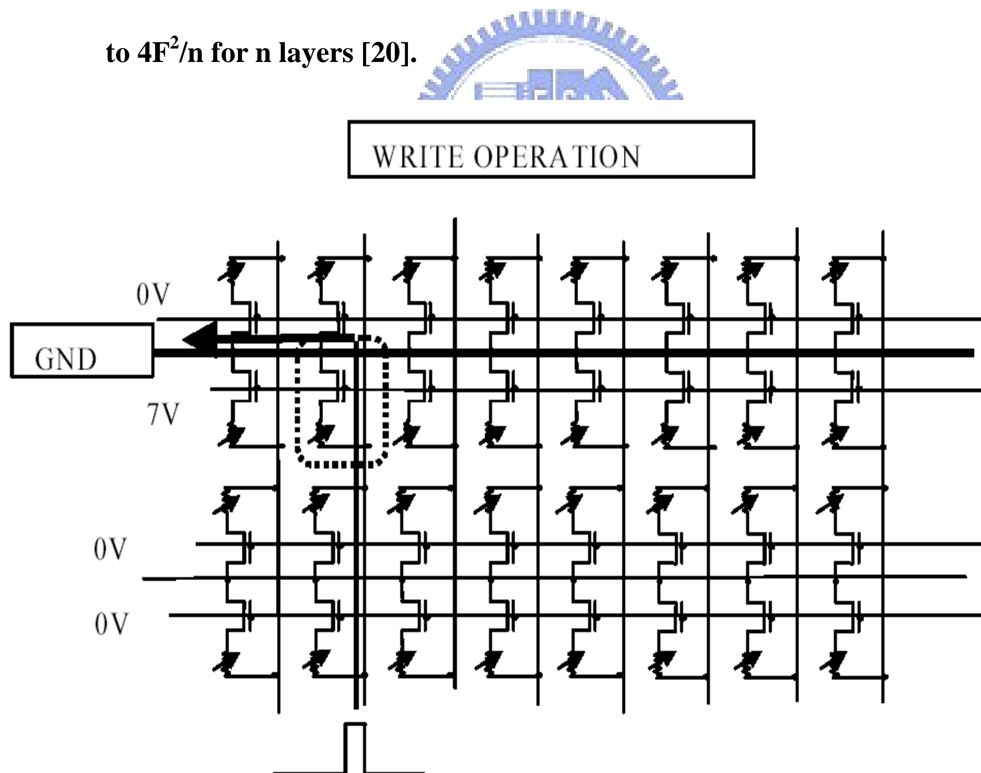

Figure 1.6 Equivalent circuit of an array for the write operation of a given bit resistor [21].

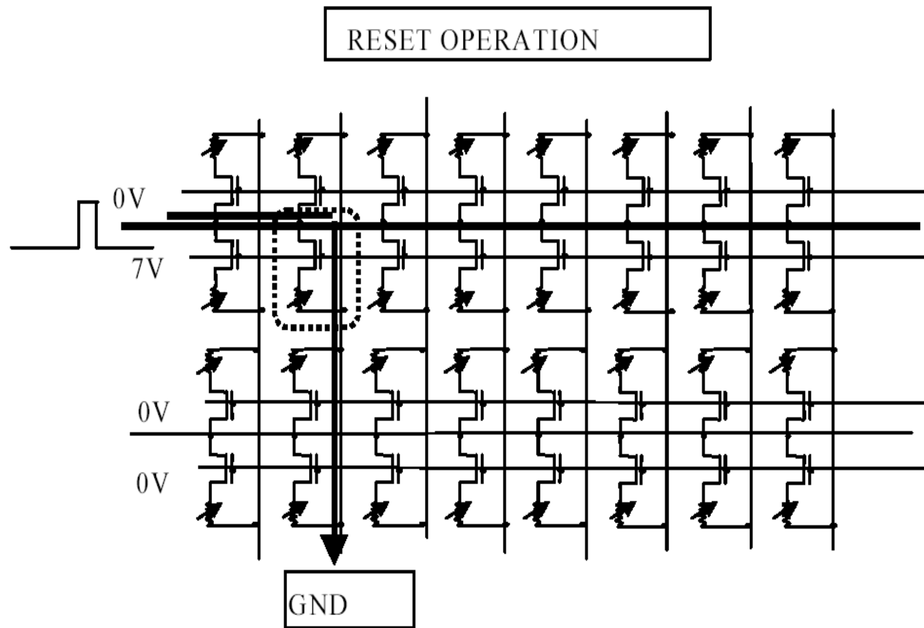

Figure 1.7 Equivalent circuit of an array for the reset operation of a given bit resistor [21].

E S A

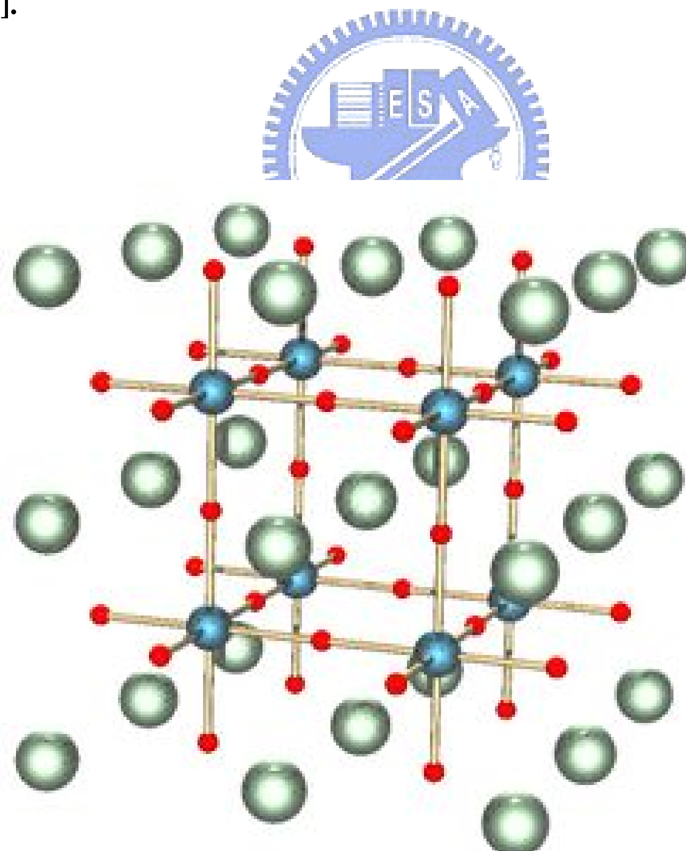

Figure 1.8 Perovskite structure. The red spheres are oxygen atoms, the deep blue are smaller metal cations and the green/blue are the larger metal cations.[18]

Chapter 2

Experiment Details

2.1 Experimental Process Flow

We focus on the resistive switching phenomenon of perovskite structure material BTi_3O_{12} (BTO). The experimental flow is shown in Figure 2.1. At first, the resistive properties are wished to be investigated in prepared samples. If not, the experimental parameters are going to be modified and investigate the switching characteristics again, until the suitable experiment parameters are obtained. After that, material analyses, electrical measurements and mechanisms discussion are all performed and demonstrated in the resistive films. The material analyses, such as SEM, TEM, XRD and SIMS, are used to investigate thickness, crystallization, grain size, inner components distribution, stoichiometry etc. Electrical measurements are the most important parts of the RRAM devices in the experiments. In this part, the distribution of operation voltages, resistance ratio, retention time, endurance test, and stress test are main characteristics which are important criteria of nonvolatile memories (NVMs), investigating the reliable and excellent electrical characteristics of BTO-based RRAM. Finally, because resistive switching mechanisms are unrevealed now, the various experimental conditions, such as various thicknesses, various rapid thermal annealing temperatures effects, and embedded metal species etc, are investigated to discuss the carrier conduction and resistive switching mechanisms. The experiment results are discussed and compared with those of other related research results. The instruments used here are also introduced in this section.

2.2 Sample Preparation

The $Bi_4Ti_3O_{12}$ (BTO) thin films with embedded metal are mainly investigated for resistive switching behaviors, and the memory devices are fabricated into a simple structure as shown in Figure 2.2 and Figure 2.3. One is conventional device, metal-insulator-metal structure with a buffer layer between insulator and bottom electrode. The top- and bottom-electrodes are both metallic materials, Pt used here and between them is the $Bi_4Ti_3O_{12}$ (BTO) insulator layer and $LaNiO_3$ (LNO) buffer. The other is the modified device by embedding a thin metal layer within BTO film, and the structure is Pt-BTO-metal-BTO-LNO-Pt. The metal layer was deposited by thermal and electron-beam evaporation. The embedded metal is utilized to diffuse into the BTO film causing the diffusion in the BTO. Taking advantage of this structure, the electrical measurements are performed by probes directly contacting with top- and bottom-electrodes.

There are several sample preparation steps, as showed in Figure 2.4. At first, the 4 inch boron-doped (100) silicon is used as device substrates, and the sample preparation procedure is depicted clearly in the following content.

2.2.1 RCA Cleaning of Silicon Substrate

4 inch boron-doped (100) silicon substrates were cleaned by standard RCA clean, which is the industry standard process to clean and remove contaminants from wafers.

2.2.2. Furnace Oxidation of Silicon Substrate

After RCA clean, the clean Si wafers were posited in the thermal furnace as soon as possible. In the furnace, those wafers were oxidized at $950^{O}C$ in O_2/H_2 atmosphere 30 minute, and the oxides were grown to the expected thickness of 200nm serving an

insulated layer in order to avoid current leakage from the substrate.

2.2.3. Deposition of Bottom Electrode

Ti metal layer, due to the great adhesion for SiO_2, was deposited on the SiO_2/Si substrates as an adhesion layer, and followed by Pt bottom-electrode deposited. Both Ti and Pt were deposited by a dual electron-beam evaporation system (EBX-10C) manufactured by ULVAC.

2.2.4. Deposition of $LaNiO_3$ Thin Films

The $LaNiO_3$ thin films were deposited by the rf magnetron sputtering system. Therefore, the various recipes of the deposition process were controlled by several parameters based on the plasma theorem and the models of the thin films growth. There were many parameters including the chamber pressure, the rf power, the working temperature, the ambient conditions, and the deposition time. The temperature and the ambient conditions could have influences on the defect density, the crystallization, the conductivity, the stoichiometry, and the dielectric constant of thin films. For the accuracy of the atmosphere, the base pressure about $3x10^{-6}$ before sputtering was necessary. To achieve the expected ambient conditions, the flow rate of Ar and O_2 was under the control of the MFC, and the working pressure was controlled by the valves to reach the low pressure where the plasma was generated.

2.2.5. Rapid Thermal Annealing Process of $LaNiO_3$ Thin Films

An as-deposited LNO thin film is performed with a post thermal treatment with rapid thermal annealing. The purpose of the post thermal treatment is to make LNO thin films crystallized with the orientation. In previous reports, the orientation of LNO has the great influences on the resistive switching properties, and better resistive

switching characteristics were obtained on the LNO with (100) orientation. In addition, LNO thin films, in this experiment, are performed with RTA at $600^{O}C$ in O_2 atmosphere for 60s, which have the (100) prefer-orientation. The RTA model is FE-004A made by JETFIRST. [42]

2.2.6. Deposition of $Bi_4Ti_3O_{12}$ Thin Films

Stoichiometric amounts of the starting materials including bismuth acetate $[Bi(OOCCH_3)_3]$ and titanium isopropoxide $Ti[OCH(CH_3)_2]_4$, were dissolved in acetic acid (CH_3COOH) and acetylacetone ($C_5H_8O_2$). The fabrication flow of the $Bi_4Ti_3O_{12}$ (BTO) thin film by sol-gel method is illustrated in Fig. 2.5. Acetic acid was adopted as solvent and heating at 80 ^{o}C for 10 min to evaporate the water. Then, the bismuth acetate was added into the acetic acid. The mixture was stirred at 80 ^{o}C for 30 min to dissolve the solute into the solvent. After that, the acetylacetone was added into the above solution and then titanium isopropoxide was also added. Then, the mixture was stirred at 80 ^{o}C for 1 h to react completely to form the final solution. The $Bi_4Ti_3O_{12}$ films were prepared by an acetate precursor sol-gel route on the LNO thin films as the resistive layer. The prepared 0.04 M precursor solution was spin-coated on the LNO/Pt/Ti/SiO_2/Si substrates to form the sol-gel film. The parameter of spin-coated is 1000rpm/3000rpm for 5s/60s. Then such deposited layer was heat-treated at 125 ^{o}C for 10 min to bake residual water and then annealed at 200 ^{o}C /400 ^{o}C for 10min/30 min. The coating and heating steps were repeated to obtain the desired film thickness.

2.2.7. Post Deposition Annealing Process of $Bi_4Ti_3O_{12}$ Thin Films

A post thermal treatment by using post deposition annealing is performed in as-deposited BTO thin films. The purpose of the post thermal treatment is to perform the crystallization of BTO thin films. In addition, the PDA atmosphere (oxygen or

nitrogen) and temperature (from 500℃ to 700℃) can be used to modify the characteristics of the memory devices. The PDA model is FE-004A made by JETFIRST.

2.2.8. Deposition of Top Electrode

The metal masks are utilized, while depositing top-electrodes to achieve various cell sizes easily. The diameters of the dot patterns on the metal mask are 350um, 250um, and 150um, and the electrode areas formed by those metal masks are around 9.62×10^{-4}, 4.91×10^{-4}, and $1.77\times10^{-4} cm^2$, respectively. The Pt top electrode is deposited by e-beam evaporation for top electrode.

2.3 Electrical Measurement and Material Analyses

After fabricating the complete devices, the electrical measurements and the material analyses are performed. Those electrical measurements can provide detailed information and the voltage is applied on Pt top electrode with the Pt bottom electrode grounded.

2.3.1 Current-Voltage (I-V) Measurement

The electrical measurement system consists of a probe station, an Agilent 4155C semiconductor parameter analyzer, an Agilent 8110A pulse generator, an Agilent E5250A low leakage switch, which are controlled by personal computer with the Agilent VEE software and GPIB controller.

The electrical measurement can be sorted into five items: bistable resistive switching measurement, retention test, stress test, endurance test, and other electrical phenomenon measurement. The initial four items are tested for criteria of memory

device and the last item is performed to understand the fundamental properties of the resistive switching memory devices. Moreover, the measurement of bistable resistive switching behaviors is characterized by applying a dc voltage sweeping forth and back between two specific values (in double sweeping mode in 4155C). By this method, the change of the conductivity state in the memory device can be demonstrated to confirm the memory effects induced by the mechanisms we expected.

2.3.2 X-Ray Diffraction (XRD)

Generally, thin films are classified according to the crystallization. There are three types of crystallization, such as amorphous, polycrystalline, and singlecrystalline. X-Ray diffraction analyses are used to investigate the crystal structure and the orientation of our sample. Furthermore, the relations between the crystallization and the heat treatment can be characterized from XRD results. In the experiment, the thin films show either amorphous or poly. Follow Scherrer's formula, we could calculate the average grain size from XRD illustration:

$$D = \frac{0.9 \times \lambda}{B \times \cos\theta}$$

The background information of our XRD analyses is that $\lambda = 1.5405\,\text{Å}$ (K_α), B is the full width at half maximum (FWHM) of the XRD peak and θ is the diffraction angle. In these analyses, X-ray is made with 0.02 degree beam divergence and operation configuration at 30KV, 20mA.

2.3.3 Atomic Force Microscopy (AFM)

The atomic force microscopy (AFM) is a very good tool to demonstrate the surface roughness and surface morphology. We use an AFM made by Digital Instruments whose model is Nano-scope III. The root mean square (RMS) value of

roughness of the film is automatically calculated by the AFM software.

2.3.4 Scanning Electron Microscopy (SEM)

Comprehensively, the surface morphology is also an important characteristics compared with those of bulk for the thin films. We could observe the surface micro-morphology and cross section image by SEM. The SEM model is S4700I with highest resolution of 15 Å made by Hitachi.

2.3.5 Transmission Electron Microscopy (TEM)

Electrons form an electron gun are accelerated to high voltages and focused on the samples by the condenser lenses. The samples are placed on a small copper grid a few millimeters in diameter. The static beam has a diameter of a few microns. The samples must be thin enough to be transparent. The transmitted and forward scattered electrons form a diffraction pattern in the back focus plane and a magnified image in the image plane. In order to study the inter-diffusion mechanics and determine the interface thickness, The Philips JEOL JEM9100 Transmission Electron Microscopy (TEM) was used to observe the interface. Furthermore, the TEM can be used to characterize the crystallized states of the films. The maximum magnification is 900000.

2.3.6 Secondary Ion Mass Spectrometer (SIMS)

It is an instrument for microscopic chemical analyses by using a beam of primary ions with energy in the range 5-20 kiloelectronvolts bombards a small spot on the surface of a sample, where the positive and negative secondary ions sputtered from the surface are analyzed in a mass spectrometer.

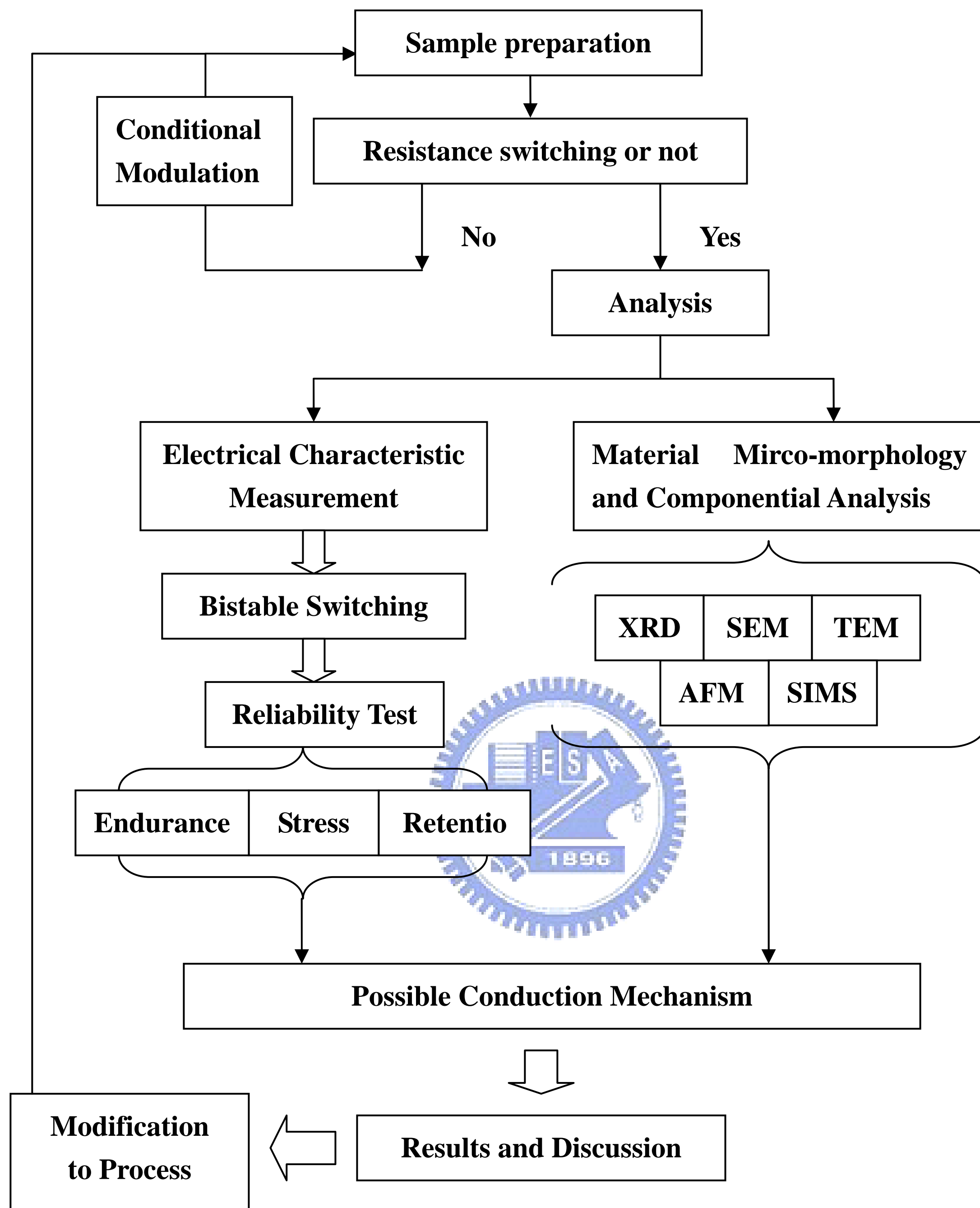

Figure 2.1 The illustration of the experiment flow

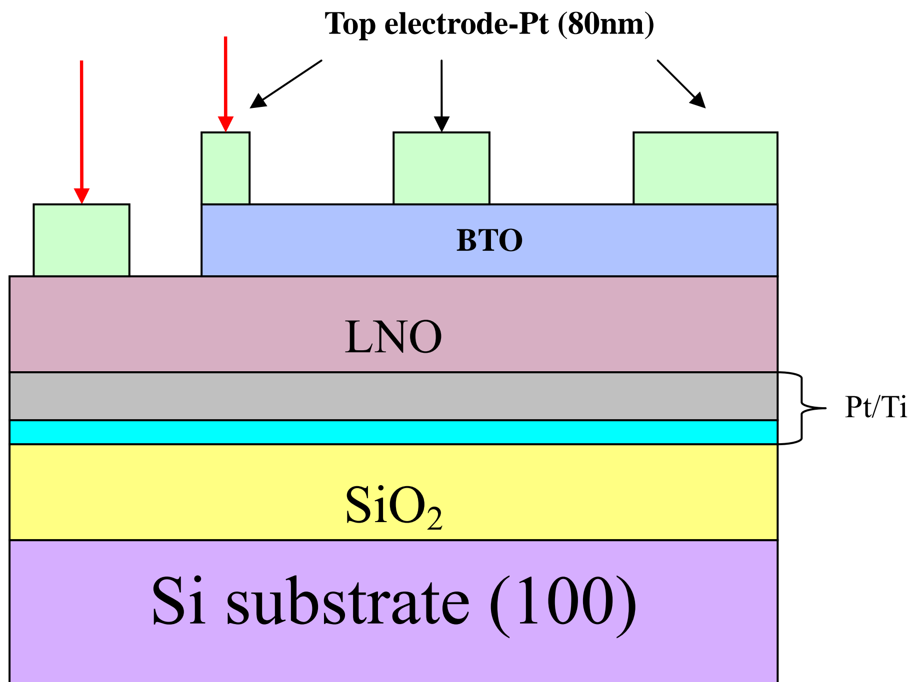

Figure 2.2 The cross section view of conventional BTO structure

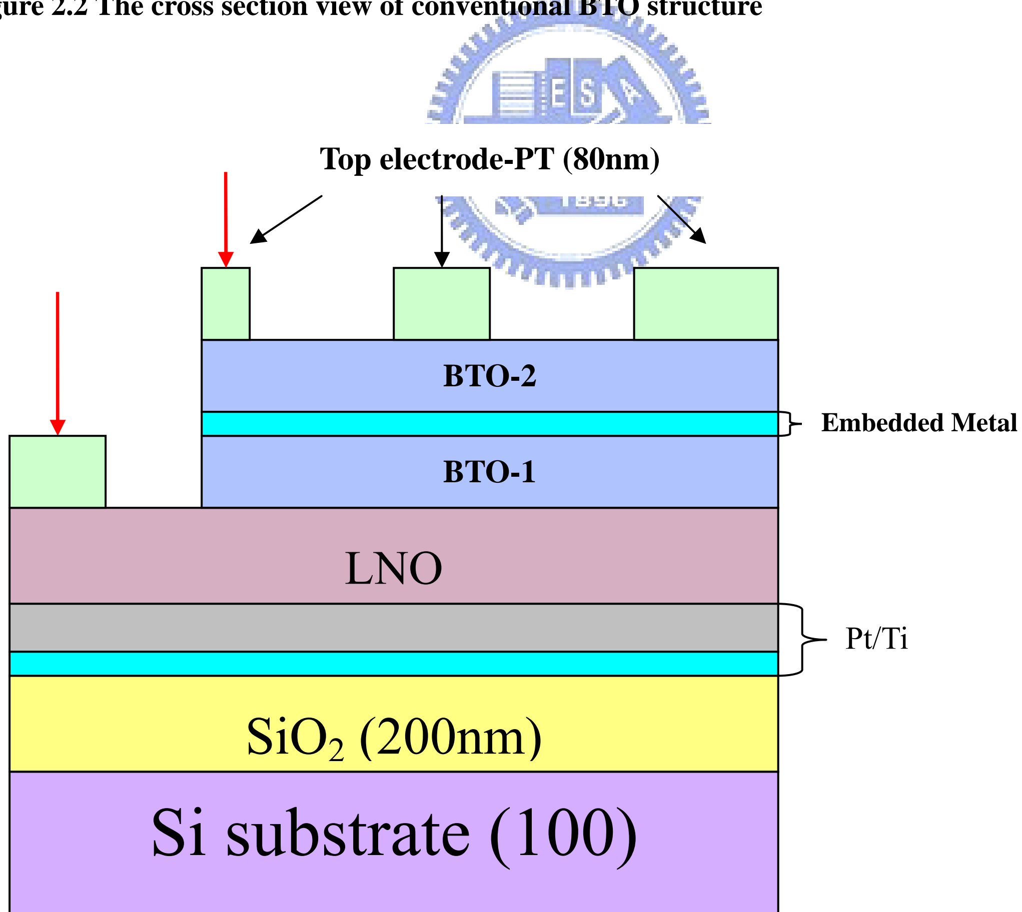

Figure 2.3 The cross section view of modified BTO structure

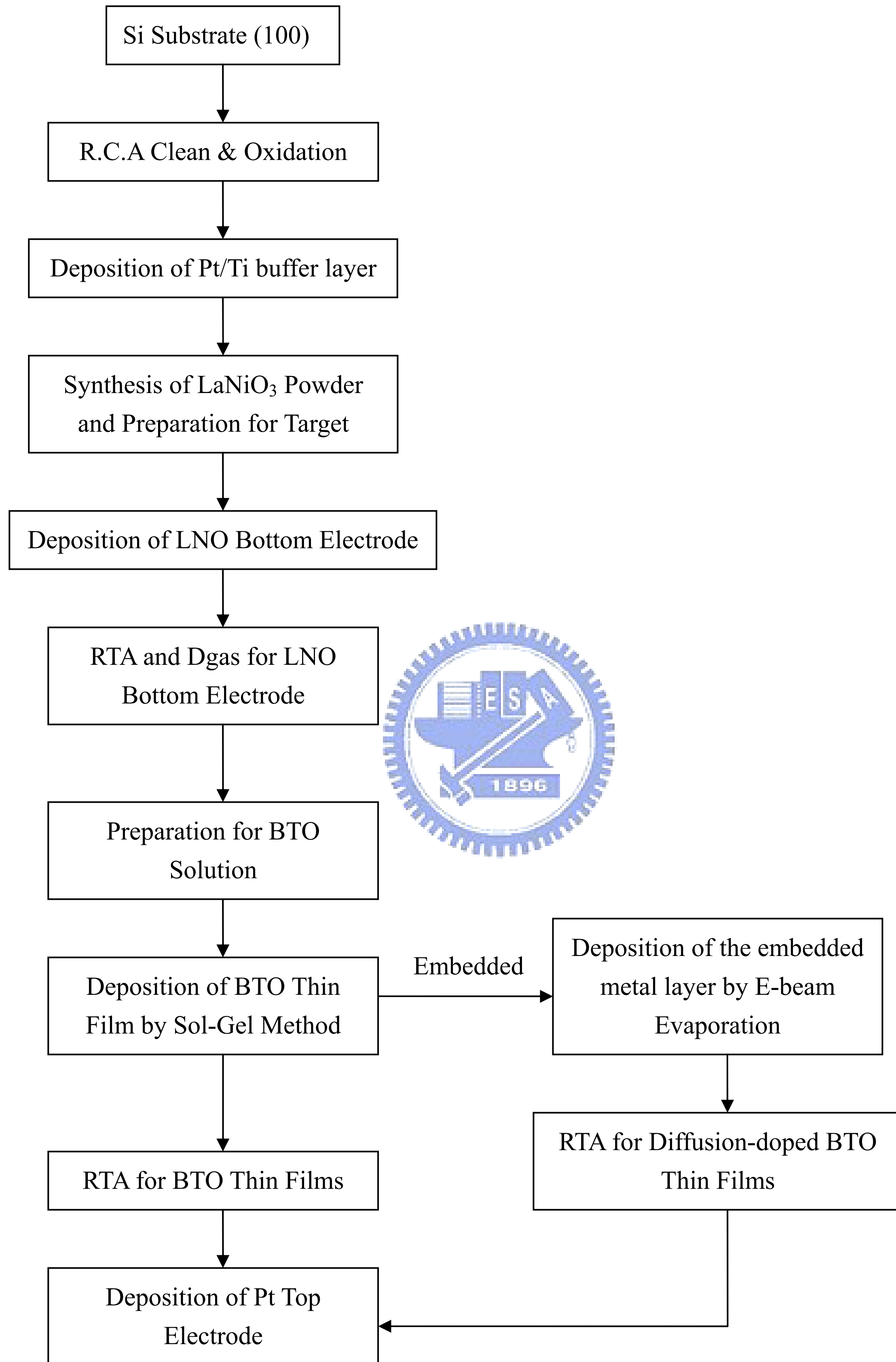

Fig. 2.4 The illustration of the sample preparation flow

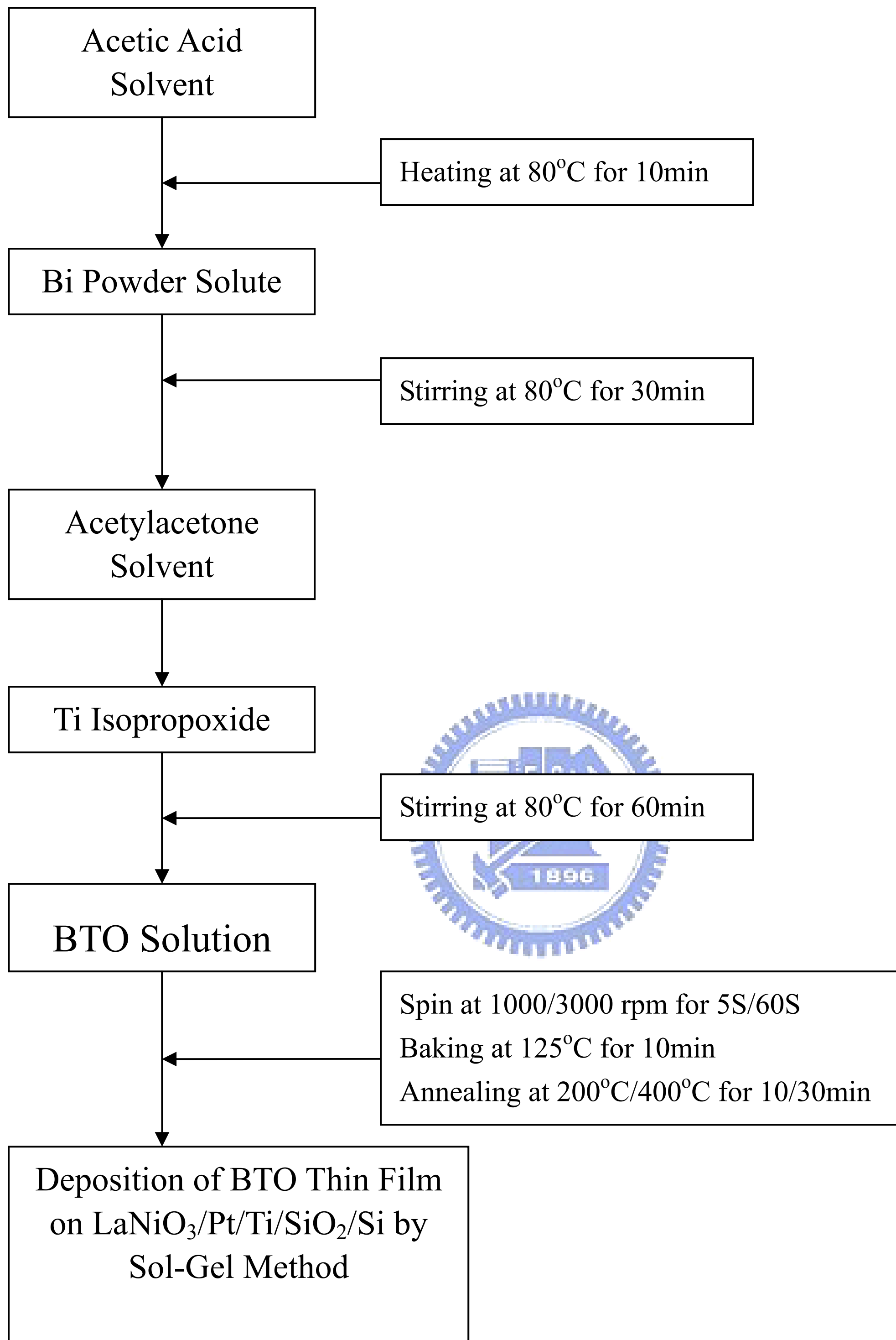

Figure 2.5 The illustration of the BTO thin film fabricated by sol-gel method flow.

Chapter 3

Experimental Results and Discussion

3.1 Pure BTO thin film

The criteria for a perfect nonvolatile memory device includes low operation voltage, low power consumption, long retention time, small cell size, high operation speed, low cost, high endurance, non-destructive readout, and simple structure. There are few reports about the memory effects and resistive switching behaviors in the BTO thin films for RRAM applications nowadays. However, recently, reproducible resistive switching in bismuth titanate (BTO) deposited by electron cyclotron resonance sputtering was successively reported. [XX] In the previous experiment, the pure BTO thin film was deposited by Sol-Gel method and performed the bistable resistive switching characteristics. However, there are still some drawbacks of the BTO-derived memory devices. In this thesis, it is interesting to promote the properties of this kind of device, like endurance and operation voltage, which are important issues for currently CMOS process.

3.1.1 Thickness of pure BTO thin film

The thickness of the original pure BTO thin film is about 45nm ~ 60 nm. Based on the previous experimental data, the forming voltage was located at the range of -4V~ -6V. This would be a big problem for application. As we know, BTO thin film was deposited by Sol-Gel method and repeated coating for 3 times to attain the thickness wanted. Nevertheless, there is a factor needed to be taken into consideration – Roughness. While coating such thin film in repeat, it doubtlessly increases the surface roughness in the aspect of micro-investigation. For this reason, we test BTO thin film in thinner thicknesses to keep a flat surface and try to diminish

the effect of roughness. In this section, we are talking about effect of thinner switching oxide on electrical properties. The BTO thin film is finished by coating for 2 times and its equivalent thickness is about 20 nm.

3.1.2 Forming process

Before any resistive switching is performed, the device is initially at an original-state (O-state) with higher resistance than OFF-state. In Figure 3.1, the voltage sweeps close to -4V and then a sudden increase in the conduction current is observed and limited at the current compliance of 20 mA, switching the device to ON-state. The forming process means a high DC bias is applied on the memory device to switch it from original-state to ON-state. During the forming process, the leakage current shows a hysteretic phenomenon in I-V curve with the double sweeping mode in Agilent 4155C.

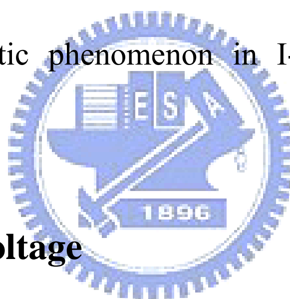
ESA 1896

3.1.3 Operation mode and voltage

After forming process, the memory device remains at ON-state. Then, we need a positive voltage to switch the memory device back to the OFF-state and this is what we call turn-off process. If the memory is switched back to the ON-state, this is a turn-on process. In previous research, even though BTO thin film belongs to non-polar switching, the best mode is located at negative turn-on and positive turn-off mode. From now on, in this thesis, we only sweep for this best mode to investigate the electrical properties. The range of the operation voltage is located at -1.2V ~ -3.8V, but depicts a larger variation.

3.1.4 Memory test for endurance

In nonvolatile memory, there is an important indication for using – Endurance. Figure 3.2 depicts the endurance test for pure BTO thin film. This is an unacceptable result. The switching cycles are less than 10. Therefore, post deposition annealing is brought in to solve such issue.

3.1.5 Thermal effect of post deposition annealing

As we know, annealing is helpful for repairing the crystalline and then improves the electrical performance. Unfortunately, it seems that post annealing does not give any promotion in this memory device, but leads to failure in the end. It is deduced that post annealing make grain become larger with high temperature and then increases the leakage current dramatically. However, thickness of BTO thin film is about 20~30nm. After post annealing at higher temperature, voltage drives thin film break down easily.

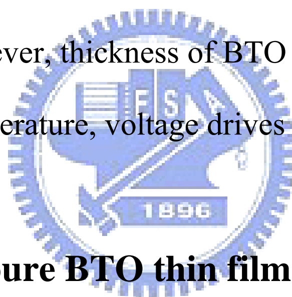

3.1.6 Summary for thinner pure BTO thin film

From these investigations of electrical properties, there are some disadvantages of BTO thin film. First, the unstable turn-on voltage increases the difficulty for RRAM applications. Miss read error between turn-on and turn-off voltage would be a serious problem in real operation. Second, reliability test for endurance is very poor, which is not suitable for applications. Third, we tried to improve its electrical properties with post annealing, but failed. That is to say that thinner BTO film could not tolerate such high temperature. Therefore, in the next section, we have a little change on structure by embedding a metal layer in between. Some interesting phenomenon are investigated and discussed later.

3.2 The effect of embedded metal in BTO thin film

Recently, many reports about the embedded perovskite thin films for non-volatile memory are proposed for RRAM application were investigated, and many kinds of embedded metal materials have been investigated and Liu et al., and Nb-doped $SrTiO_3$ films by Xiang et al. Based on the research of perovskite material $SrZrO_3$ with embedded metal, electrical properties such as operation voltage and endurance are greatly improved. BTO thin film, as known a type of perovskite structure, it is quite interesting for us to test embedded metal on it. Description about details will be referred in the following sections.

3.2.1 Materials for embedded metal

There have been many materials tested for embedded metal in perovskite structure, such as Pt, Pd, Mo, Cr, and Cu. However, it seems that device with Cr embedded has the better properties than else. It is known that Cr is a low work function metal in comparison to high work function metal Pt. In the thesis, we focus on these two different metals and give a comparison between them.

3.2.2 The effect of thermal treatment

There is an important process in this thesis, named post deposition annealing, which is abbreviated as PDA. The device will experience a high temperature process ($500^{o}C$, $600^{o}C$, $700^{o}C$) in N_2 ambient for 30 seconds before depositing top electrode. The object is to dismiss the thermal stress remained in metal materials and further to enhance the quality of thin films. It is worthy to be mentioned that the embedded metal diffuses in BTO thin film with the help of thermal treatment, and then the resistive switching property is investigated and discussed.

3.2.3 Resistive switching properties of embedded Cr BTO thin film

In this section, we are talking about the embedded metal – Chromium (Cr). In our experiments, different thicknesses (2nm, 5nm, 10nm) of Cr are used for testing resistive switching properties. In Figure 3.3, it depicts the resistive switching of 10nm Cr embedded. The drawback of this kind of device is that voltage is too large to be applied in CMOS process. Then the device is thermal treated at 500°C, 600°C and 700°C, as shown in Figure 3.4~3.6. Although the voltage is indeed lowered, it is still quite large for applications. This kind of characteristic is not fit for our expectation so that we try 5-nm-thick Cr thickness embedded in BTO film. Figure 3.7 shows that the range of voltage is slightly lower than 10nm Cr embedded. Similarly, thermal treatment is applied as well in Figure 3.8~3.10. The properties of 5-nm-thick Cr embedded are better than that of 10-nm-thick Cr embedded, so we deduce that 2-nm-thick Cr embedded, perhaps, would be better than 5-nm-thick Cr embedded. In Figure 3.11, the forming curve of each thickness is put together for comparison. To our expectation, 2-nm-thick Cr embedded shows that lowest forming voltage, which is near -4V. After forming process, resistive switching I-V curve is shown in Figure 3.12. The average operation voltage is located around -4V, which is much lower than any others. However, there are some interesting results for us to discuss. Later, the more details will be presented gradually in next section and the content is divided into two parts, including physical property analyses and electrical property analyses.

3.3 Physical property analyses of 2nm Cr embedded

It should be understood that the performance of nonvolatile memory depend on the electrical properties and the yield of nonvolatile memory depend on the physical properties, respectively. In the following sections, we will introduce the physical measurements and analyses include thermal analysis, X-ray diffraction analysis, transmission electron microscope, scanning electron microscope, and atomic force microscope. The measurements are used to see the pyrolysis temperature, crystallization temperature, preferred orientation, grain size, morphology of surface and cross-section, the surface roughness degree, the content of organic impurity, the content of major element, and the bonding energy. Besides, the physical properties measurement can help us to find the better fabrication parameters.

3.3.1 X-Ray Diffraction

The 100 nm thickness $LaNiO_3$ (LNO) buffer layer with (100) and (200) preferred orientation is deposited at 250°C on Pt/Ti/SiO_2/Si substrate by a rf magnetron sputter system. The LNO buffer layer used here is due to the better adhesion for BTO solution during spin coating. Figure 3.13 shows the XRD pattern of LNO/Pt and LNO/SiO_2. In addition, different thermal treatments are taken on the embedded 2nm-Cr BTO thin films and XRD pattern of it is shown in Figure 3.14. It looks like no difference after high temperature annealing.

3.3.2 Scanning Electron Microscope

Figure 3.15~3.18 is the top view of BTO thin film with different annealing temperature. Obviously, the grain sizes get larger and larger with the raising annealing temperature (as-deposited. 500°C. 600°C, 700°C). That can explain increasing leakage

current of OFF-State with the raising annealing temperature. To our knowledge, the leakage current in BTO film flow through the grain instead of grain boundary.

3.3.3 Atomic Force Microscope

According to the TEM image, the thickness of BTO-2/Cr-2nm/BTO-1 is 22nm, which is a very thin film. The electrical performance is sensitive to its roughness while spin coating. In order to guarantee the quality of thin film, atomic force microscope is fit for our demands. We can know for sure how rough the thin film is and how to modulate the parameters of process. Figure 3.19~3.22 show the 2D and 3D AFM images of BTO thin film. It is

3.3.4 Transmission Electron Microscope

The thickness of 2nm Cr embedded BTO thin film is investigated by transmission electron microscope. The figure 3.23 and figure 3.24 show the cross-section view of Pt/BTO-Cr-BTO/LNO without PDA and with PDA 600°C, respectively. From TEM results, lots of CrO_x clusters exist in the films. We deduce that the formation of CrO_x nanocrystal in the BTO thin film after post deposition annealing at 600°C.

2.3.6 Secondary Ion Mass Spectrometer

It is investigated that the conduction mechanism is dominated by the formation of Cr-related nanocrystal in BTO thin film while annealing at 600°C. However, when annealing temperature raises to 700°C, the electrical performance would be poor. The reason is that Lanthanum(La) of the bottom electrode LNO diffuses seriously, as shown in Figure 3.25.

3.4 Electrical Property Analyses of 2nm Cr Embedded

3.4.1 Resistive Switching Characteristics

Because of the advantage of low operation voltage, we especially focus on the electrical properties of 2nm Cr embedded. As referred above, the forming voltage of 2nm Cr embedded without post deposition annealing is near -4V, which is lower than any others. It is interesting to see if the forming voltage is lowered down by thermal annealing. Therefore, we treat our samples in N_2 ambient for 30 seconds at 500°C, 600°C, and 700°C. The object is to see how the thermal treatment affects the performance of devices. The measured results are presented in the Figure 3.26, which are plots in the form of statistics for forming voltage. Unfortunately, it looks like the forming voltage is independent of annealing temperature. But, in the figure 3.27, there exists an obvious trend that the Original-State current increases with the raising annealing temperature. From the SEM images, the grain size gets larger with higher annealing temperature. As we know, in BTO thin film, conducting path is built by the grain and leads to leakage current. That is the reason for interpreting such phenomenon.

Figure 3.28 depicts the resistive switching properties. There also exists the same trend with forming curves and that is the raising OFF-State current with raising annealing temperature. But, what surprises us is that annealing at 600°C shows the lowest turn on voltage (-2V) in comparison to other temperatures. That is an amazing result. In order to verify the good property of annealing at 600°C, we perform the statistics of twenty devices and as shown in Figure 3.29, annealing at 600°C indeed shows the lowest variation of turn on voltage. Also, the determination to judge whether the memory device is good for using is the resistance ratio between ON-State and OFF-State. Figure 3.30 shows the statistics of ON-State and OFF-State resistance

at 0.3V. The statistical resistance ratio is more than 100, which is enough for identifying logic "1" or logic"0". For further investigation, we plot the accumulative probability, as shown in Figure 3.31. It is easy to tell that annealing at 600°C gives the most stable voltage. Based on the above properties, the device with 600°C thermal annealing shows the best electrical property. In the following section,

3.4.2 Memory Test

In this section, we are talking about the reliability test for memory devices. In reality, whether the memory shows the good properties or not, the memory tests are the indication for applications. For this purpose, memory tests such as endurance, retention time and voltage stress are discussed below:

A. Endurance Test

Endurance is another important index for nonvolatile memory. Endurance means that how many cycles the memory device can be operated between ON-State and OFF-State. A good memory device must maintain its resistance ratio in an acceptable range after continuously "writing" and "erasing". The switching cycles of each annealing temperature are shown in Figure 3.32~3.35. In order to realize the variation of operation voltage, Figure 3.36~3.39 are plots for write/erase cycles of ON-State and OFF-State. Besides, In Figure 3.40, comparison of endurance cycles in different process conditions are performed. After all, annealing at 600°C shows the impressive performance.

B. Retention Test

For a nonvolatile memory, retention time means how long that the data can be kept within an acceptable range without any power supply, which is an important

index. Therefore, it is reasonable that 2nm Cr embedded with PDA 600°C has the best result in electrical properties, so we choose it to measure the retention test at room temperature and 85°C, as shown in Figure 3.41 and Figure 3.42, respectively. At room temperature, it shows slight variation for both ON-State and OFF-State after several weeks, indicating that the retention time exceeds 1000000 seconds and the resistance ratio is still more than 3 orders of magnitude.

C. Voltage Stress Test

Voltage stress test is performed to check reliability for reading data (0/1, or ON-State/OFF-State) frequently or successively for a long time. Figure 3.43 depicts the voltage stress of 2nm Cr embedded BTO thin film by applying 0.3V voltage on ON-State and OFF-State during 14400 seconds, and no degradation is observed in both memory states. In addition, the resistance ratio of memory device is over 3 orders of magnitude for a long time, and both states are very solid. As usual, the voltage stress test is performed at 85°C in Figure 3.44. The resistance ratio remains over 3 orders of magnitude for at least 12000 seconds although the OFF-State current drop a little in the end.

3.4.3 Curve Fitting of Current-Voltage Plots

The electrical properties of the Pt/BTO-2/2nm-Cr/BTO-1/LNO/PT structure without PDA are characterized by curve fitting method. The positive and negative bias regions of the I-V curve are shown in the double logarithmic plots in the Figure 3.45 and Figure 3.46, respectively. According to the curve fitting analyses, Ohmic conduction (Slope=1) dominates the ON-State in both positive and negative bias regions. For OFF-State, Ohmic conduction dominates at low electric field contributed by thermal carriers. Followed by a $I \sim V^2$ where the slope is 2 in the double logarithmic

plots, indicating theat the trap-filled space charge limited current (SCLC) behavior. The same electron conduction behavior is also observed in the Pt/BTO-2/2nm-Cr/BTO-1/LNO/PT structure with PDA 600°C treatment, as shown in Figure 3.47 and Figure 3.48, respectively. From investigation between without PDA and with PDA 600°C, no transformation is found in mechanism.

3.4.4 The relation between temperature and current

Owing to the good properties of embedded 2nm-Cr device, curiosity drives us to find out what is the domination of each state. Therefore, we measure the I-V curve of the device at different temperatures (room temperature, 50°C, 75°C, 100°C, 125°C and 150°C) and then to analysis the variation of current in each temperature. At ON-State, as shown in Figure 3.49 no obvious different in conductivity is investigated. Current seems like independent of temperature. It is hard for us to judge what the property of ON-State is. At OFF-State, as shown in Figure 3.50, an obvious trend is shown in figure. The current is increasing while increasing measurement temperature. The change of conductivity can indicate that the property of OFF-State is semiconductor-like or insulator behavior. By the way, the calculation for activation energy (Ea) is depicted in Figure 3.51. The slope of the linear fitting in Arrhenius plots is proportional to the activation energy, having the relationship as following :

$$Slope = \frac{\ln I_1 - \ln I_2}{\frac{1000}{T_1} - \frac{1000}{T_2}} = -1000k \times E_a$$

where k is Boltzman's constant. The ON-State have activation energy (Ea) of 0.011eV while the OFF-State have the activation energy (Ea) of 0.18eV.

3.4.5 Possible mechanism

According to the previous research on embedded metal, the diffusion of metal in thin film dominates the switching mechanism. It confirms that the filament is connected by the diffusion metal with the help of thermal treatment. In our experiment, such phenomenon should be taken for interpreting the mechanism of embedded 2nm-Cr device. However, something different happens after post deposition annealing at 600°C. From the investigation of TEM, as shown in Figure 3.24, we deduce that the formation of clusters exists in BTO thin film. The clusters are the gathering of Cr, which easily traps oxygen to form the Cr-related nanocrystal. As a result, the conducting path is confined and the filaments are formed in the weaker places near the Cr-related nanocrystal.

3.5 Electrical Property Analyses for 2nm Pt Embedded

In above research, the focus is on the embedded Cr BTO thin film. Chromium has a shallow work function of 4.5 and easily to be oxidized. Therefore, we prepare for another material – Pt, which is a deep work function of 5.65 and an inert metal, to replace Cr as an embedded metal and to figure out what is the difference between them. Further, explanation for the mechanism of each material is necessary.

3.5.1 Resistive Switching Characteristics

Figure 3.52~3.55 depict that the resistive switching properties of 2nm Pt embedded with no PDA, PDA 500°C, 600°C and 700°C, respectively. It is investigated that the characteristics are not as good as 2nm Cr embedded. To our surprise, the forming voltage is below -3V, which is lowest ever. However, after forming process, the resistive switching behavior disappoints us. There are some

drawbacks existed in it. First, the endurance cycles are very poor, which is less than 10. Even though the operation voltage is very low, in reality, such property does not fit for applications. Second, it is obvious that the resistance ratio between ON-State and OFF-State is less than 10. In order to prove the resistance ratio, the statistics for ON-State and OFF-State resistance is shown in Figure 3.56. This is a very serious problem for judging the logic"1" and logic "0" and easily leads to read error. Third, after post deposition annealing, the electrical property gets worse and worse. It is of no use with high temperature annealing. Although the issues referred above are quite poor in electrical properties, there are still something interesting for discussion.

3.5.2 Curve Fitting of Current-Voltage Plots

In order to compare with the Cr embedded structure, it is necessary to fit curve for the Pt/BTO-2/2nm-Pt/BTO-1/LNO/PT structure. At first, as usual, we deal with the embedded 2nm-Pt device without PDA. The positive and negative bias regions of the I-V curve are shown in the double logarithmic plots in the Figure 3.57 and Figure 3.58, respectively. According to the curve fitting analyses, Ohmic conduction (Slope=1) dominates the ON-State in both positive and negative bias regions. For OFF-State, Ohmic conduction dominates at low electric field contributed by thermal carriers. Followed by a $I \sim V^2$ where the slope is 2 in the double logarithmic plots, indicating that the trap-filled space charge limited current (SCLC) behavior. Then, we fit curve for the device with 2nm-Pt embedded with PDA 600°C. The curve fitting at positive and negative regions are shown in Figure 3.59 and Figure3.60, respectively. At ON-State, Ohmic conduction (Slope=1) dominates in both positive and negative regions. However, at OFF-State, great transition takes place in high field at both positive and negative regions. Simply ohmic conduction dominates in OFF-State.

3.5.3 The relation between temperature and current

As usual, it is necessary to figure out what dominates in both states of embedded 2nm-Pt device with PDA 600°C, so we measure the I-V curve of the embedded 2nm-Pt device with PDA 600°C at different temperatures (room temperature, 50°C, 75°C, 100°C, 125°C and 150°C) and then to analysis the variation of current in each temperature. At ON-State, as shown in Figure 3.61, the current is decreasing with raising measurement temperature. This trend indicates that the property of ON-State is metal-like behavior. It is owing to the formation of metallic filaments in thin film. At OFF-State, as shown in Figure 3.62, an obvious trend is investigated. The current is increasing while increasing measurement temperature. The change of conductivity can indicate that the property of OFF-State is semiconductor-like or insulator behavior.

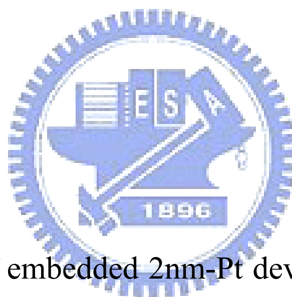

3.5.4 Possible mechanism

In the electrical properties of embedded 2nm-Pt devices without PDA and with PDA 600°C, the OFF-State current is different. The leakage current is higher in devices with PDA 600°C. It reveals that the serious diffusion of Pt ions in BTO thin film happens. The diffusion phenomenon is proved in SIMS analysis, as shown in Figure 3.63. Therefore, we suggest a model for interpreting the conduction mechanism. In Figure 3.64, it shows the illustrations of conduction mechanism in embedded 2nm-Pt devices. After PDA 600°C, the diffused Pt ions are distributed globally in BTO thin film so that the leakage current of OFF-State is larger than that without PDA treatment. As a result, too much remaining filaments lead to the ohmic conduction at OFF-State and the fact is proved with measurement at different temperatures. At last, the comparison in device yield is shown in Figure 3.65

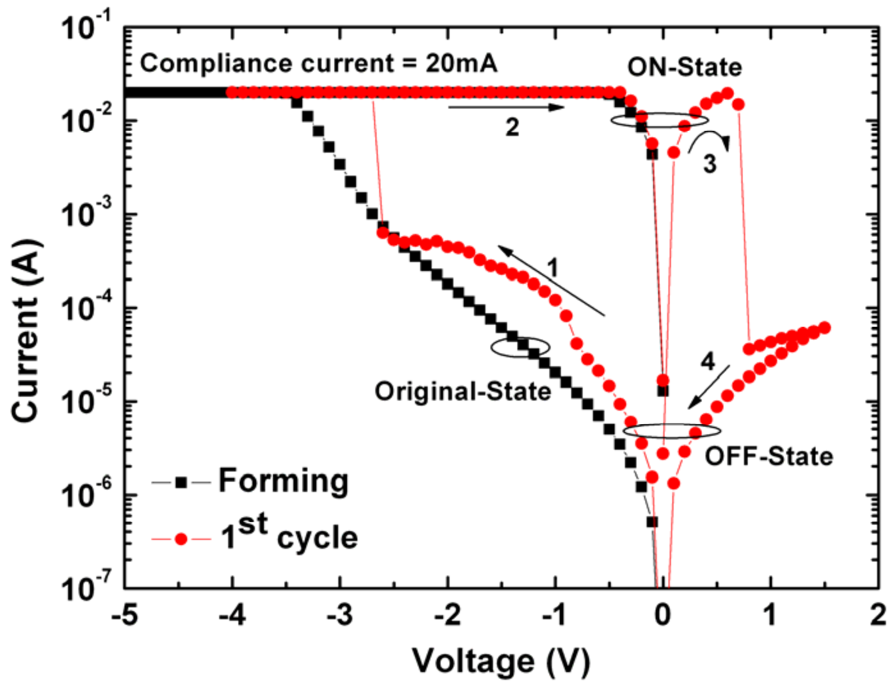

Figure 3.1 The forming curve and first cycle of pure BTO thin film without PDA

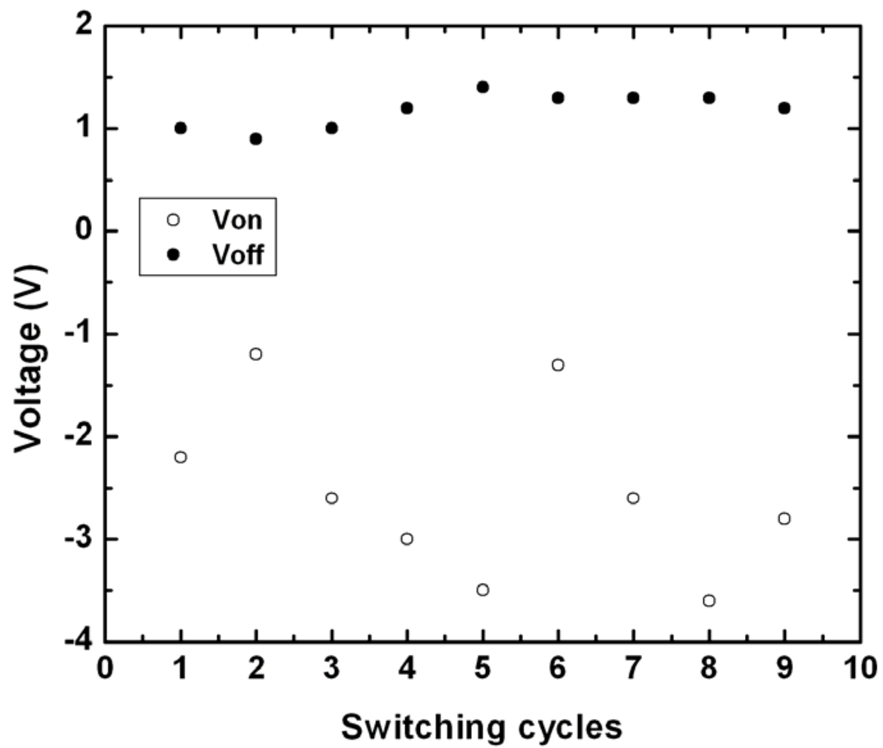

Figure 3.2 Endurance of pure BTO thin film without PDA

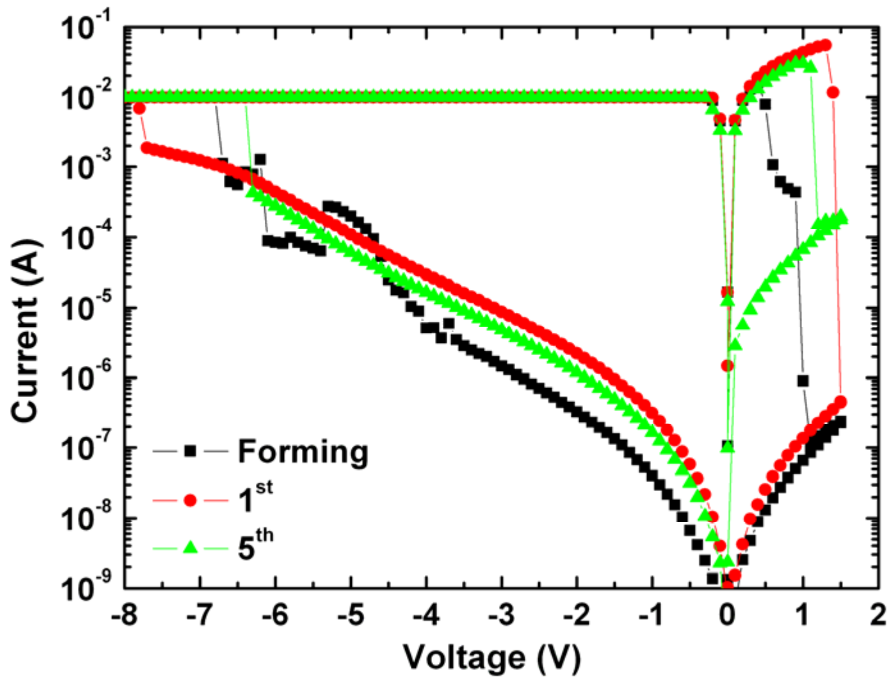

Figure 3.3 Electrical properties of 10nm Cr embedded BTO thin film without PDA

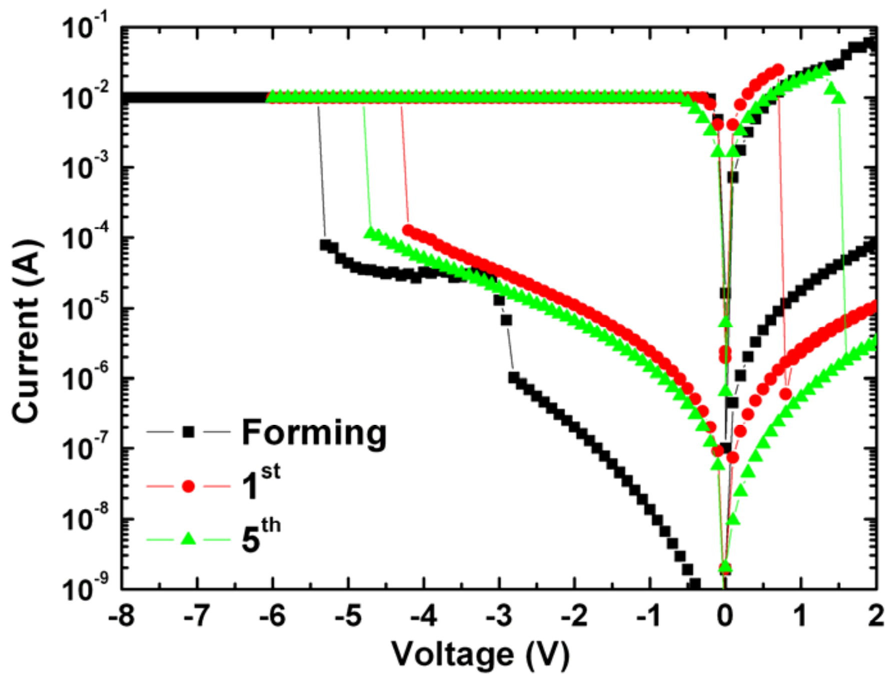

Figure 3.4 Electrical properties of 10nm Cr embedded BTO thin film with PDA 500°C

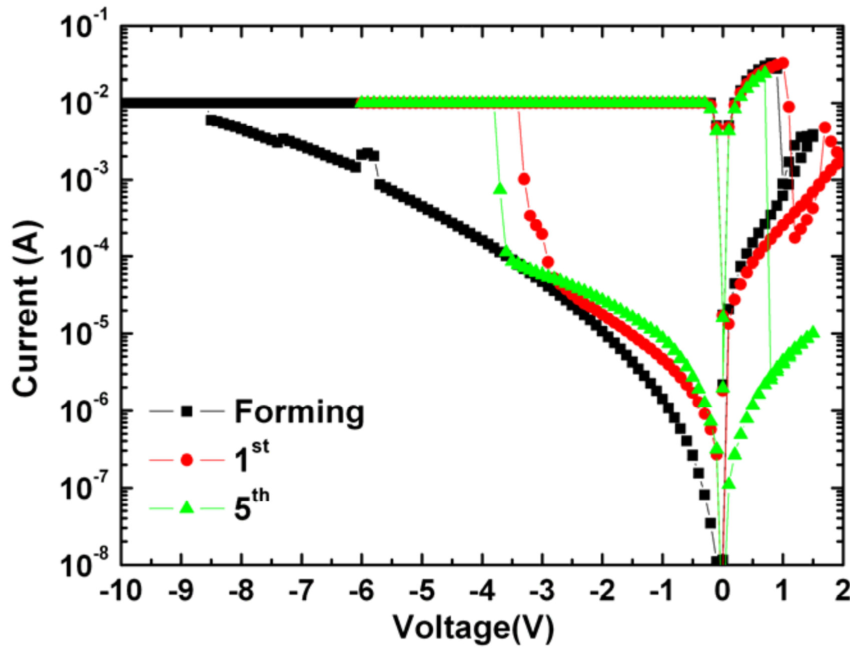

Figure 3.5 Electrical properties of 10nm Cr embedded BTO thin film with PDA 600°C

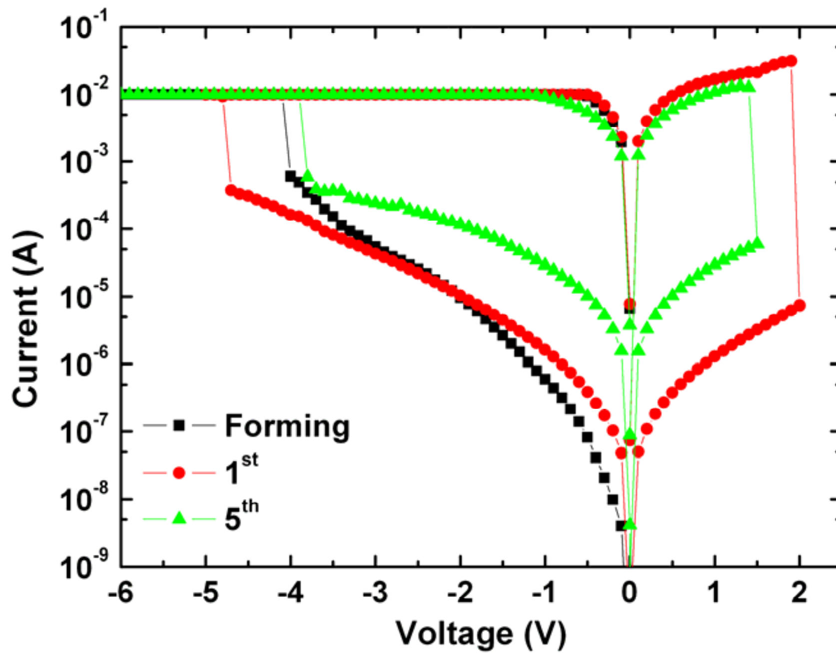

Figure 3.6 Electrical properties of 10nm Cr embedded BTO thin film with PDA 600°C

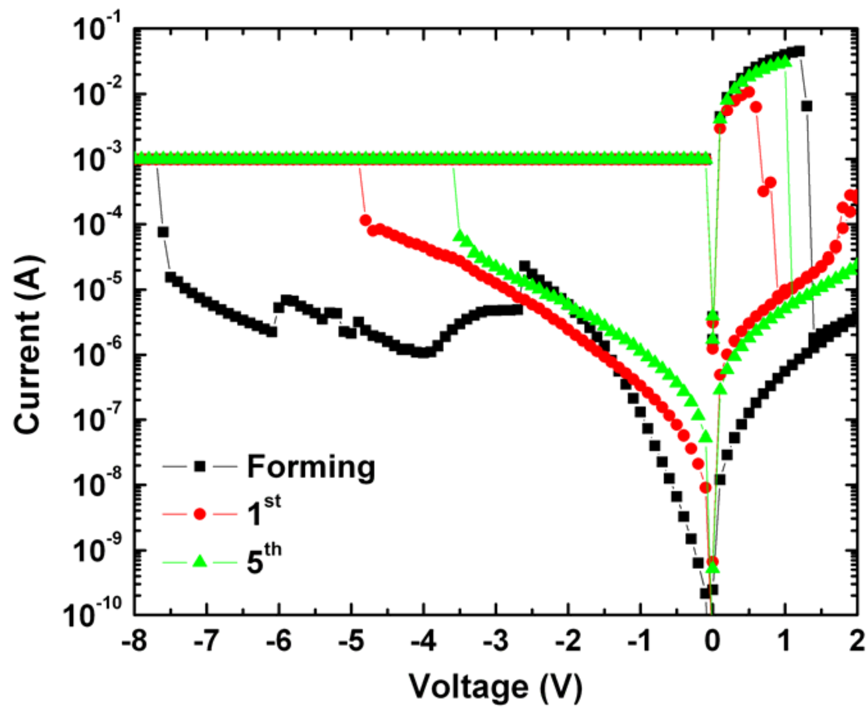

Figure 3.7 Electrical properties of 5nm Cr embedded BTO thin film without PDA

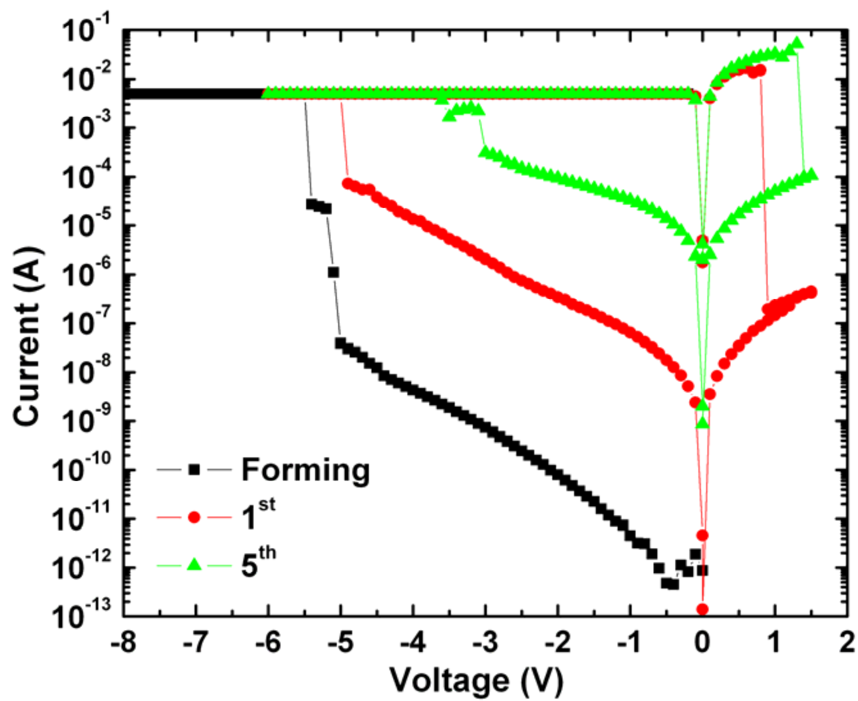

Figure 3.8 Electrical properties of 5nm Cr embedded BTO thin film with PDA 500°C

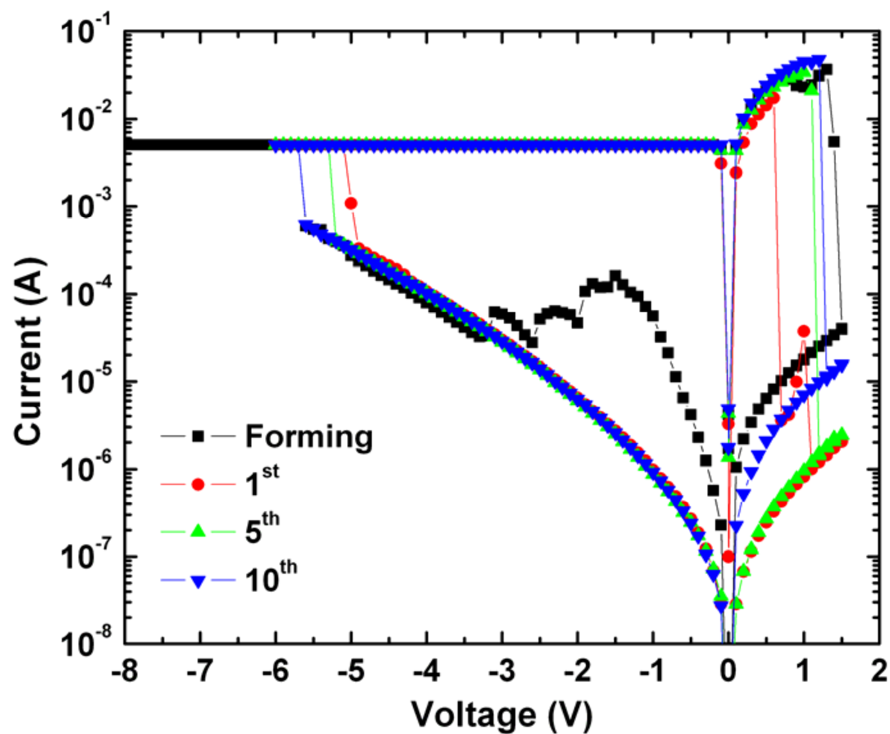

Figure 3.9 Electrical properties of 5nm Cr embedded BTO thin film with PDA 600°C

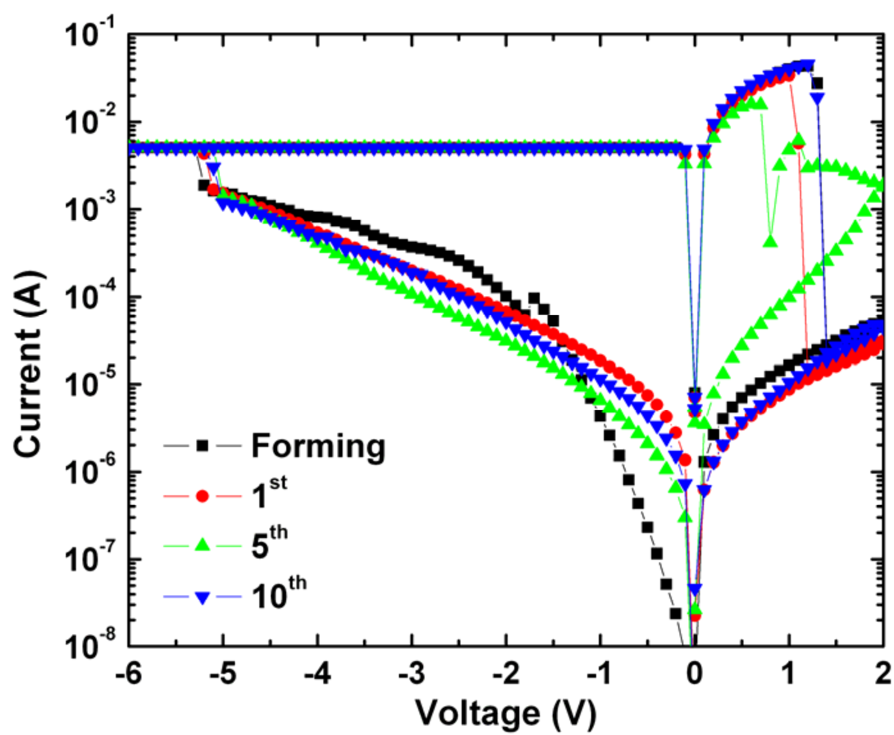

Figure 3.10 Electrical properties of 5nm Cr embedded BTO thin film with PDA 700°C

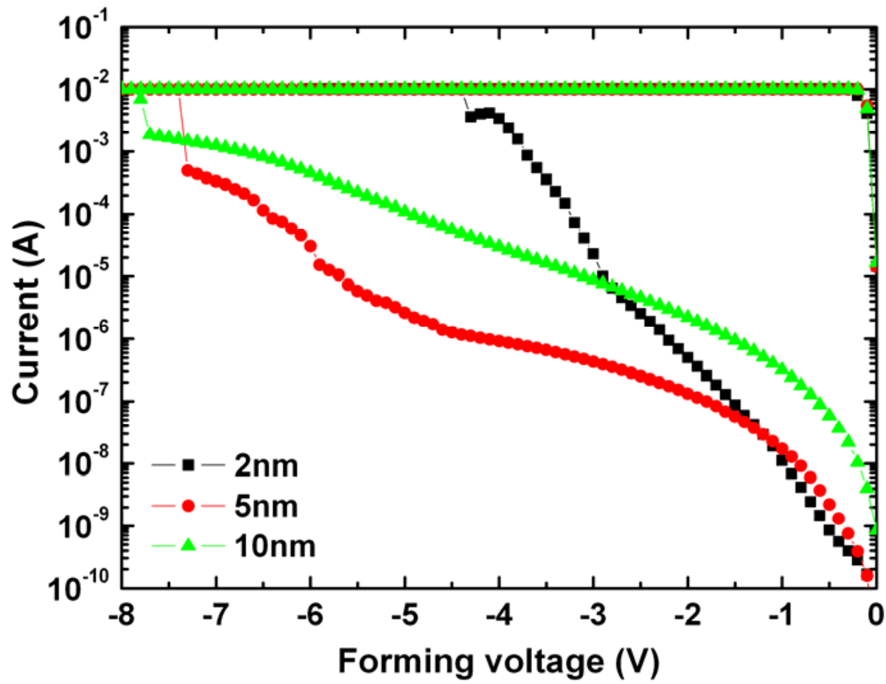

Figure 3.11 Forming process of various Cr thicknesses in the embedded BTO thin film

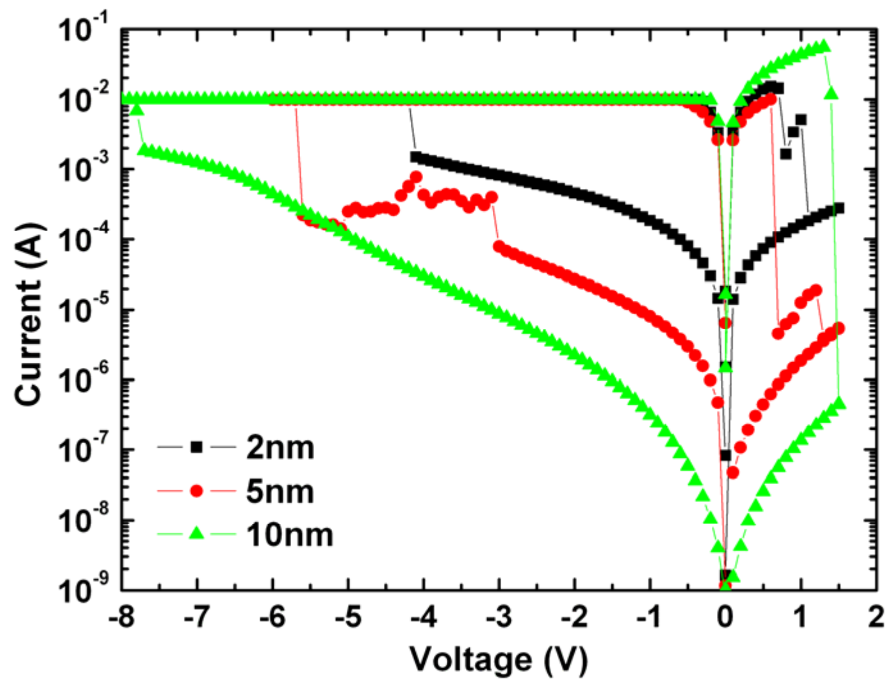

Figure 3.12 Resistive switching I-V curves of various Cr thicknesses in the embedded BTO thin film.

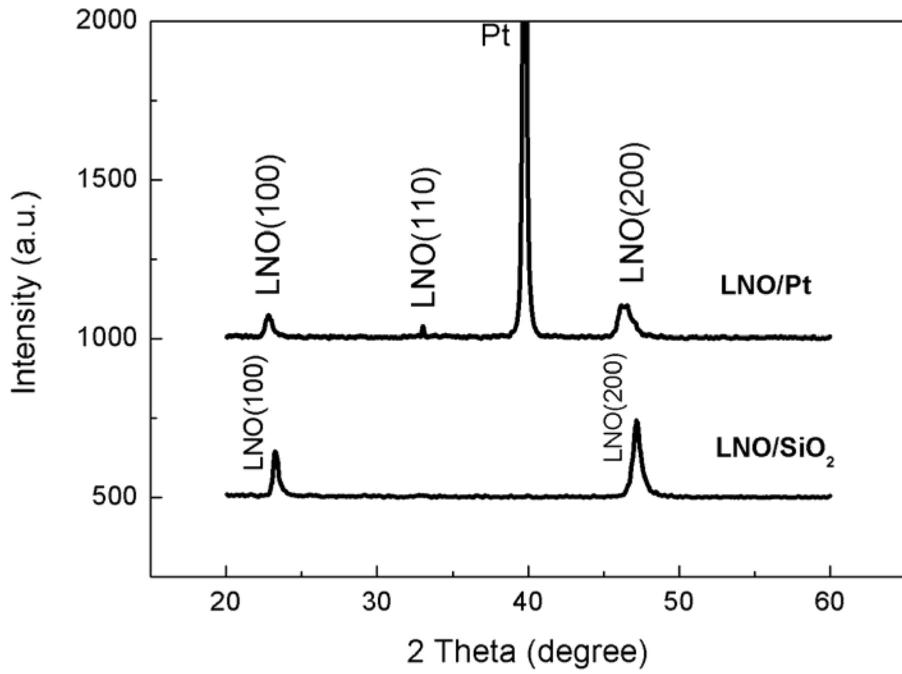

Figure 3.13 XRD pattern of LNO/Pt and LNO/SiO_2 bottom electrode

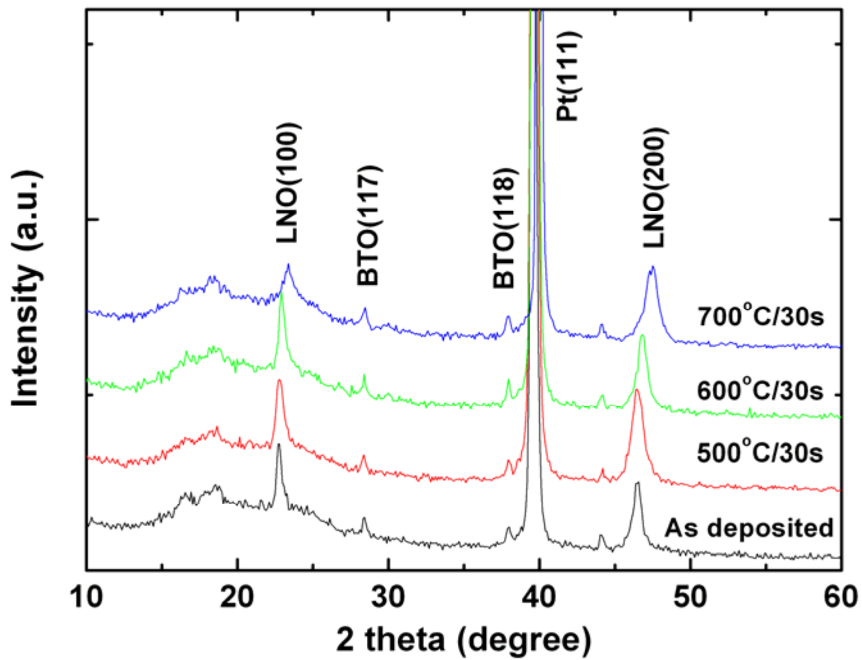

Figure 3.14 XRD pattern of embedded Cr BTO thin film with different thermal treatment

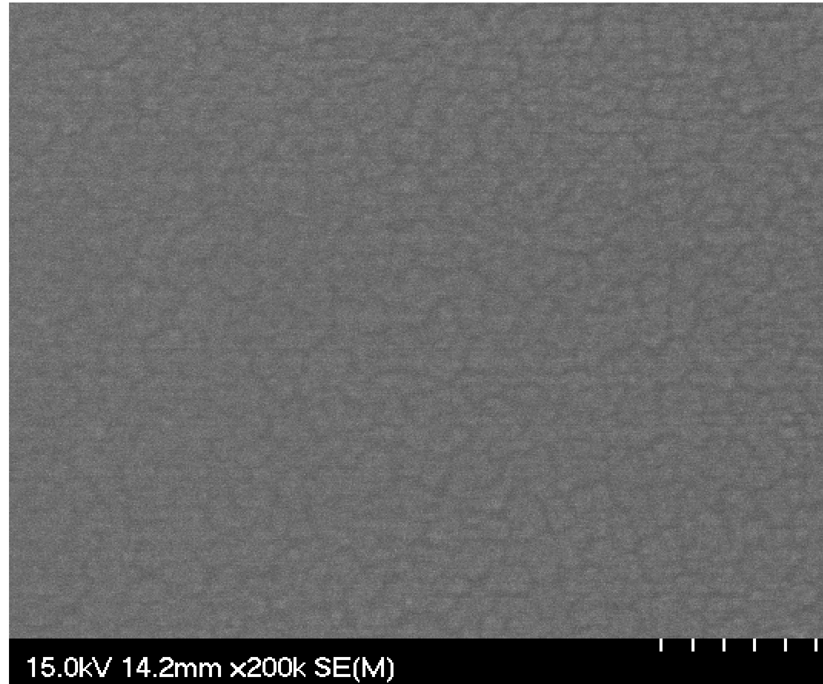

Figure 3.15 Top view SEM images of embedded Cr BTO thin film without PDA

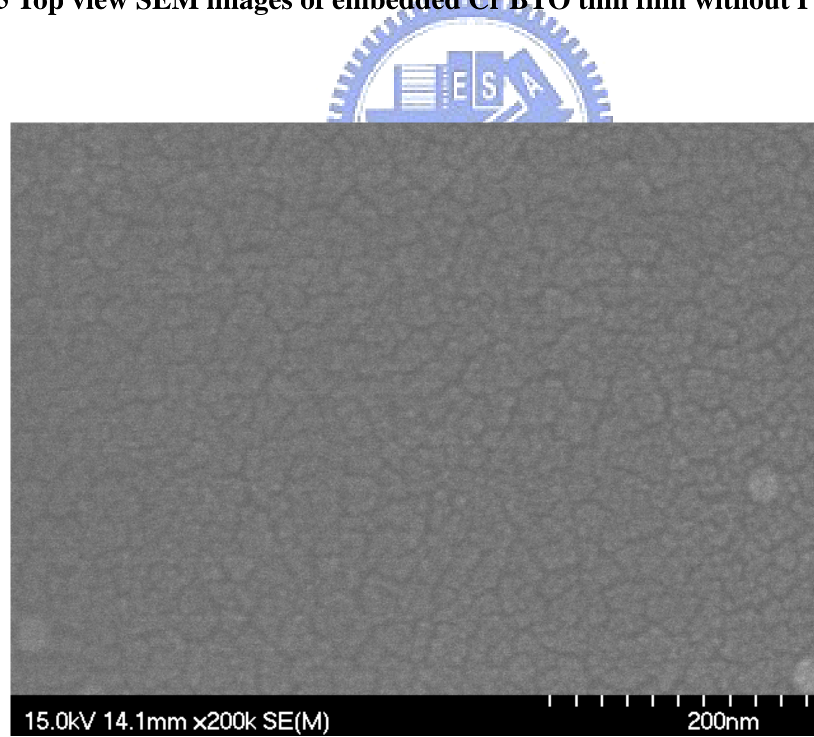

Figure 3.16 Top view SEM images of embedded Cr BTO thin film with PDA 500°C

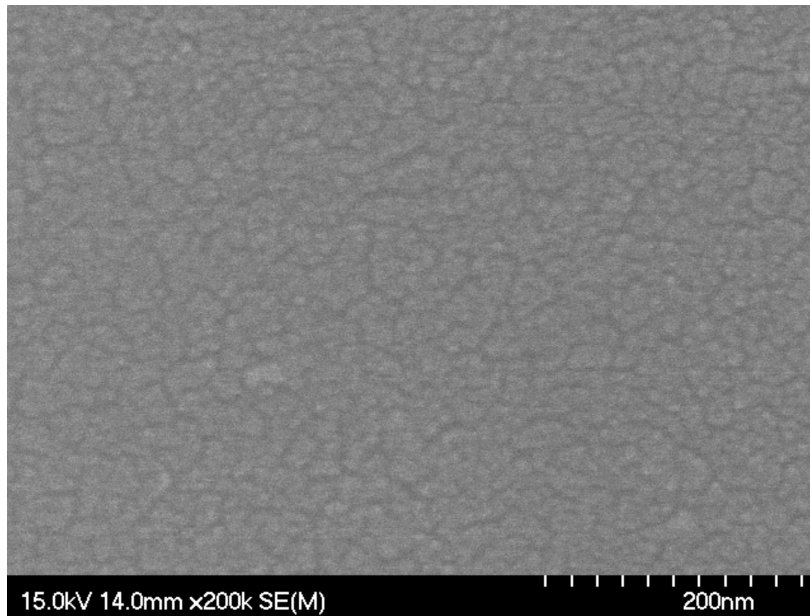

Figure 3.17 Top view SEM images of embedded Cr BTO thin film with PDA 600°C

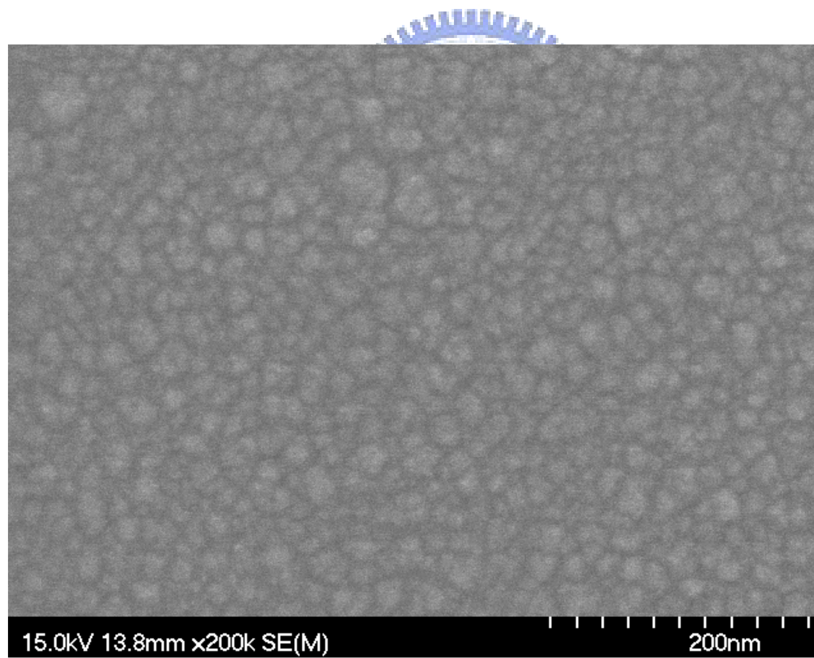

Figure 3.18 Top view SEM images of embedded Cr BTO thin film with PDA 700°C

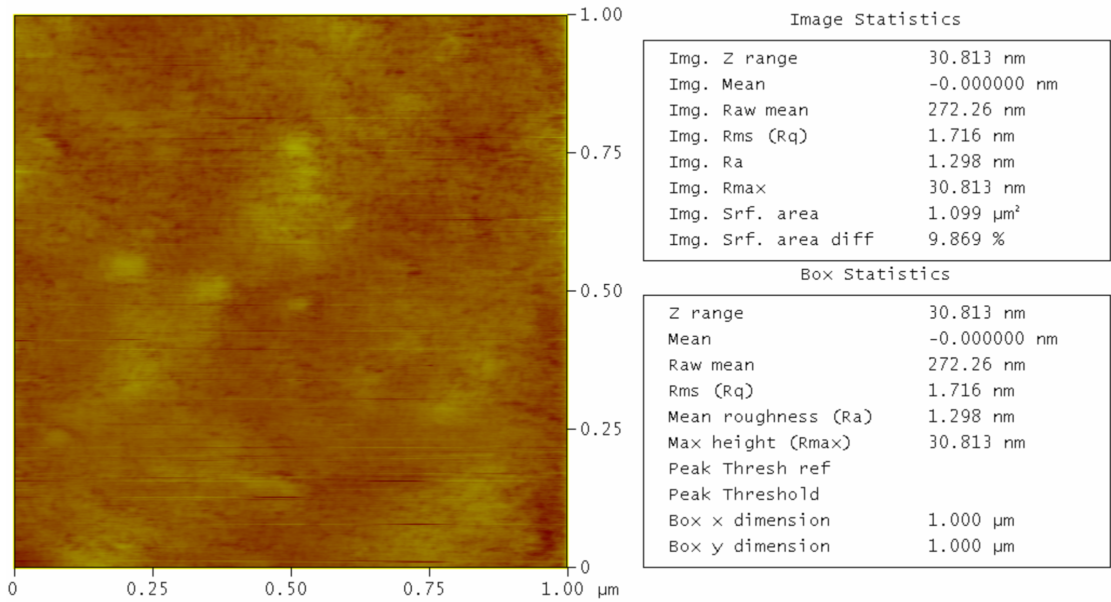

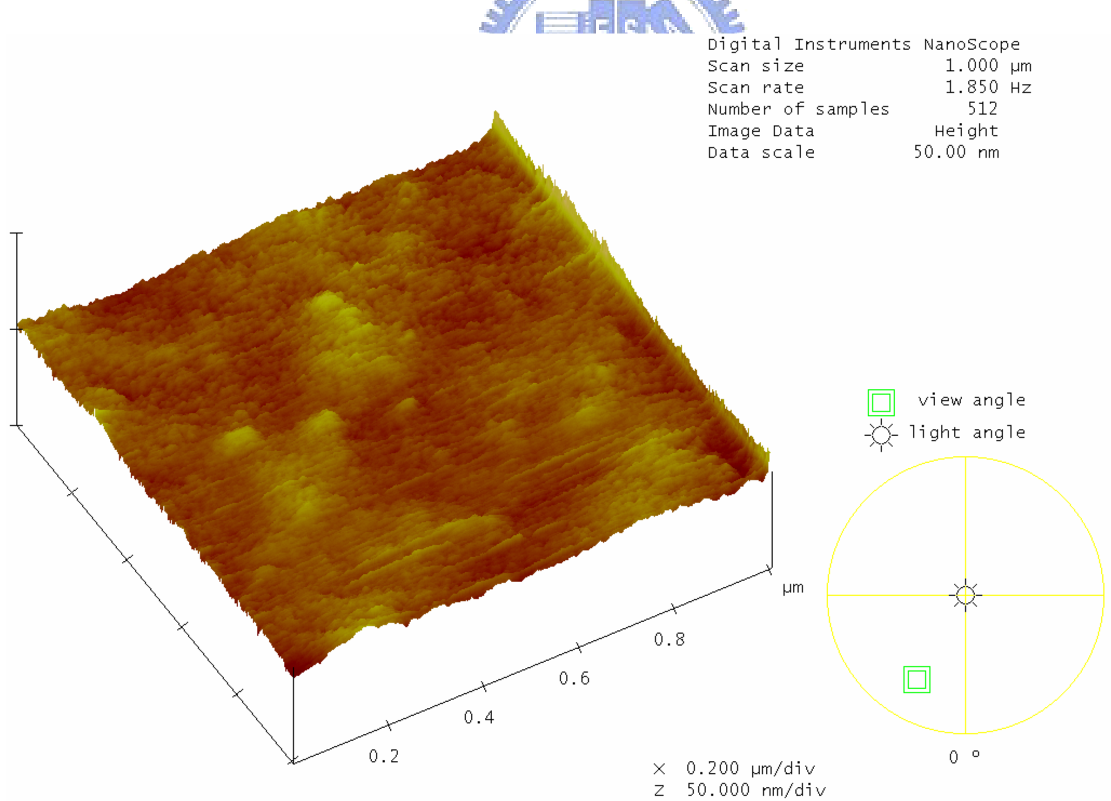

Figure 3.19 2D and 3D AFM image of the embedded Cr BTO thin film without PDA

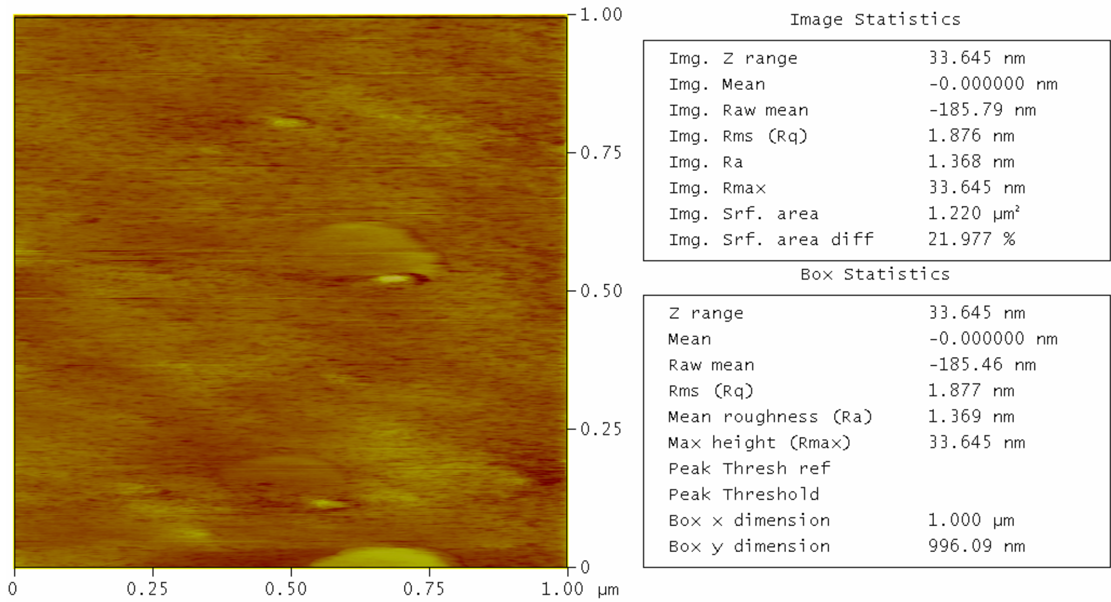

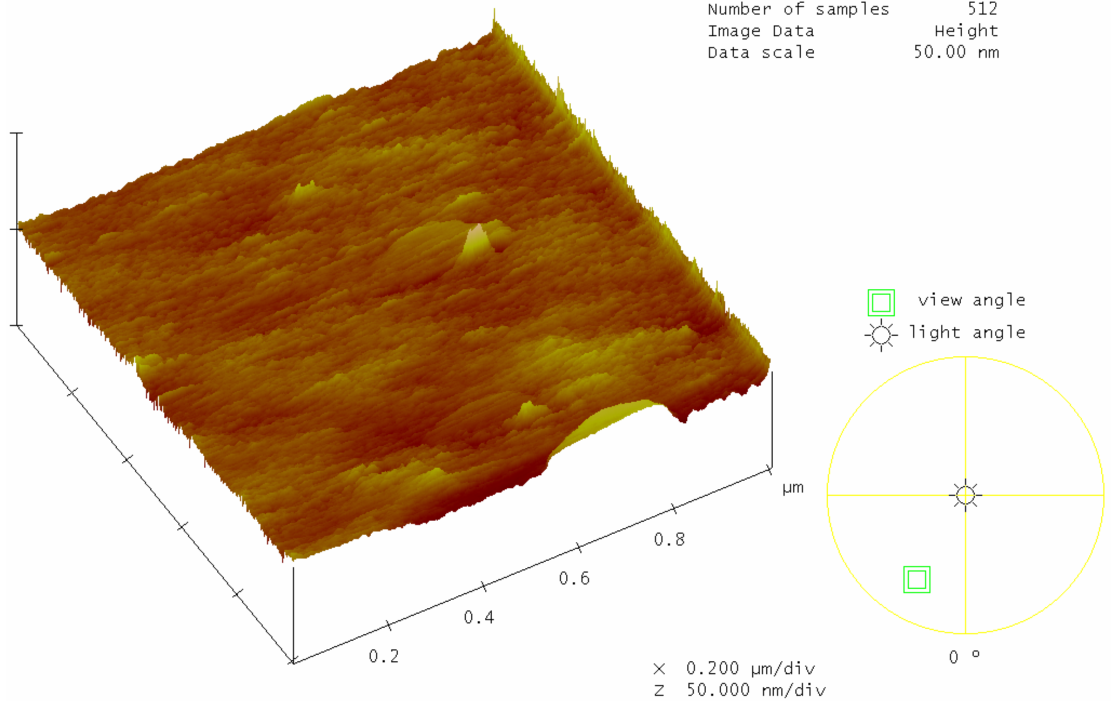

Figure 3.20 2D and 3D AFM image of the embedded Cr BTO thin film with PDA 500°C

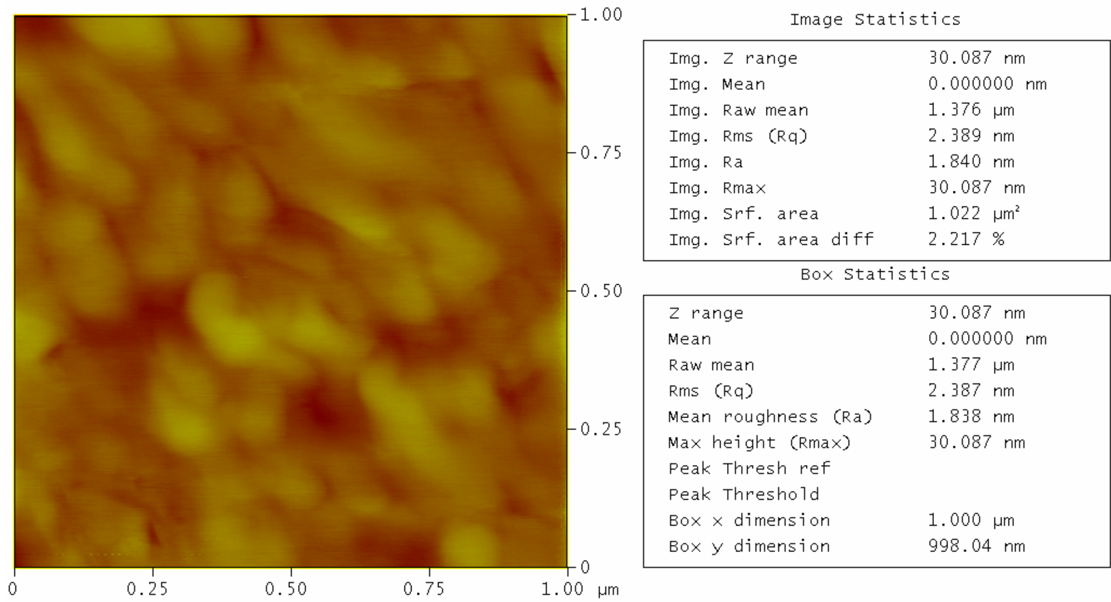

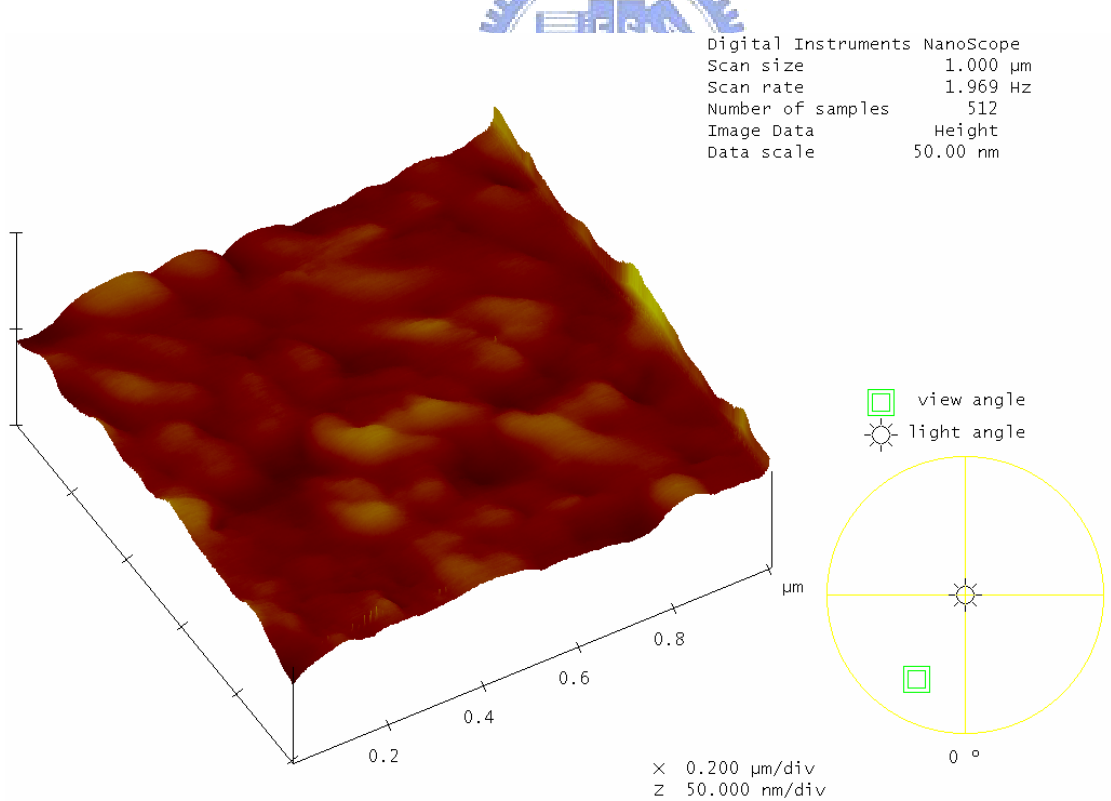

Figure 3.21 2D and 3D AFM image of the embedded Cr BTO thin film with PDA 600°C

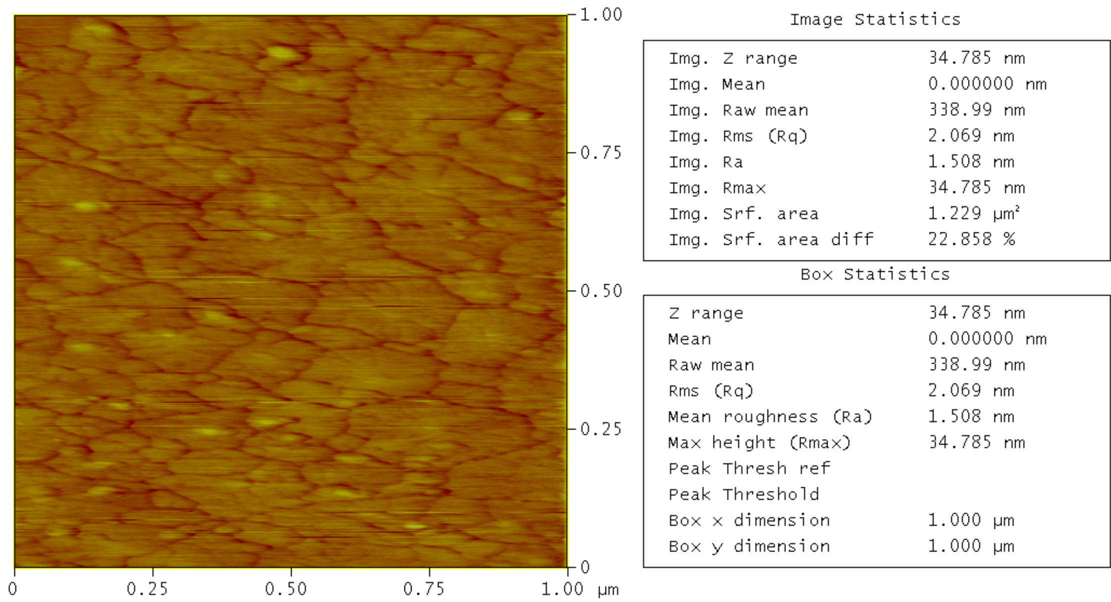

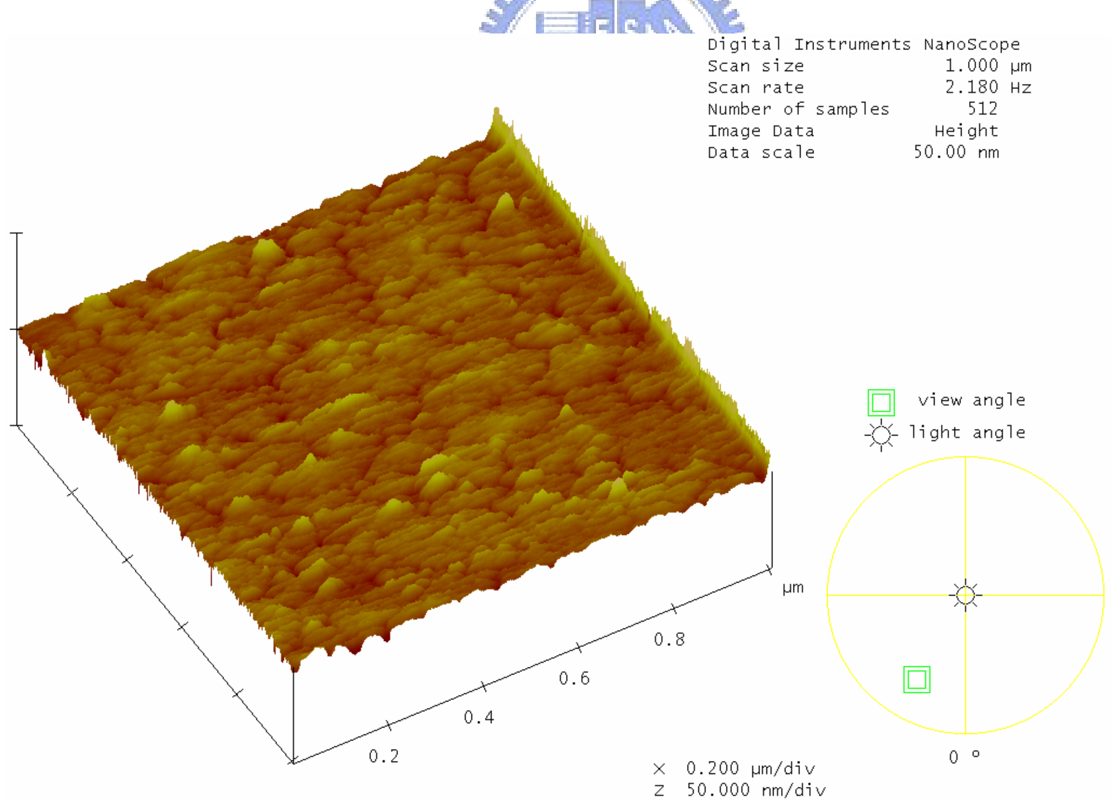

Figure 3.22 2D and 3D AFM image of the embedded Cr BTO thin film with PDA 700°C

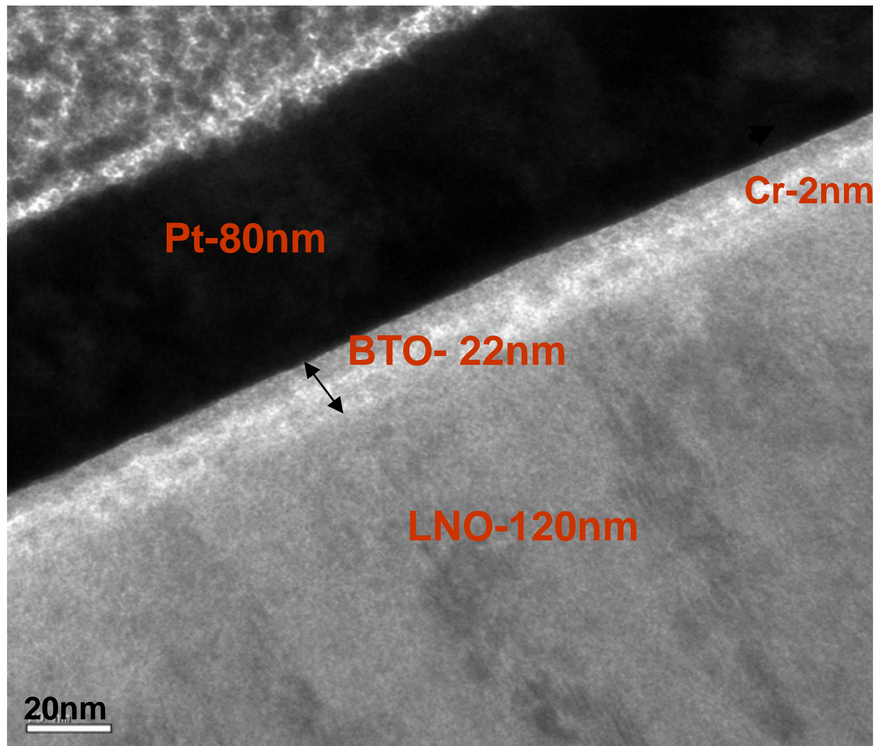

Figure 3.23 TEM image of the embedded Cr BTO thin film without PDA

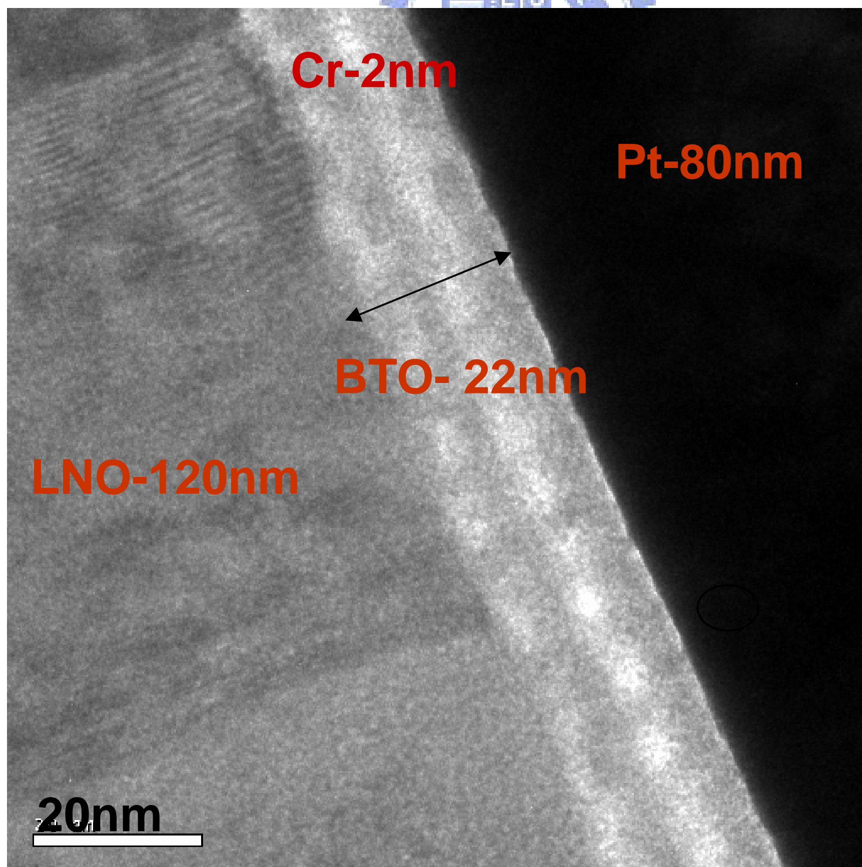

Figure 3.24 TEM image of the embedded Cr BTO thin film with PDA 600°C

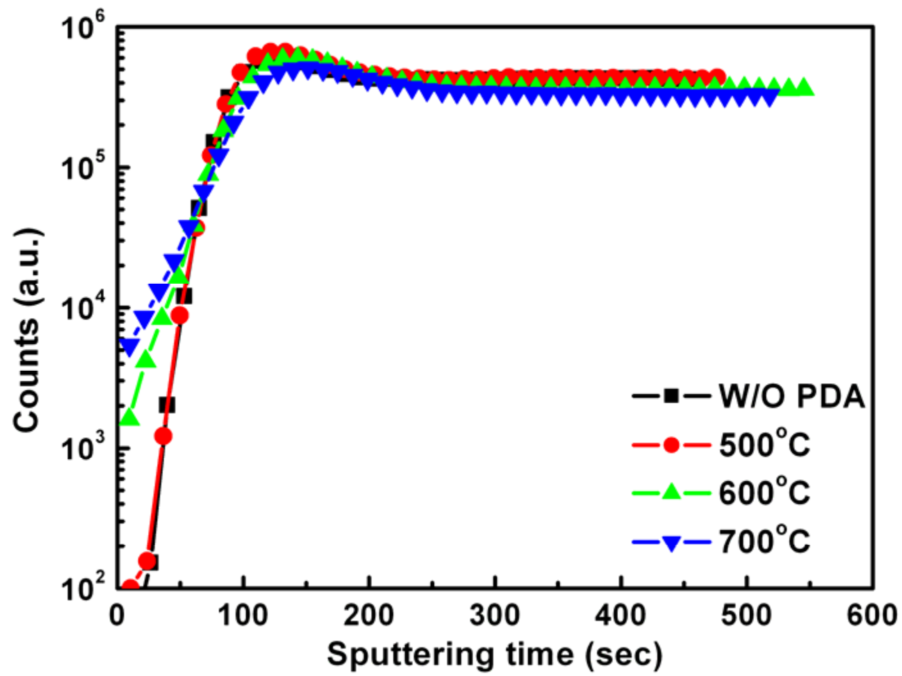

Figure 3.25 SIMS for proving the La diffusion of bottom electrode LNO

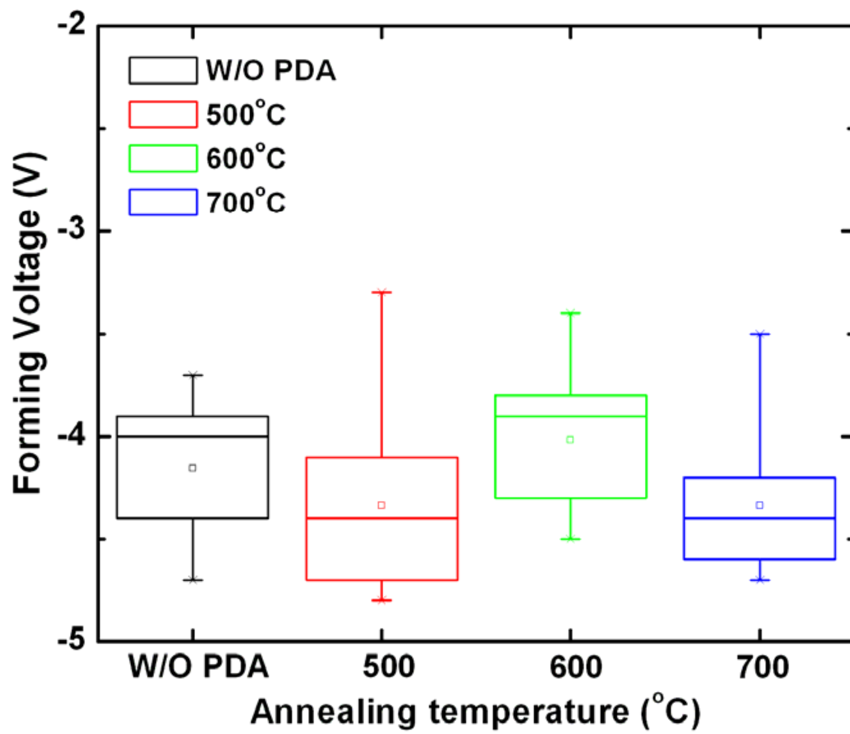

Figure 3.26 Statistics for forming voltage of different annealing temperatures

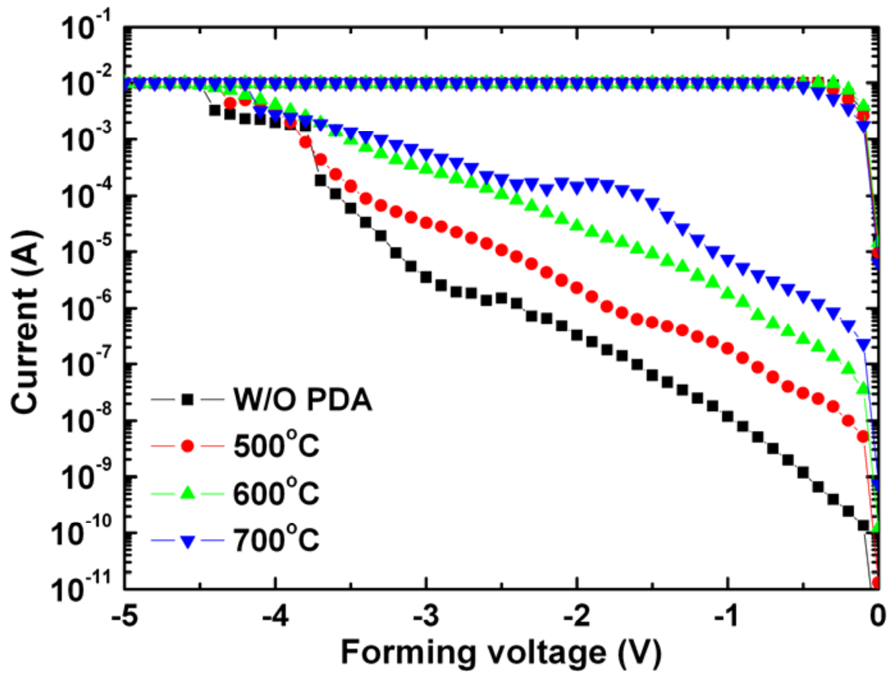

Figure 3.27 Forming I-V curves of different annealing temperatures

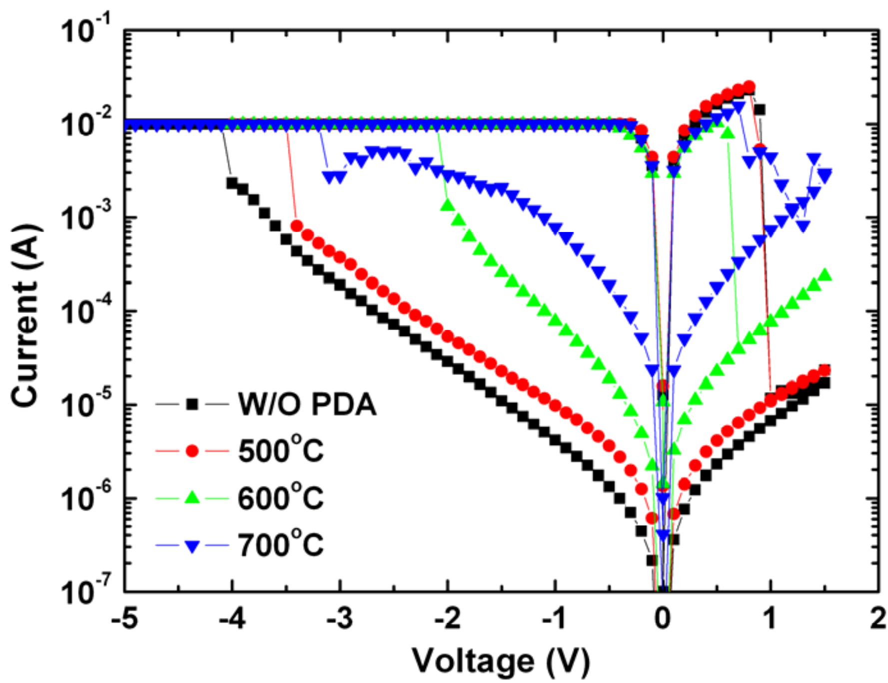

Figure 3.28 Switching I-V curves of different annealing temperatures

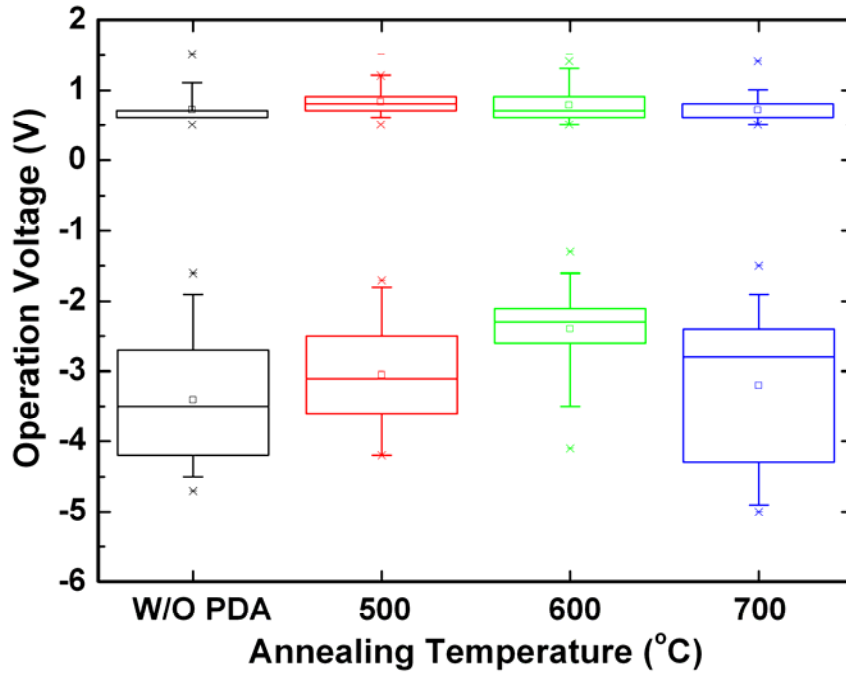

Figure 3.29 Statistics of operation voltage with different annealing temperatures

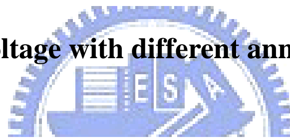

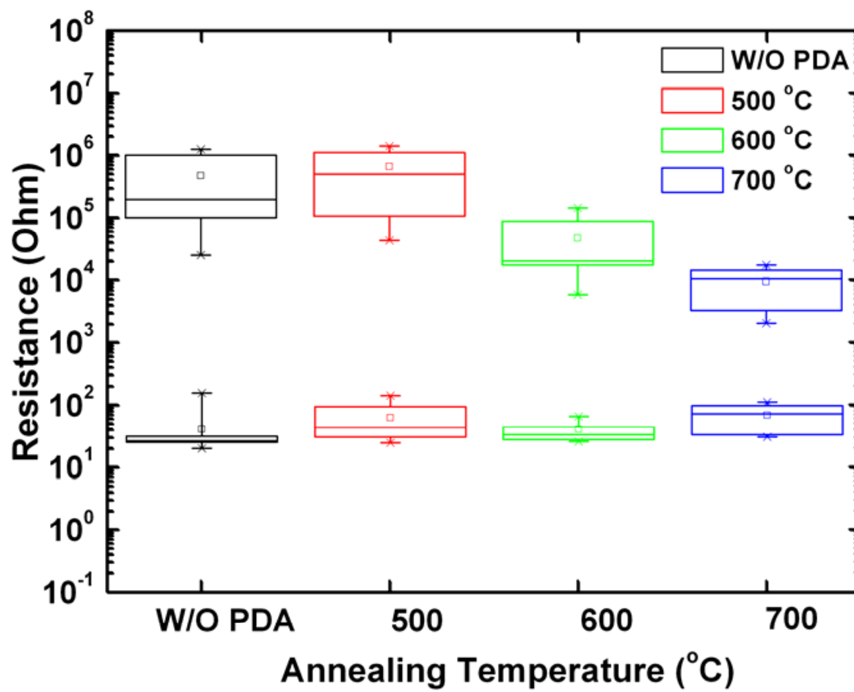

Figure 3.30 Statistics of ON and OFF state resistance with different annealing temperatures

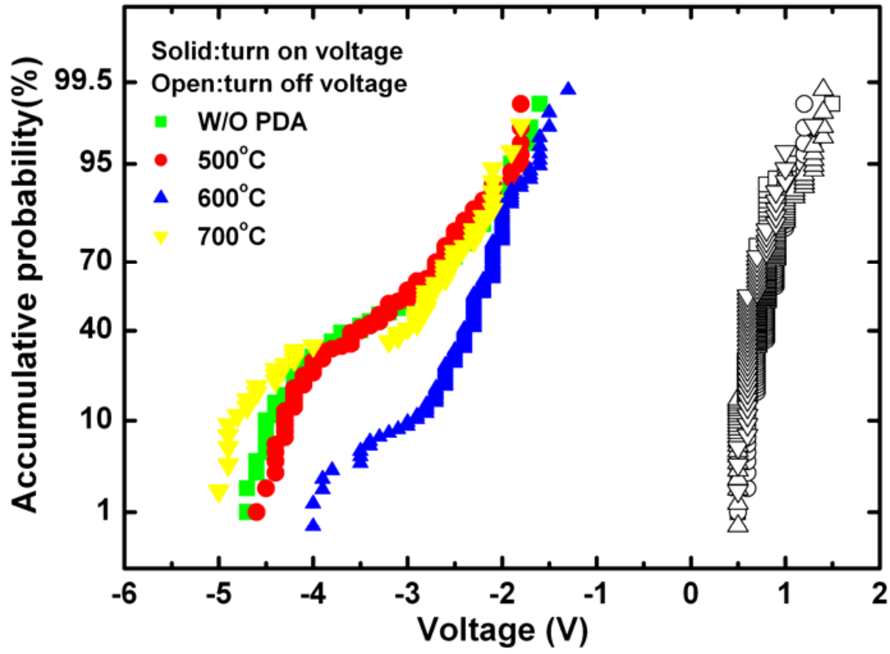

Figure 3.31 Accumulative plots for turn-on and turn-off voltage

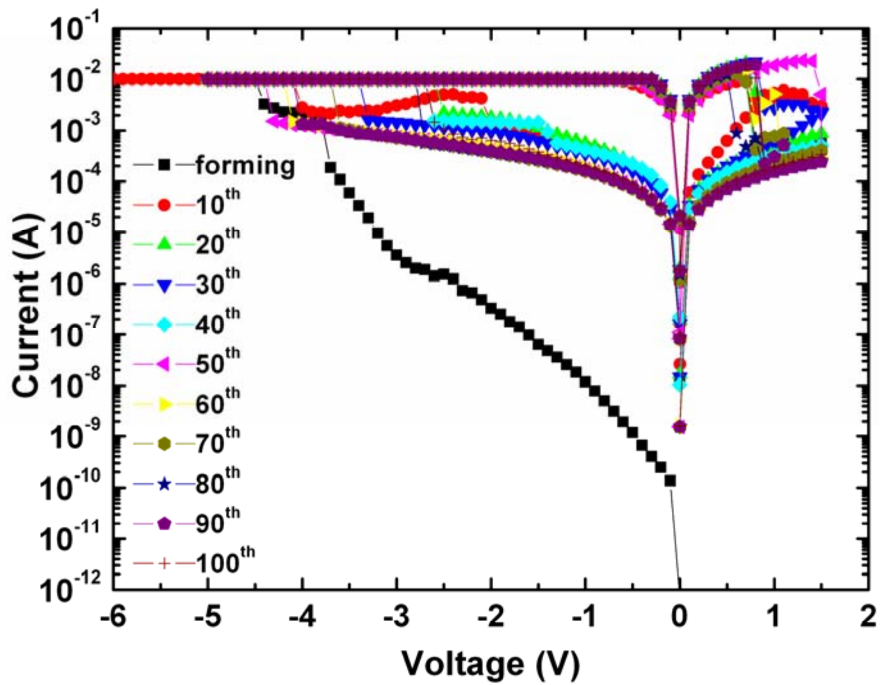

Figure 3.32 Switching cycles of embedded 2nm-Cr device without PDA

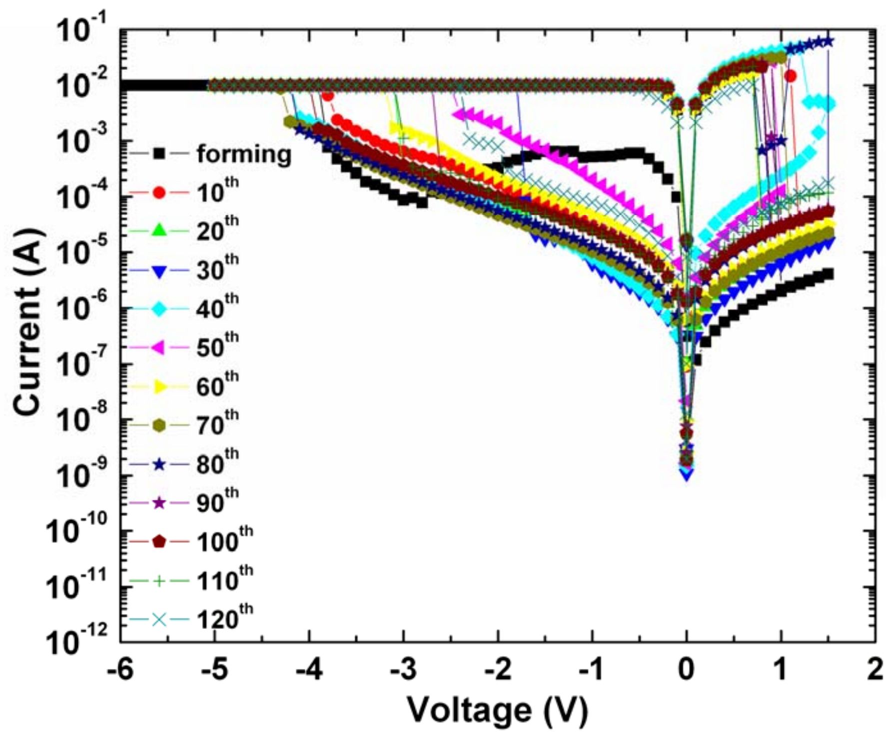

Figure 3.33 Switching cycles of embedded 2nm-Cr device with PDA 500°C

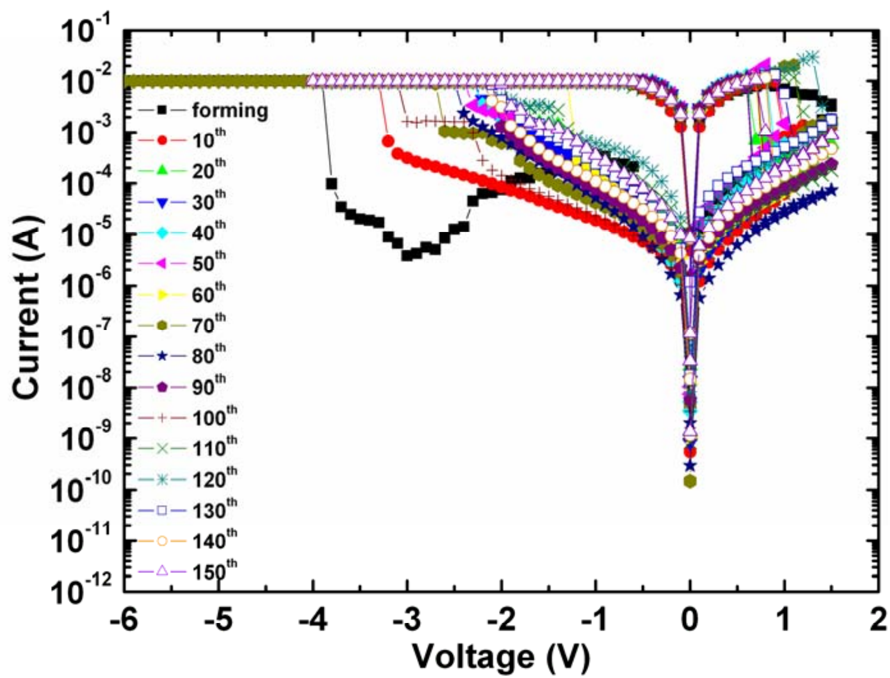

Figure 3.34 Switching cycles of embedded 2nm-Cr device with PDA 600°C

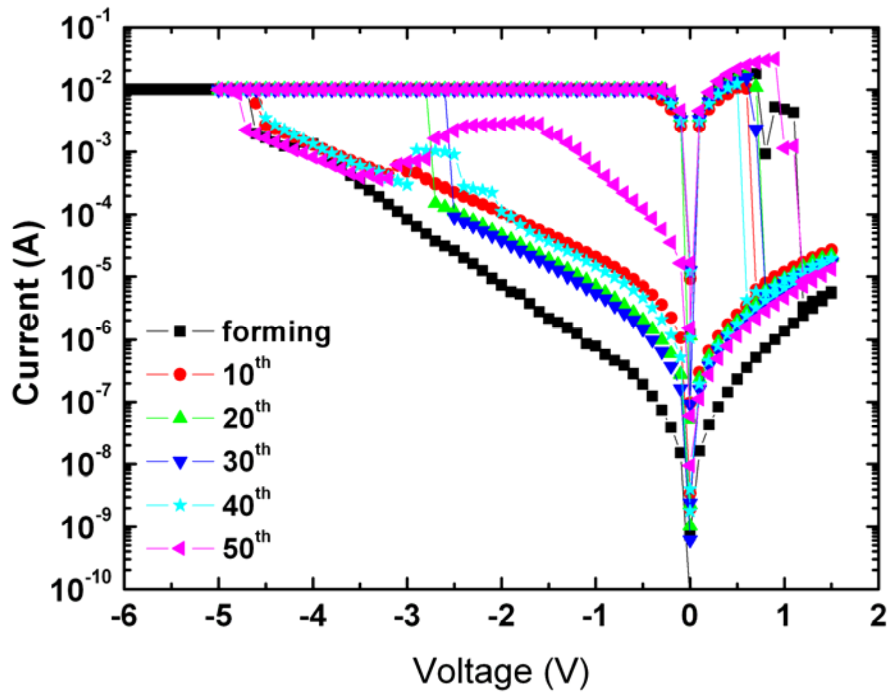

Figure 3.35 Switching cycles of embedded 2nm-Cr device with PDA 700°C

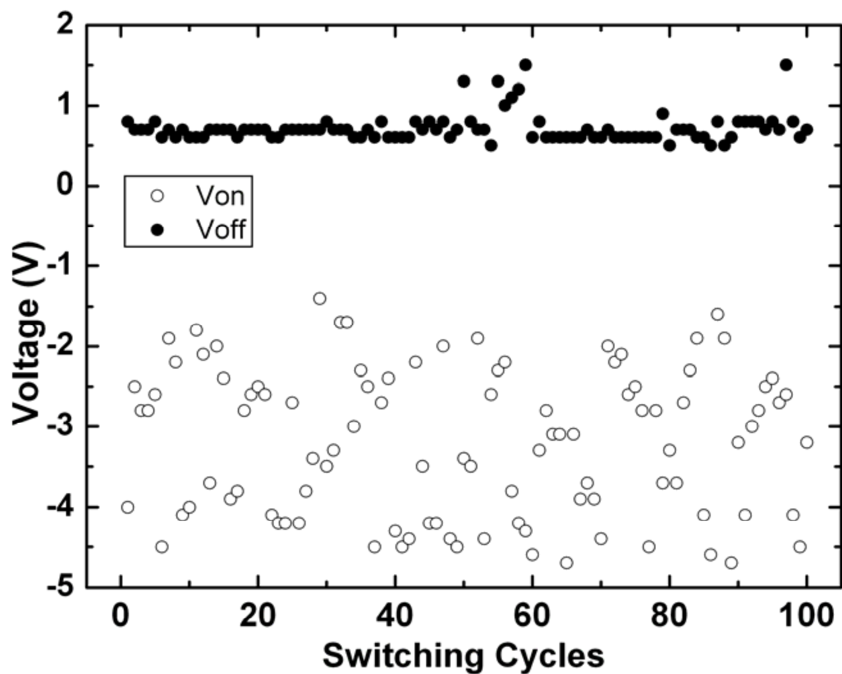

Figure 3.36 Write/Erase cycles for ON-State and OFF-state of sample without PDA

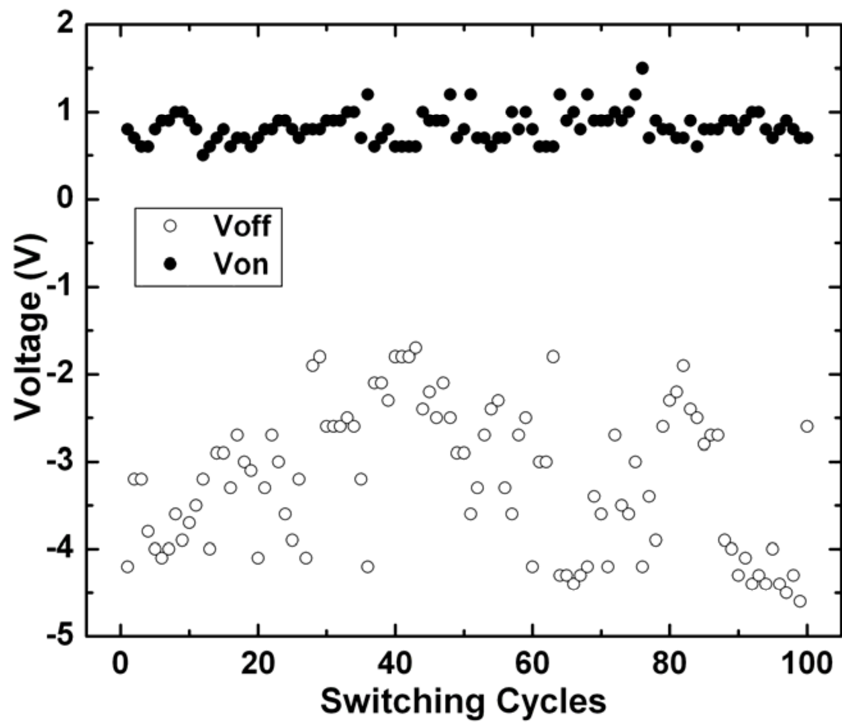

Figure 3.37 Write/Erase cycles for ON-State and OFF-state of sample with PDA 500°C

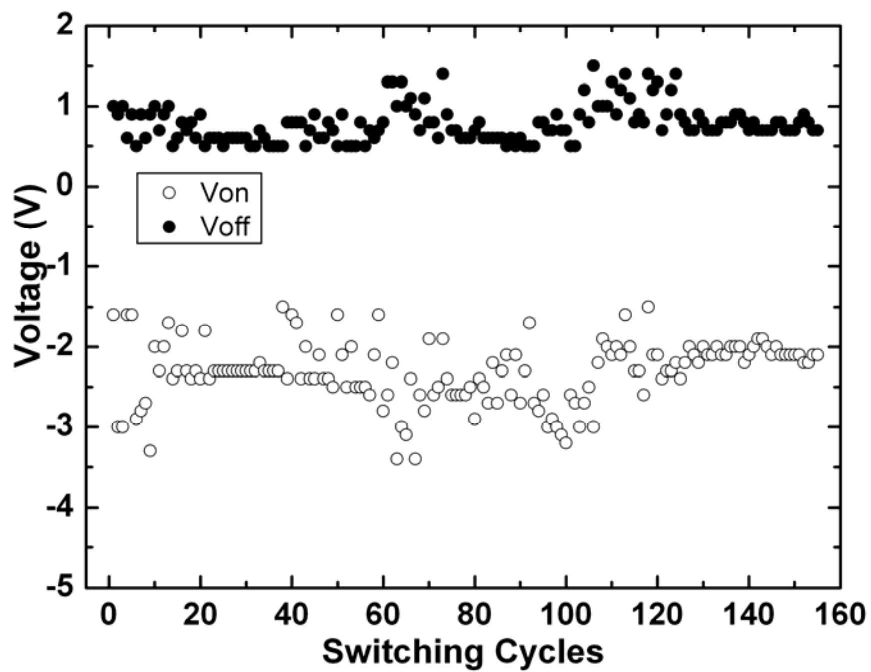

Figure 3.38 Write/Erase cycles for ON-State and OFF-state of sample with PDA 600°C

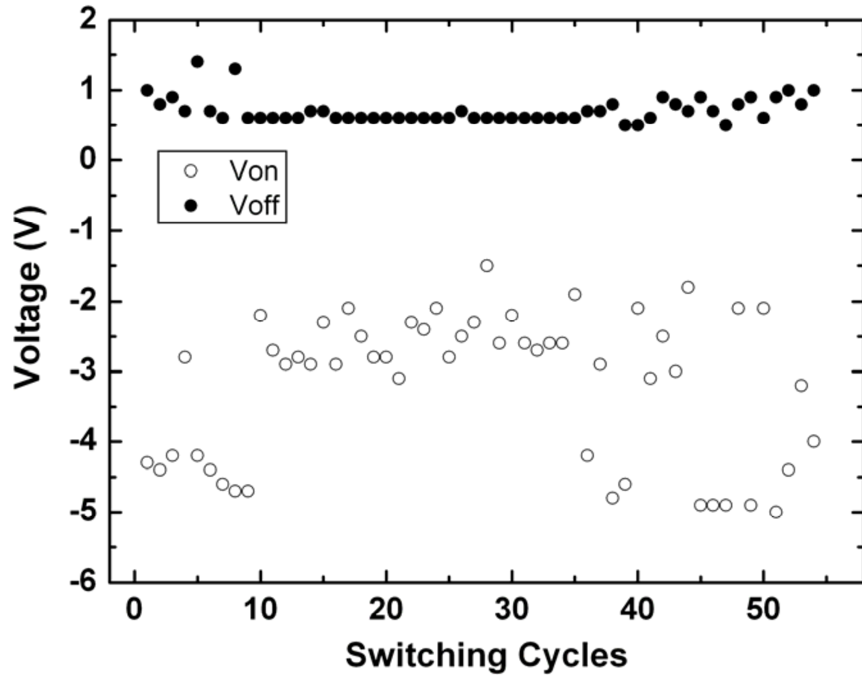

Figure 3.39 Write/Erase cycles for ON-State and OFF-state of sample with PDA 700°C

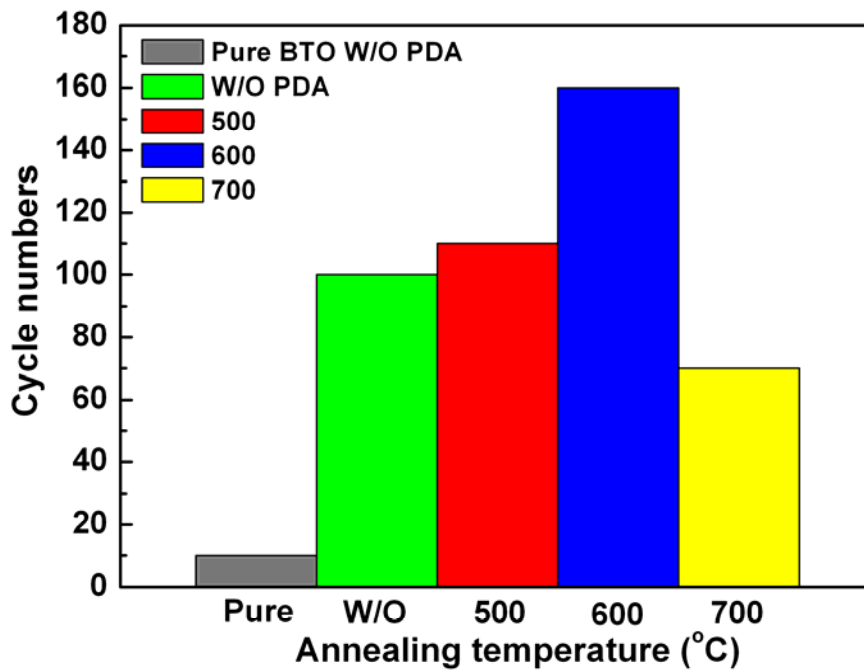

Figure 3.40 Endurance comparisons of different devices

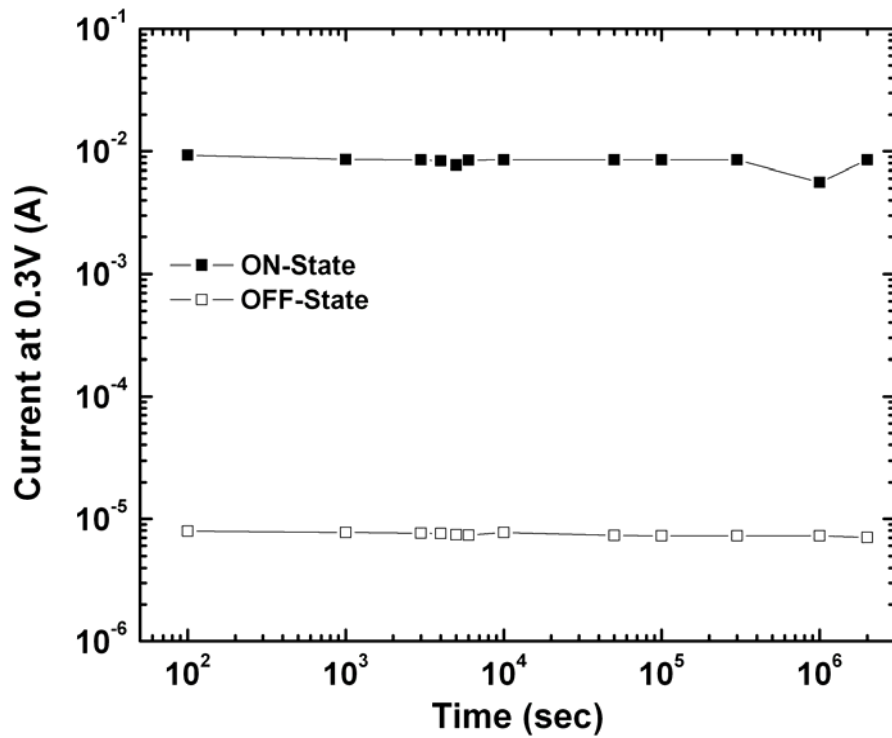

Figure 3.41 Retention test at room temperature of embedded 2nm-Cr with PDA 600°C device

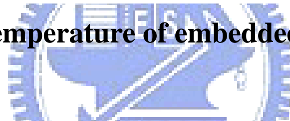

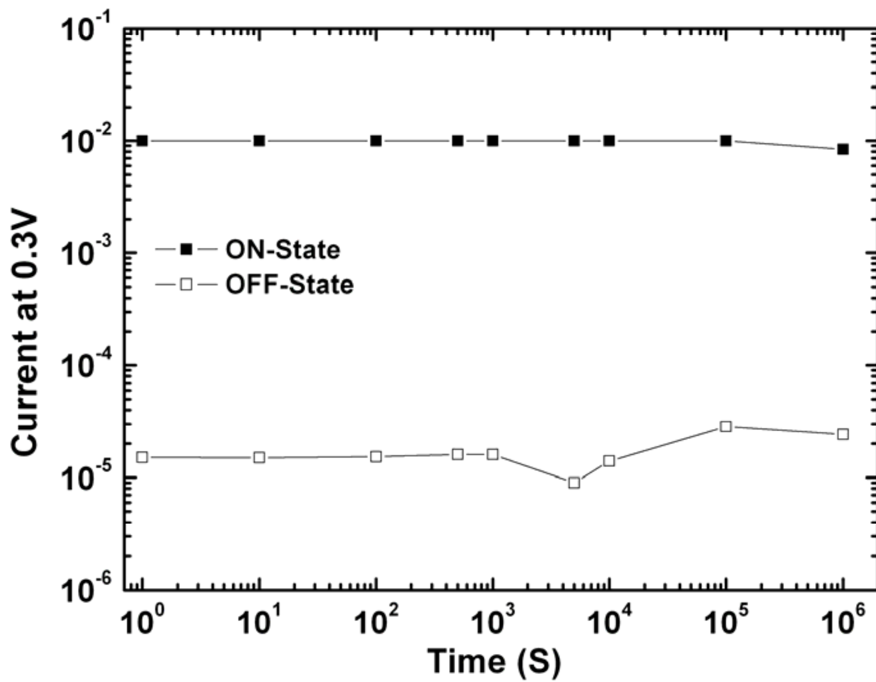

Figure 3.42 Retention test at 85°C of embedded 2nm-Cr with PDA 600°C device

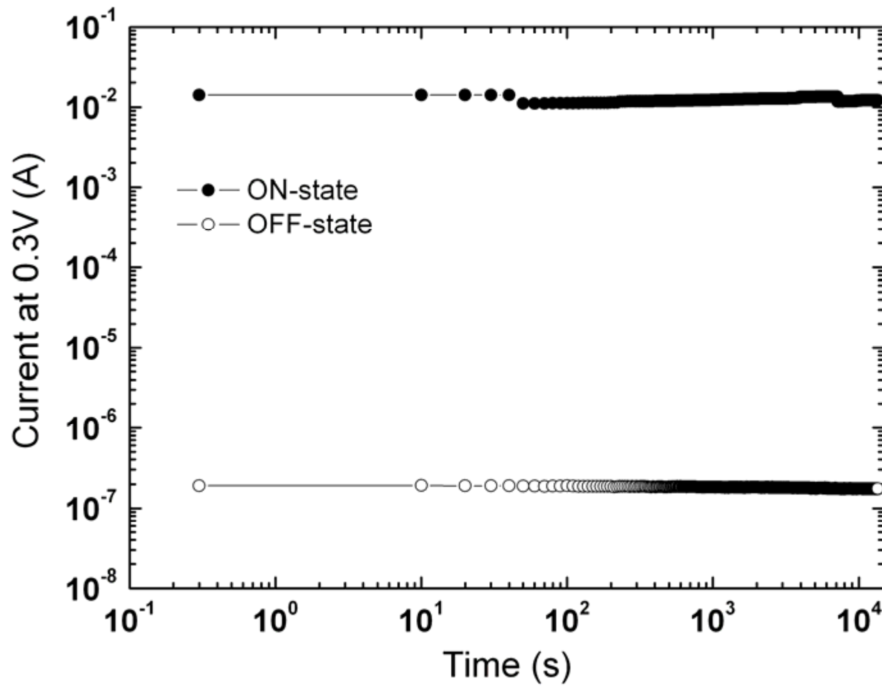

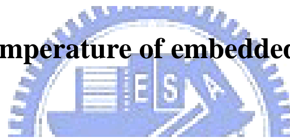

Figure 3.43 Voltage stress at room temperature of embedded 2nm-Cr with PDA 600°C device

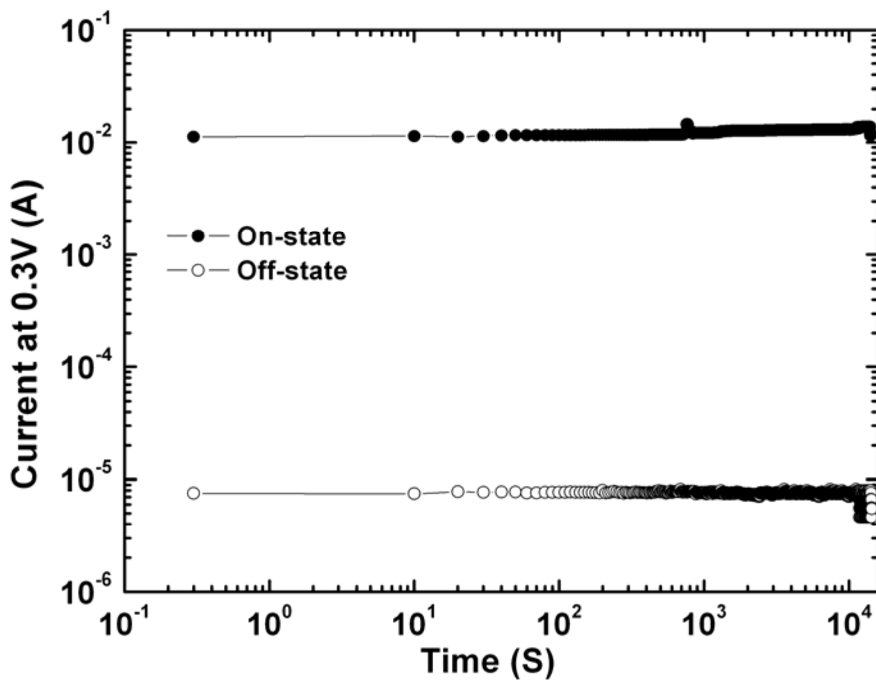

Figure 3.44 Voltage stress at 85°C of embedded 2nm-Cr with PDA 600°C device

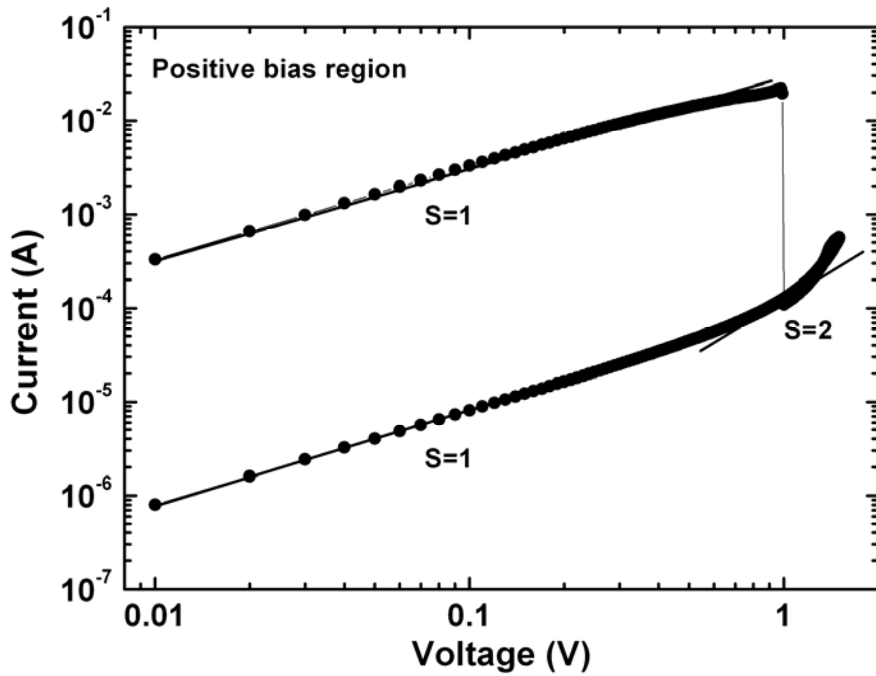

Figure 3.45 Curve fitting at positive bias region for embedded 2nm-Cr device without PDA

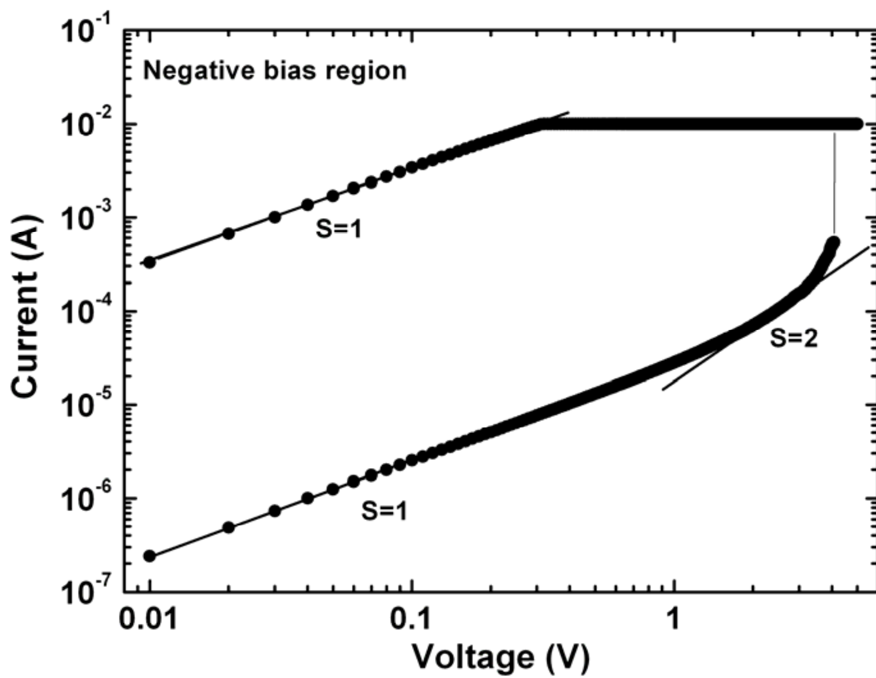

Figure 3.46 Curve fitting at negative bias region for embedded 2nm-Cr device without PDA

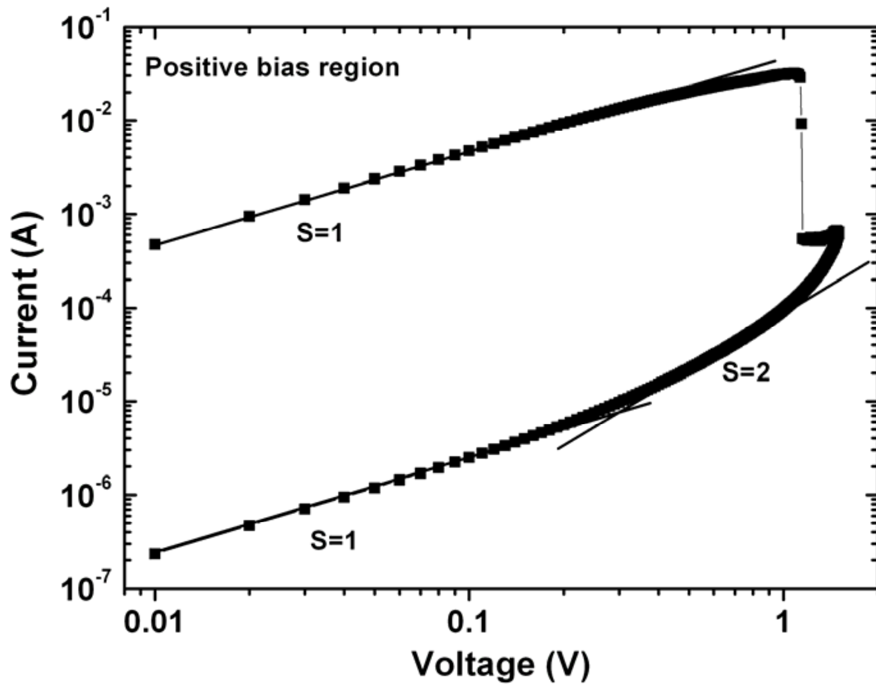

Figure 3.47 Curve fitting at positive bias region for embedded 2nm-Cr device with PDA 600°C

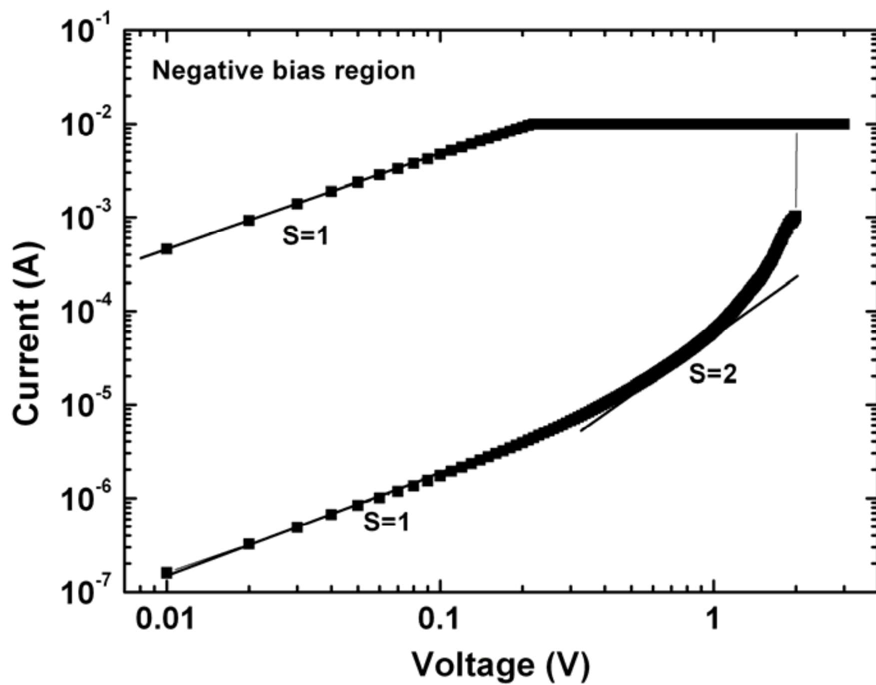

Figure 3.48 Curve fitting at negative bias region for embedded 2nm-Cr device with PDA 600°C

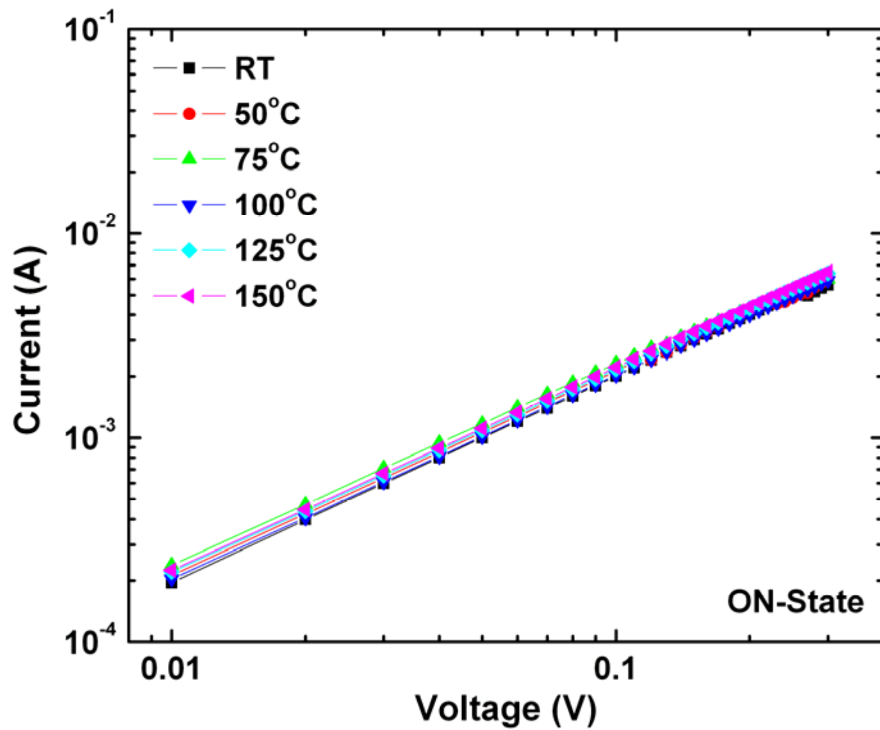

Figure 3.49 ON-State conductivity of measurement at various temperatures

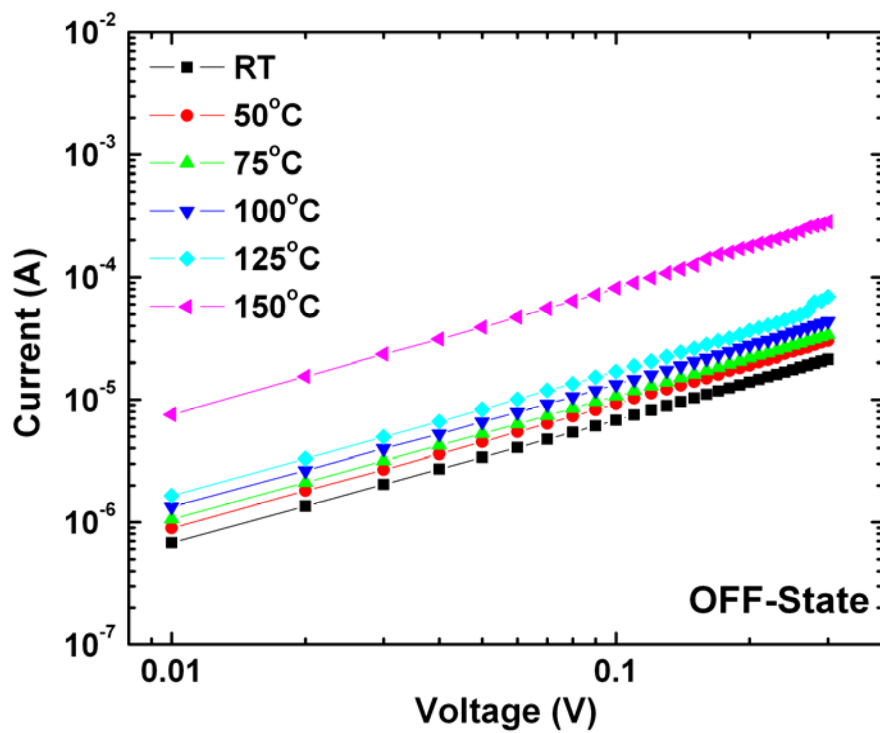

Figure 3.50 OFF-State conductivity of measurement at various temperatures

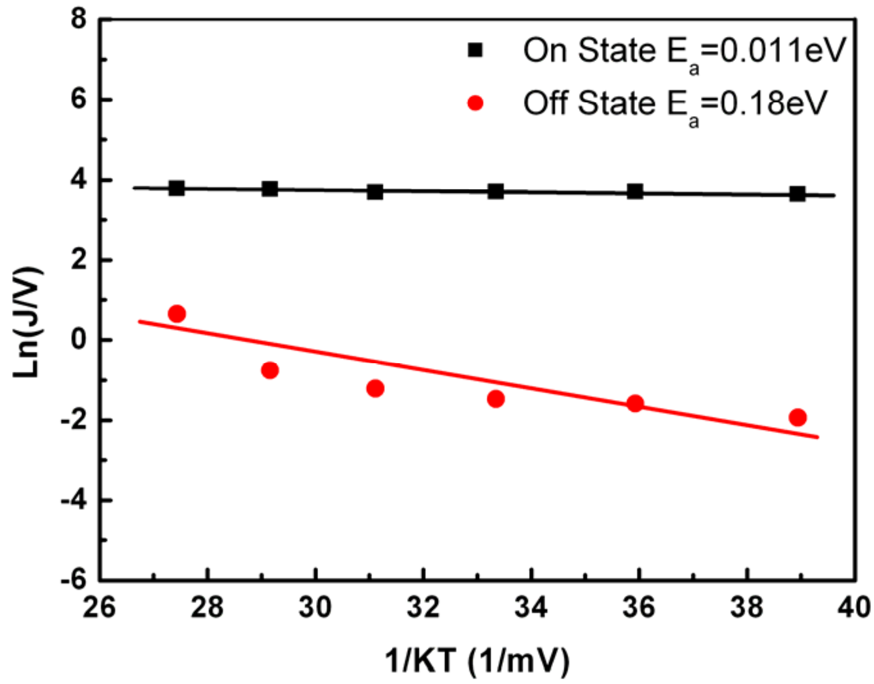

Figure 3.51 The activation energy of ON and OFF states

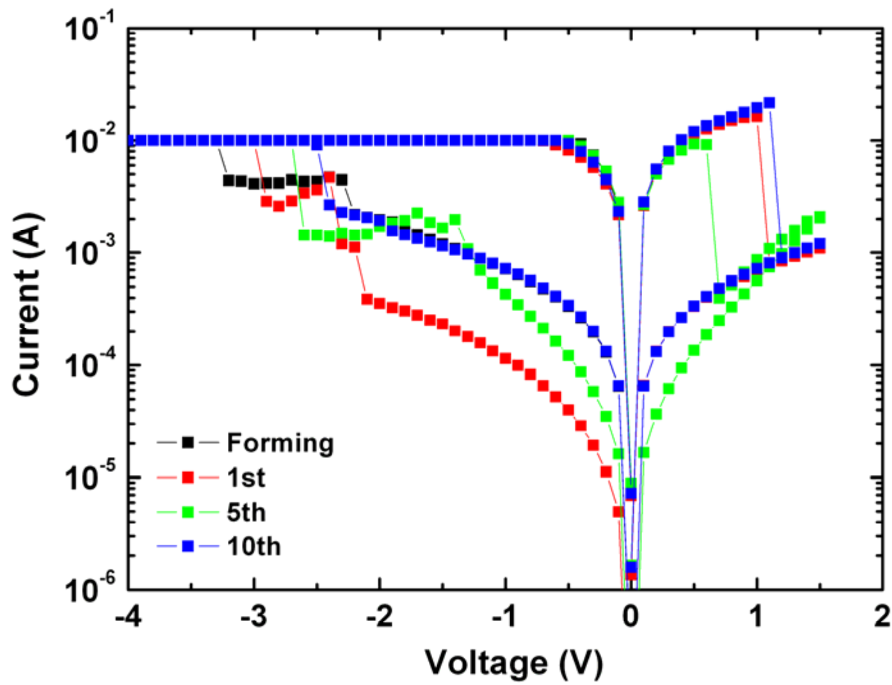

Figure 3.52 Electrical property of embedded 2nm-Pt device without PDA

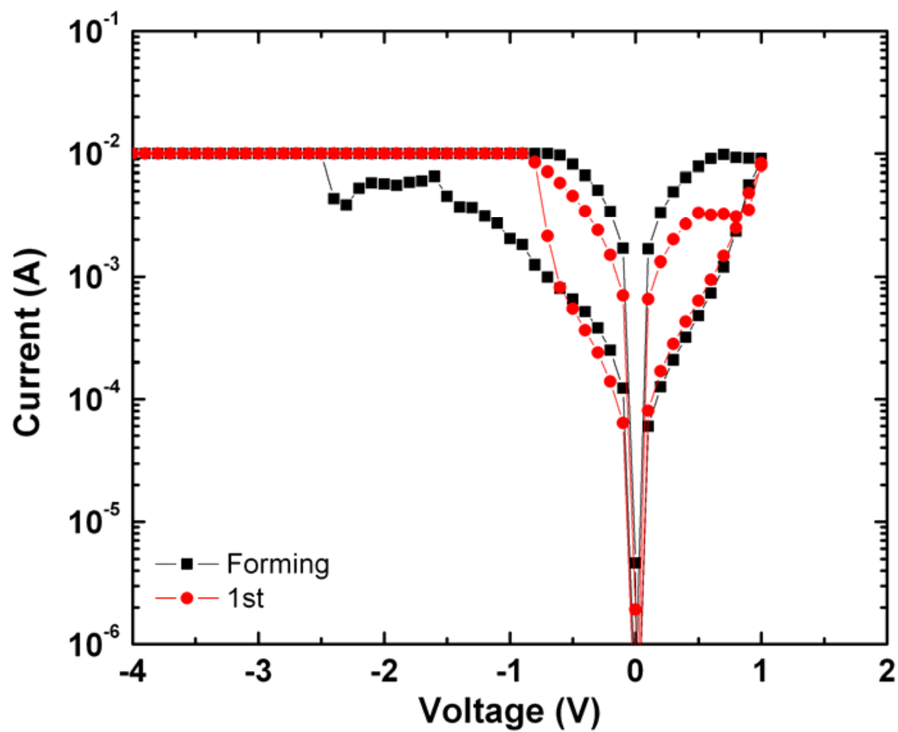

Figure 3.53 Electrical property of embedded 2nm-Pt device with PDA 500°C

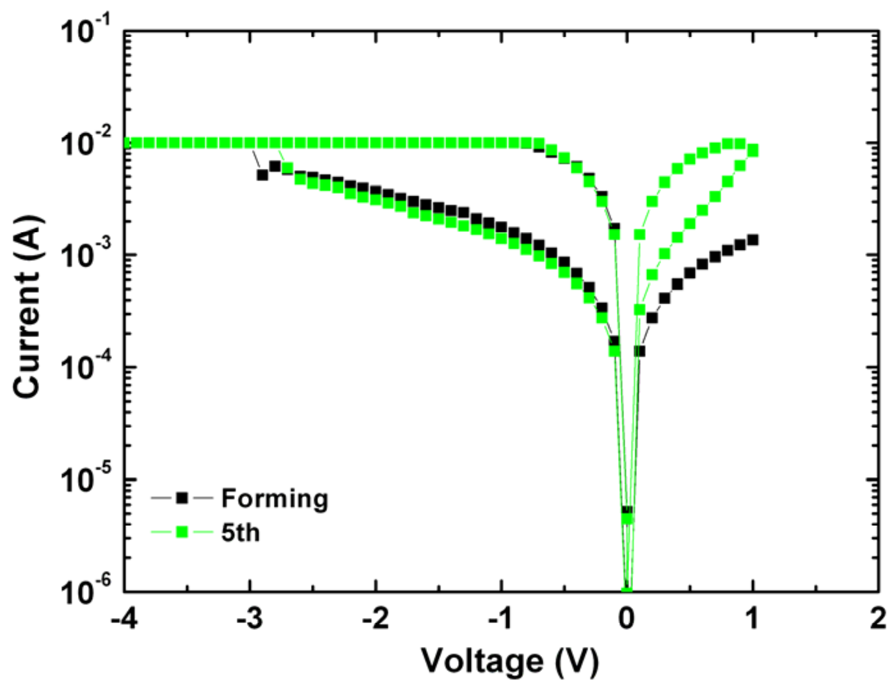

Figure 3.54 Electrical property of embedded 2nm-Pt device with PDA 600°C

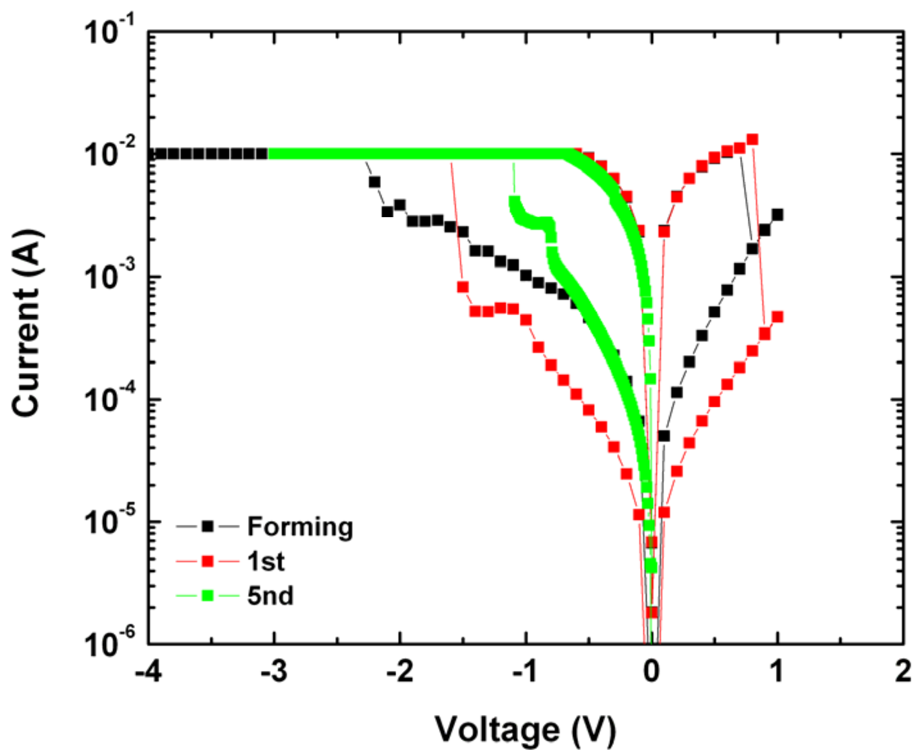

Figure 3.55 Electrical property of embedded 2nm-Pt device with PDA 700°C

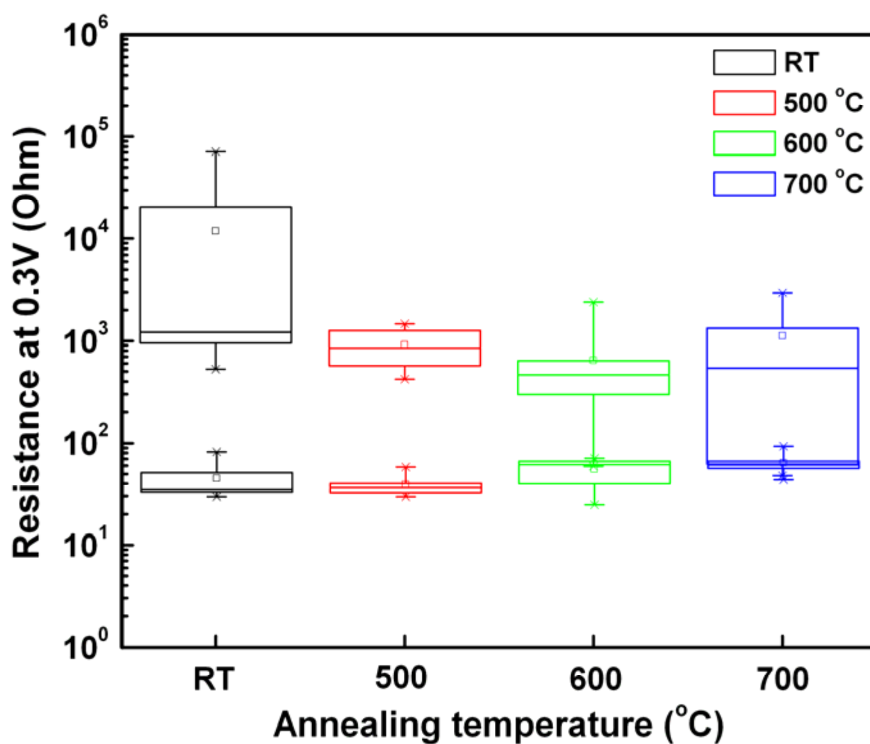

Figure 3.56 Statistics for resistance of ON-State and OFF-State at various temperatures

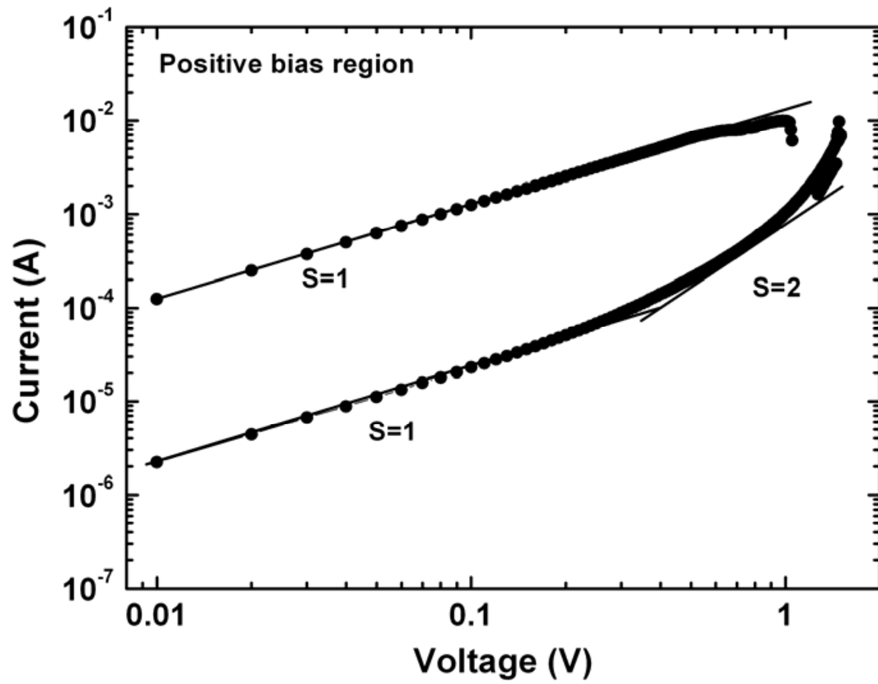

Figure 3.57 Curve fitting at positive bias region for embedded 2nm-Pt device without PDA

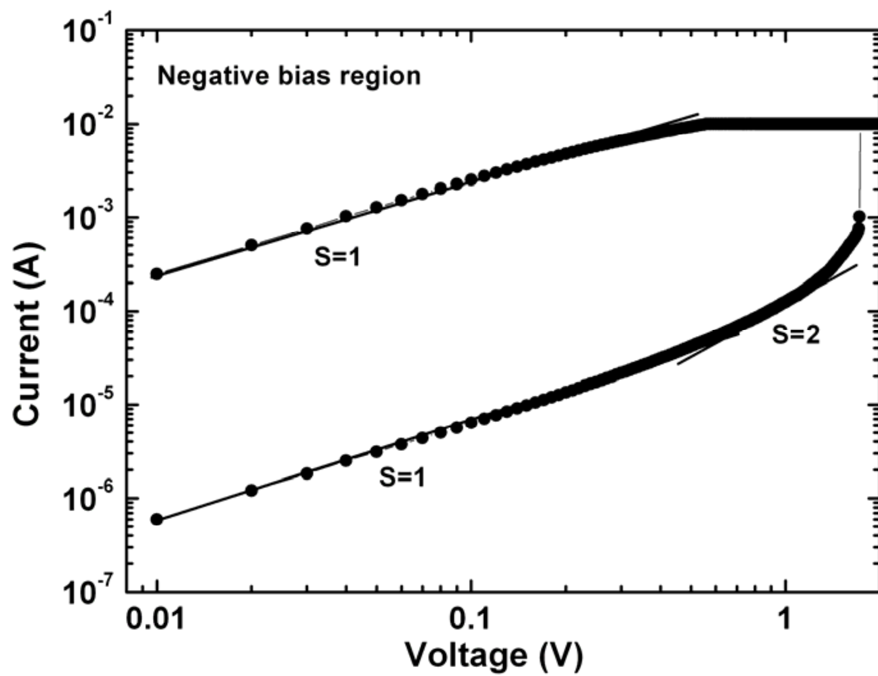

Figure 3.58 Curve fitting at negative bias region for embedded 2nm-Pt device without PDA

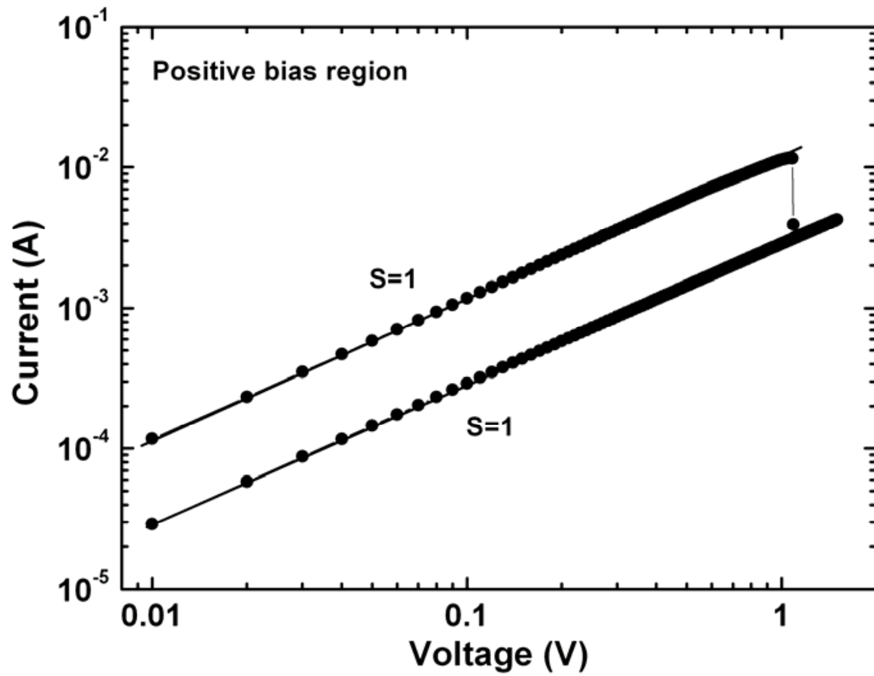

Figure 3.59 Curve fitting at positive bias region for embedded 2nm-Pt device with PDA 600°C

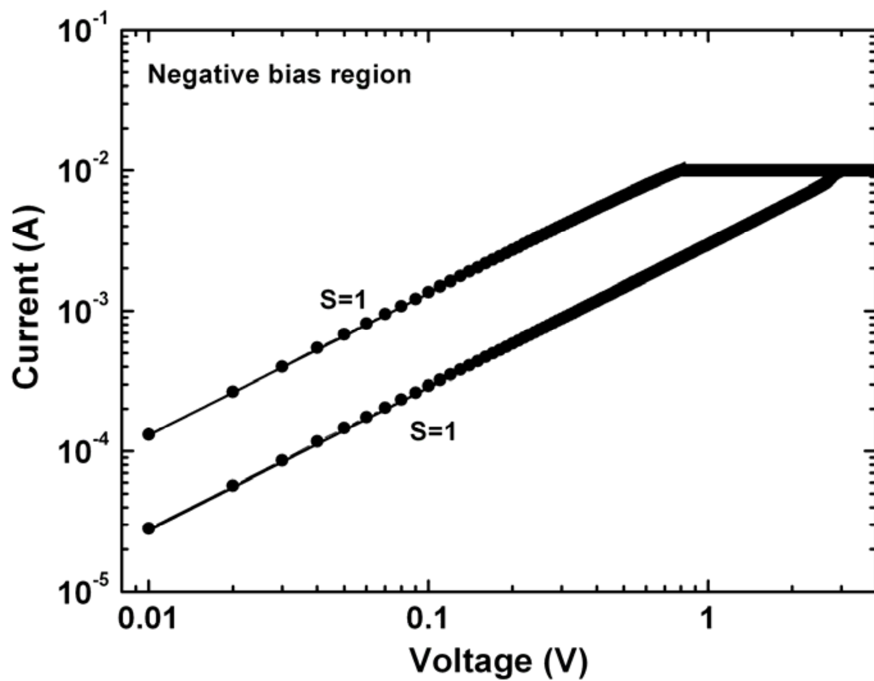

Figure 3.60 Curve fitting at negative bias region for embedded 2nm-Cr device with PDA 600°C

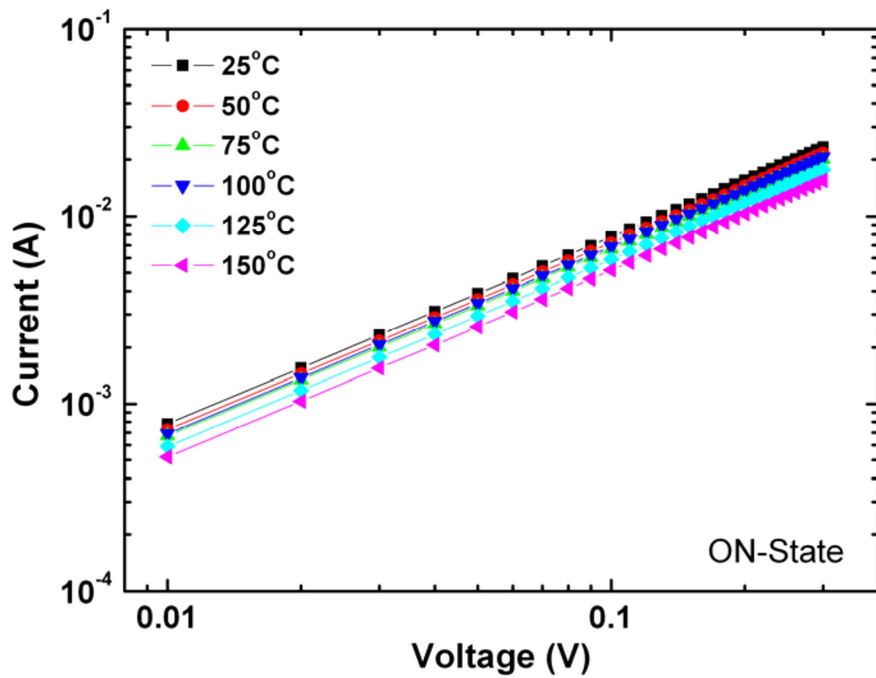

Figure 3.61 ON-State conductivity of measurement at various temperatures for embedded 2nm-Pt device with PDA 600°C

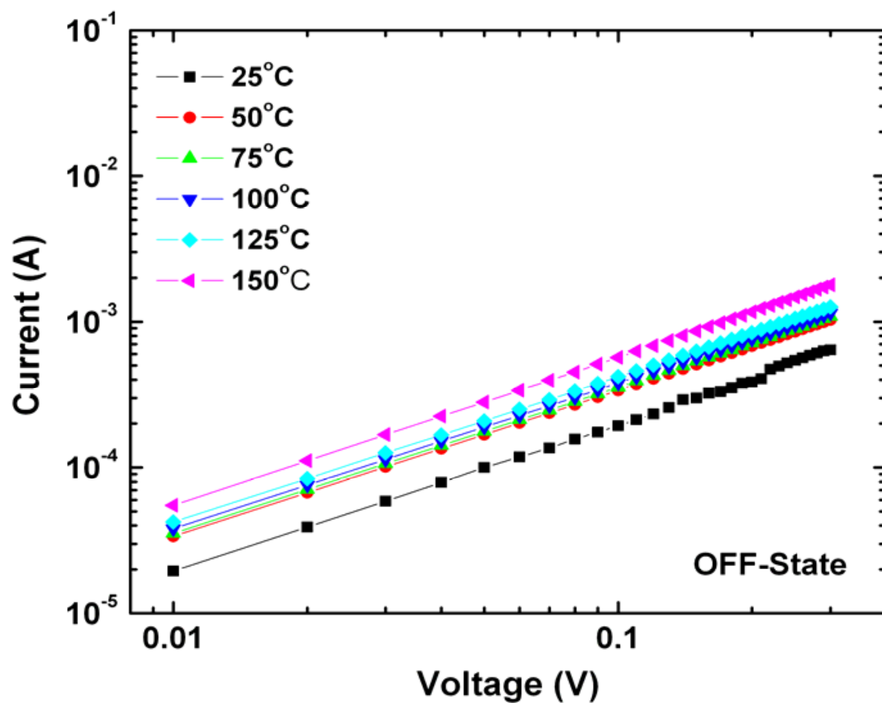

Figure 3.62 OFF-State conductivity of measurement at various temperatures for embedded 2nm-Pt device with PDA 600°C

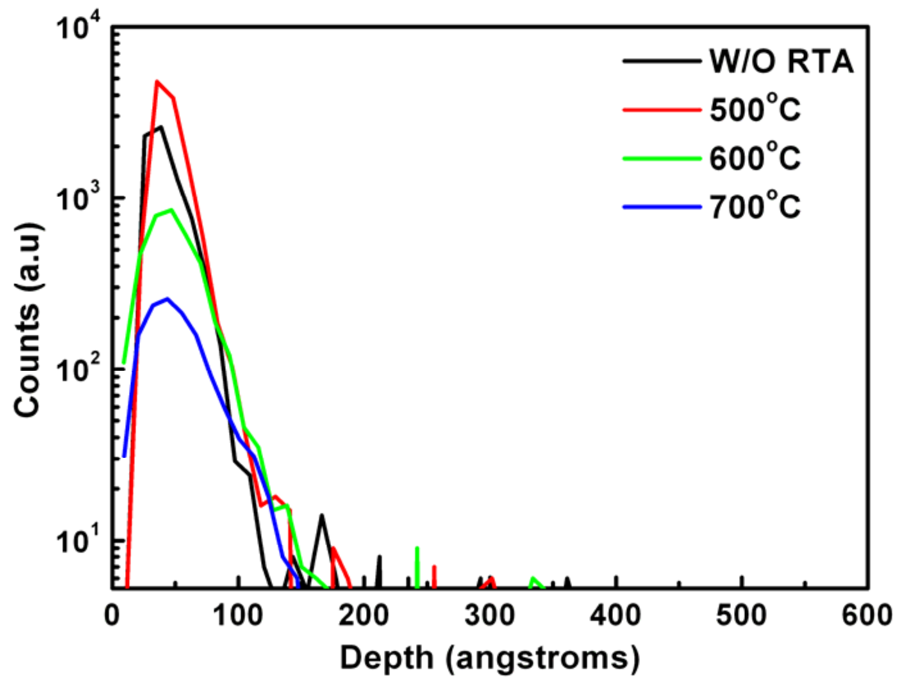

Figure 3.63 SIMS for proving the Pt diffusion in BTO thin film

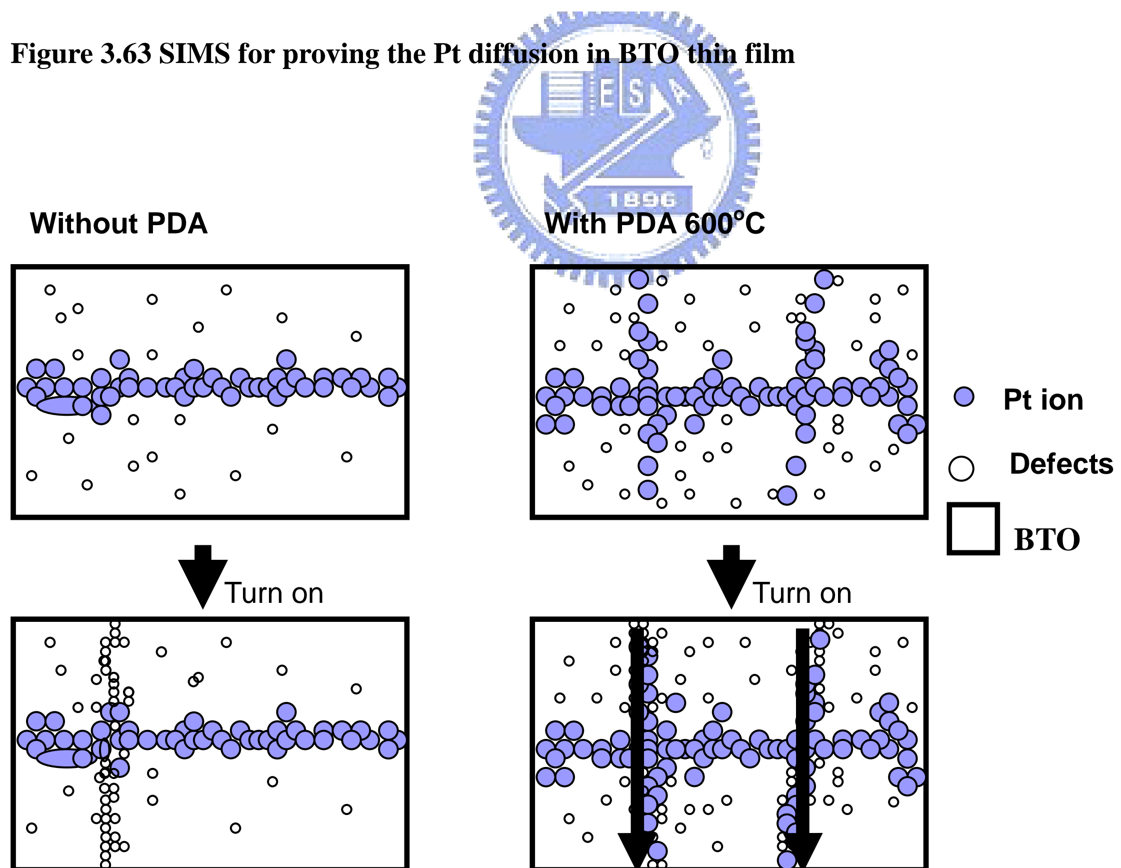

Figure 3.64 Illustrations of conduction mechanism in embedded 2nm-Pt devices.

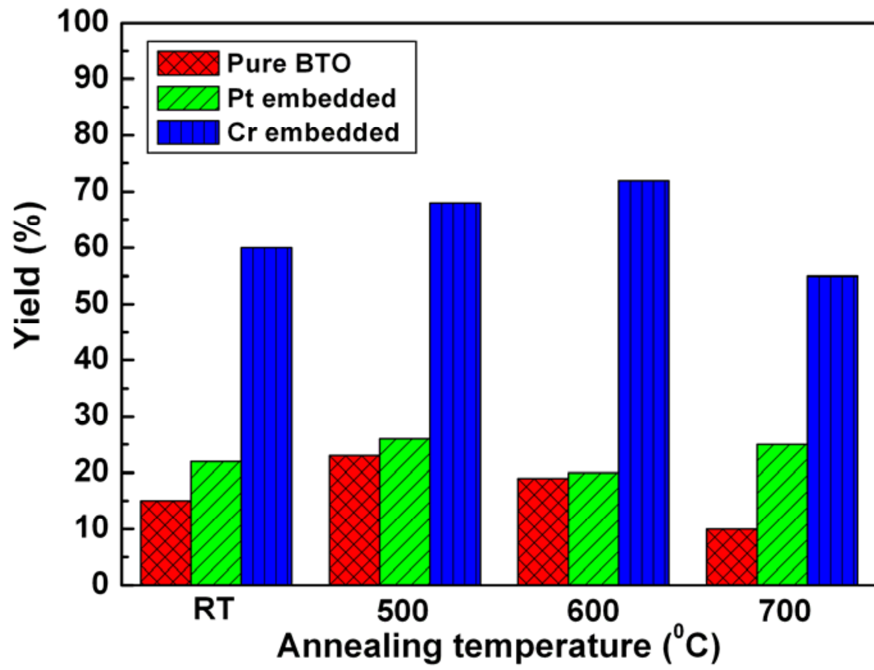

Figure 3.65 Comparison in device yield.

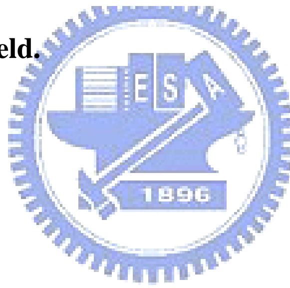

Chapter 4

Conclusions

4.1 Conclusions

In this thesis, we modify the conventional structure Pt/BTO/LNO/Pt by embedding Cr layer in BTO layer. The different thicknesses (10nm, 5nm, 2nm) of Cr are tested. The forming voltage and operation voltage are both decreased by embedding 2nm-Cr in BTO thin film. Further, the operation voltage can be more decreased and stabilized by post deposition annealing (PDA) in N_2 ambient, especially at 600°C. From material analyses, the stabilization of electrical properties is attributed to the formation of Cr-related nanocrystal after post deposition annealing at 600°C. Also, in memory effect tests such as endurance, retention and voltage stress, the device shows excellent performance as well. As we know, Cr is an active metal, which means easily reacted with oxygen. In order to compare with it, we choose Pt, an inert metal, to be the embedded metal. The resistive switching characteristics are poor while raising annealing temperature. From SIMS, Pt ions diffuse seriously in BTO film with higher annealing temperature so that the off-state current increase dramatically. Therefore, from the comparison in device yield, the embedded 2nm-Cr device with PDA 600°C shows the best performance among them.

References:

[1] D. Kahng and S. M. Sze, "A floating gate and its application to memory devices. "Bell Systems Technical Journal, Vol. 46, pp. 1283.1967.

[2] M.J. Rozenberg, I. H. Inoue, and M. J. Sanchez, "Nonvolatile Memory with Multilevel Switching: A Basic Model", Physical Review Letters, Vol. 92, No. 17, 2004

[3] C.Y. Lin, C.C. Lin, C.H.Huang, C.H. Lin, and T.Y. Tseng, "Resistive Switching Properties of Sol-Gel Derived Mo-doped $SrZrO_3$ Thin Films", Surface and Coatings Technology, 2007.

[4] W. Chen, W. J. Liu, M. Zhang, S. J. Ding, D. W. Zhang, and M F. Li, "Multistacked $Al_2O_3/HfO_2/SiO_2$ Tunnel Layer for High-density Nonvolatile Memory Application", Apply Physics Letters, Vol. 91, pp. 22908, 2007.

[5] M. Kwon, H. Choi, M. Chang, M. Jo, S. J. Jung, and H. Hwang, "Droplet Evaporation-Induced Ferritin Self-Assembled Monolayer as A Template for Nanocrystal Flash Memory", Apply Physics Letters, Vol. 90, pp. 193512, 2007.

[6] S. Maikap, P.J. Tzeng, T. Y. Wang, H.Y. Lee, C.H. Lin, C.C. Wang, L.S. Lee, J.R. Yang, and M. J. Tasi, "HfO2/HfAlO/HfO2 Nanolaminate Charge Trapping Layers for High-Performance Nonvolatile Memory Device Applications", Japanese Journal of Applied Physics, Vol. 46, No. 4A, pp. 1803, 2007.

[7] S. V. Pietambaram, N. D. Rizzo, R. W. Dave, J. Goggin, K. Smith, J. M. Slaughter, and S. Tehrani, "Low-Power Switchhing in Magnetoresistive Random Access Memory Bits Using Enhanced Permeability Dielectric Films", Apply Physics Letters, Vol. 90, pp. 143510, 2007.

[8] N.D. Rizzo, M. DeHerrera, J. Janesky, B. Engel, J. Slaughter, and S. Tehrani, "Thermally Activated Magnetization Reversal in Submicron Magnetic Tennel Junctions for Magnetoresistive Random Access Memory", Apply Physics

Letters, Vol. 80, No.13, pp. 2335, 2002.

[9] I. G. Baek, J. E. Lee, H. J. Kim, Y. K. Ha, J. S. Bae, S. C. Oh, S. O. Park, U. I. Chung, N. I. Lee, H. K, Kang, J. T. Moon, “MRAM with Lamellar Structure as Free Layer” IEDM Tech. Dig., pp. 831, 2003.

[10] J. S. Moodera, L. R. Kinder, T. M. Wong, and R. Meservey, “Large magnetoresistance at room temperature in ferromagnetic thin film tunnel junctions,” *Phys. Rev. Lett.*, vol. 74, pp. 3273–3276. April 1995.

[11] J. S. Kovacs, and P. Signell, “Magnetic induction,” Project PHYSNET document MISN-0-145, 2001.

[12] L. L. Hinchey and D. L. Mills, “Magnetic properties of superlattices formed from ferromagnetic and antiferromagnetic materials,” *Physical Review B*, vol. 33, no. 5, pp. 3329, March 1986.

[13] P. Grünberg, R. Schreiber, Y. Pang, M. B. Brodsky, and H. Sowers, “Layered Magnetic Structures: Evidence for Antiferromagnetic Coupling of Fe Layers across Cr Interlayers,” *Physical Review Letters*, vol. 57, no. 19, pp. 2442, November 1986.

[14] C. Carbone and S. F. Alvarado, “Antiparallel coupling between Fe layers separated by a Cr interlayer: Dependence of the magnetization on the film thickness,” *Physical Review B*, vol. 36, no. 4, pp. 2433, August 1987.

[15] M. N. Baibich, J. M. Broto, A. Fert, F. Nguyen Van Dau, F. Petroff, P. Eitenne, G. Creuzet, A. Friederich, and J. Chazelas, “Giant Magnetoresistance of (001)Fe/(001)Cr Magnetic Superlattices,” *Physical Review Letters*, vol. 61, no. 21, pp. 2472, November 1988.

[16] Rouquette J, Haines J, Bornand V, Pintard M, Papet Ph, Bousquet C, Konczewicz L, Gorelli FA,Hull S, “Pressure tuning of the morphotropic phase boundary in

piezoelectric lead zirconate titanate," *Phys. Rev. B*, vol. 70, pp. 14108, 2004.

[17] Liu W, Jiang B, Zhu W, "Self-biased dielectric bolometer from epitaxially grown Pb(Zr,Ti)O3 and lanthanum-doped Pb(Zr,Ti)O3 multilayered thin films," *Appl. Phys. Lett.,* vol. 77 pp. 1047-1049, 2000.

[18] T. Y. Tseng, "Extended Abstracts of the First International Meeting on Ferroelectric Random Access Memories," Gotemba, Japan, 20, 2001.

[19] I. G. Baek, M. S. Lee, S. Seo, M. J. Lee, D. H. Seo, D. S. Suh, J. C. Park, S. O. Park, H. S. Kim, I. K. Yoo, U. I. Chung, and J. T. Moon, "Highly Scalable Non-volatile Resistive Memory using Simple Binary Oxide Driven by Asymmetric Unipolar Voltage Pulses," in *IEDM Tech. Dig*., 2004.

[20] R. Sezi, A. Walter, R. Engl, A. Maltenberger, J. Schumann, M. Kund, and C. Dehm, "Organic Materials for High-Density Non-Volatile Memory Application," in *IEDM Tech. Dig*., pp. 259-262, 2003

[21] W. W. Zhuang, W. Pan, B. D. Ulrich, J. J. Lee, L. Stecker, A. Burmaster, D. R. Evans, S. T. Hsu, M. Tajiri, A. Shimaoka, K. Inoue, T. Naka, N. Awaya, K. Sakiyama, Y. Wang, S. Q. Liu, N. J. Wu, and A. Ignatiev, "Novell Colossal Magnetoresistive Thin Film Nonvolatile Resistance Random Access Memory (RRAM)," in *IEDM Tech. Dig*., pp. 193-196, 2002.

[22] A. Beck, J. G. Bednorz, Ch. Gerber, C. Rossel and D. Widmer, "Reproducible switching effect in thin oxide films for memory applications," *Appl. Phys. Lett.*, vol. 77, pp. 139, March 2000.

[23] Y. Watanabe, J. G. Bednorz, A. Bietsch, Ch. Gerber, D. Widmer, A. Beck and S. J. Wind, "Current-driven insulator–conductor transition and nonvolatile memory in chromium-doped $SrTiO_3$ single crystals," *Appl. Phys. Lett*., vol. 78, pp. 3738, March 2001.

[24] S. Q. Liu, N. J. Wu and A. Ignativ, "Electric-pulse-induced reversible resistance

change effect in magnetoresistive films," *Appl. Phys. Lett.,* vol. 76, pp. 2749, March 2000.

[25] S. Seo, M. J. Lee, D. H. Seo, E. J. Jeoung, D.-S. Suh, Y. S. Joung, I. K. Yoo, I. R. Hwang, S. H. Kim, I. S. Byun, J.-S. Kim, J. S. Choi and B. H. Park, "Reproducible resistance switching in polycrystalline NiO films," *Appl. Phys. Lett.,* vol. 85, pp. 5655 July 2004.

[26] M. J. Rozenberg, I. H. Inoue and M. J. S´anchez, "Nonvolatile Memory with Multilevel Switching: A Basic Model," *Phys. Rev. Lett.,* vol. 92, 178302, April 2004.

[27] A. E. Owen, J. Hu, and A. J. Snell, "Electronic switching in amorphous silicon devices: properties of the conducting filament," pp. 830~833 IEEE 1999.

[28] J. Hajto, A. E. Owen, A. J. Snell, P. G. LeComber, and M. J. Rose, "Chap. 14 pp. 641-701 in amorphous and Microcrystalline Semiconductor Device," Ed: J. Kanicki, Artech House (1992).

[29] K. Aoyama, K. Waku, A. Asanuma, Y. Uesu, and T. Katsufuji, "Electric-pulse-induced reflectance change in the thin film of perovskite manganite," *Appl. Phys. Lett.*, vol. 85, pp. 1208-1211, June 2004.

[30] S. Seo, M. J. Lee, D. H. Seo, S. K. Choi, D. S. Suh, Y. S. Joung, I. K. Yoo, I. R. Hwang, S. H. Kim, and B. H. Park, "Conductivity switching characteristics and reset currents in NiO films," *Appl. Phys. Lett.*, vol. 86, pp. 093509, February 2005.

[31] S. Q. Liu, N. J. Wu, and A. Ignatiev, "Electrica-pulse-induced reversible resistance change effect in magnetoresistive films," *Appl. Phys. Lett.*, vol. 76, pp. 2749-2751, March 2000.

[32] S. Gangopadhyay, J. Geiger, B. Schroder, H. Rubel, and S. Iselborn, "Memory switching in sputtered hydrogenated amorphous silicon (a-Si:H)," *Jpn. J. Appl.*

Phys., vol. 24, pp. 1363-1364, July 1985.

[33] Y. Segui, B. Ai, and H. Carchano, “Switching in polystyrene film: Transistion from on to off state,” *J. Appl. Phys.*, vol. 47, pp. 140-142, January 1976.

[34] H. Carchano, R. Lacoste, and Y. Segui, “Bistable electrical switching in polymer thin film,” *Appl. Phys. Lett.*, vol. 19, pp. 414-415, September 1971.

[35] A. E. Owen, J. Hu, J. Hajto, and A. J. Snell, in *Proceedings of 5th International.*

[36] A. Beck, J. G. Bednorz, C. Gerber. C. Rosseel, and D. Widmer, “Reproducible switching effect in thin oxide films for memory application,” *Appl. Phys. Lett.*, vol. 77, pp.139-141, 2000.

[37] I. G. Baek, M. S. Lee, S. Seo, M. J. Lee, D. H. Seo, D. S. Suh, J. C. Park, S. O. Park, H. S. Kim, I. K. Yoo, U. I. Chung, and J. T. Moon, “Highly Scalable Non-volatile Resistive Memory using Simple Binary Oxide Driven by Asymmetric Unipolar Voltage Pulses,” in *IEDM Tech. Dig.*, 2004.

[38] L. D. Bozano, B. W. Kean, V. R. Deline, J. R. Salem, and J. C. Scott, “Mechanism for bistable in organic memory elements,” *Appl. Phys. Lett.*, vol. 84, pp. 607-609, November 2004.

[39] A. Bandyopadhyay and A. J. Pal, “Multilevel conductivity and conductance switching in supramolecular structures of an organic molecule,” *Appl. Phys. Lett.*, vol. 84, pp. 999-1001, December 2003.

[40] S. Lai and T. Lowrey, “OUM - A 180 nm Nonvolatile Memory Cell Element Technology for Stand Alone and Embedded Applications,” in *IEDM Tech. Dig.*, 2001, pp. 803-806.

[41] D. M. Taylor and C. A. Mills, “Memory effect in the current–voltage characteristic of a low-band gap conjugated polymer,” *J. Appl. Phys.*, vol. 90, pp. 306-309, April 2001.

[42] C. Y. Liu, C. C. Chuang, J. S. Chen, A. Wang, W. Y. Jang, J. C. Young, K. Y. Chiu, and T. Y. Tseng, “Memory effect of sol-gel derived V-doped $SrZrO_3$ thin films”. Thin Solid Films, pp.287, 2006.